

INFORMATION TO USERS

This was produced from a copy of a document sent to us for microfilming. While the most advanced technological means to photograph and reproduce this document have been used, the quality is heavily dependent upon the quality of the material submitted.

The following explanation of techniques is provided to help you understand markings or notations which may appear on this reproduction.

1. The sign or "target" for pages apparently lacking from the document photographed is "Missing Page(s)". If it was possible to obtain the missing page(s) or section, they are spliced into the film along with adjacent pages. This may have necessitated cutting through an image and duplicating adjacent pages to assure you of complete continuity.
2. When an image on the film is obliterated with a round black mark it is an indication that the film inspector noticed either blurred copy because of movement during exposure, or duplicate copy. Unless we meant to delete copyrighted materials that should not have been filmed, you will find a good image of the page in the adjacent frame.
3. When a map, drawing or chart, etc., is part of the material being photographed the photographer has followed a definite method in "sectioning" the material. It is customary to begin filming at the upper left hand corner of a large sheet and to continue from left to right in equal sections with small overlaps. If necessary, sectioning is continued again—beginning below the first row and continuing on until complete.
4. For any illustrations that cannot be reproduced satisfactorily by xerography, photographic prints can be purchased at additional cost and tipped into your xerographic copy. Requests can be made to our Dissertations Customer Services Department.
5. Some pages in any document may have indistinct print. In all cases we have filmed the best available copy.

University
Microfilms
International

300 N. ZEEB ROAD, ANN ARBOR, MI 48106
18 BEDFORD ROW, LONDON WC1R 4EJ, ENGLAND

7919613

MORGAN, JOHN ADRIAN
NUCLEOSYNTHESIS IN SUPERNOVAE AND THE ORIGIN
OF ISOTOPIC HETEROGENEITY IN THE EARLY SOLAR
SYSTEM.

RICE UNIVERSITY, PH.D., 1979

University
Microfilms
International 300 N. ZEEB ROAD, ANN ARBOR, MI 48106

RICE UNIVERSITY

NUCLEOSYNTHESIS IN SUPERNOVAE AND THE ORIGIN
OF ISOTOPIC HETEROGENEITY IN THE EARLY SOLAR SYSTEM

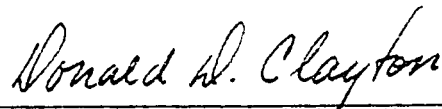
by

John A. Morgan

A THESIS SUBMITTED
IN PARTIAL FULFILLMENT OF THE
REQUIREMENTS FOR THE DEGREE

DOCTOR OF PHILOSOPHY

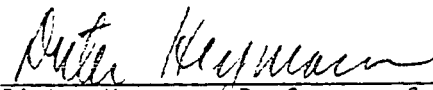
APPROVED, THESIS COMMITTEE:



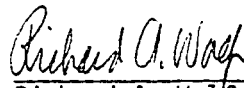
Donald D. Clayton, Andrew Hays
Buchanan Professor of Astrophysics
Chairman



Ian Duck, Professor of Physics



Dieter Heymann, Professor of
Space Physics and Geology



Richard A. Wolf, Professor of
Space Physics and Physics

HOUSTON, TEXAS

MAY 1979

NUCLEOSYNTHESIS IN SUPERNOVAE AND THE ORIGIN
OF ISOTOPIC HETEROGENEITY IN THE EARLY SOLAR SYSTEM

John A. Morgan

ABSTRACT

A model for the nucleosynthetic yields for $20 \leq A \leq 30$ from a massive supernova (spectral class O or B on the main sequence) is developed and compared with the requirements of a hypothetical trigger for solar system formation, as proposed by Cameron and Truran. A static network simulates the presupernova nuclear evolution of the neon- and carbon-bearing zones of a $25 M_{\odot}$ star. The peak burning conditions for explosive nucleosynthesis from shock passage are obtained by applying the Rankine-Hugoniot relations in a borderline radiation-dominated gas with borderline relativistic and degenerate electrons to conditions estimated from a presupernova stellar model, assuming that the dimensionless entropy per nucleon increases by about 0.28 across the shock. Comparisons are made with similarity solutions and results of hydrodynamic calculations of shock passage. Except for ^{26}Al , which is made almost entirely by the explosion, the products of static carbon burning dominate abundance patterns in the ejecta. Both explosive carbon burning and explosive neon burning contribute significantly to ^{26}Al production. Free neutron levels in this part of the supernova may allow synthesis of ^{40}K , ^{107}Pd , ^{129}I and possibly other rare, heavy nuclei in interesting amounts.

ACKNOWLEDGEMENTS

I would like to thank the many people who assisted me in the course of this study. My research director, Professor Clayton, gave me much shrewd and practical advice as the problem unfolded, and especially when things went awry. Professor Heymann's constant enthusiasm and interest in the wider ramifications of my work helped buoy my own interest -- and also helped keep me honest about its generality. I would like to express my appreciation for the stimulating and cordial atmosphere of the 1977 University of California, Santa Cruz supernova workshop. Thanks also go to Brian Whitehead and Professor Wolf for pointing out errors, to Ruth Parks for typing the final manuscript, to Beverly McCabe for drafting the figures, and to Ann E. Wehrle who mercilessly criticized my writing style and my spelling. Indebtedness to Rice University, the National Science Foundation, and the National Aeronautics and Space Administration for financial support during my years of graduate study is acknowledged.

Finally, this dissertation bears a double dedication to my mother, Lois H. Morgan, whose unwavering confidence in me made the road a little less rocky, and to the memory of my father, John Tramble Morgan, M.D., 1916-1976, who first showed me the beauty of things scientific.

TABLE OF CONTENTS

	Page
I. Of the Birth and Death of Stars.....	1
II. Thermonuclear Burning Stages in Advanced Stellar Evolution.....	13
III. Presupernova Nuclear Evolution.....	34
IV. Strong Shocks in the Mantle of a Supernova.....	62
V. A Nucleosynthetic Model for the Explosion of a Massive Star.....	107
VI. Discussion.....	149
Bibliography.....	153

A new difficulty came into Alice's head.
"Supposing it couldn't find any?" she suggested.
"Then it would die, of course."
"But that must happen very often," Alice
remarked thoughtfully.
"It always happens," said the Gnat.

Through the Looking-Glass,

Lewis Carroll

CHAPTER I

OF THE BIRTH AND DEATH OF STARS

A. Introduction

In this study we will develop a model for the nucleosynthetic yields from the supernova explosion of a massive star of the sort which has been proposed as the initiating event in the formation of the solar system by Cameron and Truran (1977). The notion that a supernova played a role in the earliest history of the solar system has been advanced at times by Hoyle (1944), Kohman (1961), Manuel et al. (1972), Cameron (1962) and others, but has only become accepted as a major element in origin theories with the discovery of evidence for live ^{26}Al in the Allende meteorite at the time of its formation. Evidence for the injection of any detectable amount of live ^{26}Al from a single supernova is a remarkable and very important discovery about the history of the early solar system, but the coincidence that this should happen within at most a few million years of the formation of the radiometrically oldest solid bodies in the solar system, the Ca-Al rich inclusions in Allende, is considered by many too unlikely to be plausible, unless the events are causally related. The model to be developed will concentrate on the relative yields of the isotopes with $20 \leq A \leq 30$, although limits can be set on the synthesis of heavy nuclei, as a first step towards reconstructing the responsible event and, perhaps, toward assessing its role in the early solar system.

B. Historical Remarks

The question of the origin of the solar system has a long and tortuous history, into which ideas concerning supernovae have entered only recently. Classical antiquity saw the emergence of speculations with a suggestively modern cast. The Epicurean materialist Lucretius, in his De Rerum Natura (ca. 55 BCE) begins with the words,

"I will now set out in order the stages by which the initial concentration of matter laid the foundations of earth and sky, of the ocean depths and the orbits of sun and moon."

an account of cosmology which asserts the earth, sun and moon formed through the agency of natural laws acting on matter already extant,

"...nothing but a hurricane raging in a newly congregated mass of atoms of very sort."

In the period following the Copernican revolution, Descartes (1644) made the first attempt to formulate a theory of solar system origins on the basis of the new astronomy and physics whose flowering would shortly culminate in the Newtonian synthesis, but Newton himself engaged in little cosmogonical speculation. During the eighteenth century, the introduction of Buffon's tidal theory (1745) and of early forms of the nebular hypothesis, advanced independently by Kant (1755) and by Laplace (1796, in the same book as his celebrated anticipation of the notion of a black hole) mark the division for the next two centuries of solar system origin theories into two basic classes: The cataclysmic theories, relying upon rare, violent events exemplified by Buffon's postulated grazing encounter of the sun with a comet of roughly solar mass (!), leading to the tidal ejection of the matter

which formed the planets, and the nebular theories, which assume that planets form from a more-or-less quiescent rotating disk or series of concentric rings which is coeval with the sun. The inferred frequency of planetary system formation as an astrophysical process differs drastically between the two classes.

The first half of the twentieth century produced a large and diverse body of attempts to formulate a workable theory of solar system origins. Without attempting to do justice to the variety and scope of these investigations, we shall mention some highlights. Chamberlin (1901) and Moulton (1905), in the early years of the century, developed the notion of a tidal encounter between the sun and a passing star, while nebular theories have been elaborated by von Weizacker (1944), ter Haar (1948), Whipple (1948), Kuiper (1949) and Cameron (1963), to name a few. A new element in origin theories, the possible role of solar electric and magnetic fields, was introduced by Birkeland (1912) and has been developed by Berlage and, independently, by Alfvén. Lyttleton (1941) and Hoyle (1944) proposed cataclysmic theories intended to circumvent difficulties encountered in tidal theories; in light of later developments, Hoyle's suggestion that the sun had a binary companion which became a supernova is noteworthy.

The theoretical approaches listed above attempt to account in a gross manner for the origin of planetary bodies in near-circular orbits with angular momentum parallel to the sun's spin, and devote a great deal of attention to such regularities in the present solar system as the Titius-Bode law. The 1950's saw the emergence of a radically different approach based on understanding the physical and chemical

properties of meteorites, pioneered by Urey (1951); it is at this point that the question of the origin of the solar system becomes entangled with that of the origin of the elements.

C. Isotopic Chronologies of the Solar System

The development of stellar nucleosynthesis theory as described in the review article of Burbidge et al. (1957) rests on the realization that abundances of the chemical elements reflect nuclear, rather than chemical, systematics, which are characteristic of the physical conditions at their place of formation. The empirical evidence against which such theories are to be tested is the "cosmic abundance table" whose first incarnation was prepared by Goldschmidt (1937) and which was updated by Suess and Urey (1956) on the assumption that chondritic meteorites are samples of pristine "average" solar system material. The idea that all heavy elements in the solar system are products of a continuous enrichment due to nucleosynthesis inside stars followed by dispersal in the interstellar medium underlies the use of long-lived radioactivities present in protosolar matter as radioactive clocks to date events in the early history of the solar system. Already in 1929 Rutherford had pioneered the development of radiometric chronologies for solar system bodies by deducing a U/Th age for the earth; as mass spectroscopic techniques improved, and as theoretical understanding of astrophysical nuclear processes advanced, there emerged a chronology of events in the history of meteorite parent bodies. Clayton (1968) and Wetherill (1975) give accounts of this body of knowledge. Prior to 1975, the major conclusions were: 1) The oldest meteorites have

Rb/Sr ages of $\approx 4.6 \times 10^9$ yr, and 2) Fossil ^{129}I and ^{244}Pu radioactivities indicate a "free decay" interval of order 10^8 yr between the time the material in the solar nebula became isolated from galactic nucleosynthesis and the time meteorite parent bodies began to retain Xe daughters of these activities. This interval is suggestively close to the time between spiral arm passages, and figured in schemes for the history of meteoritic material. However, a series of dramatic discoveries in the Allende meteorite has called the accepted interpretation of solar system chronometers into question and has come to influence theories of the origin of the solar system profoundly. Briefly, these are:

1. The discovery by R. N. Clayton et al. in 1973 of isotopically anomalous oxygen in Allende; enrichments of ^{16}O were found, corresponding to the addition of up to 5% of pure ^{16}O to average solar system oxygen in some inclusions.

2. Gray and Compston (1974), Lee and Papanastassiou (1974), and Lee et al. (1977; 1977a; 1977b) have established the existence in Allende Ca-Al rich inclusions of excesses in $^{26/24}\text{Mg}$ which correlate linearly with the Al/Mg content of distinct mineral phases coexisting in the inclusions. If interpreted as an internal isochron for a fossil of live ^{26}Al , the initial $^{26/27}\text{Al}$ ratio in the inclusions was approximately 6×10^{-5} . ^{26}Mg excesses indicating a comparable formation ratio have also been found in Leoville (Lorin et al., 1978) and possibly in Murchison (McDougall and Phinney, 1978). Excesses of ^{26}Mg of up to 10% are known in Allende.

3. A spate of heavy elements has been found to exhibit anomalies which may be interpreted as due to addition of an r-process component to the solar nebula (but see Clayton, 1978, for an alternate point of view). These are found in Ca, Ba, Nd and Sm (McCulloch and Wasserburg, 1978; Lee et al., 1978). In general, these anomalies have not been found to correlate with ^{26}Mg excesses.

The second class of anomalies mentioned above is perhaps the most striking. If the ^{26}Mg excesses are interpreted as fossils of live ^{26}Al in the early solar system, then there are two basic astrophysical mechanisms for accounting for its presence. In one, the infant sun emits a large flux of energetic charged particles during its T-Tauri phase, possibly in conjunction with significant mass loss, as originally suggested by Fowler et al. (1962) and developed by Heymann and Dzickanec (1976), Heymann et al. (1978), Clayton et al. (1977), Dwek (1978) and Lee (1978). This category of model has difficulty accounting for ^{26}Al production on energetic grounds. As an example, Lee (1978) finds that the ^{16}O and ^{26}Al anomalies can be produced in 3×10^{25} g of normally-constituted matter if 3% of the gravitational binding energy of the sun is expended in an energetic proton irradiation. Surely this is extravagant. Moreover, expected light element anomalies from such an irradiation are not observed (Phinney et al., 1978). The second possibility is that the ^{26}Al , along with ^{16}O and possibly other isotopic anomalies, be injected in a single, late spike from galactic nucleosynthesis, i.e., a supernova. To the nucleosyntheticist, the ^{16}O anomaly virtually screams "supernova," but does

not establish a timescale for the addition of fresh nucleosynthetic products to the solar system. ^{26}Al , however, does so with a vengeance.

D. Supernovae

Beyond a doubt, the best way to introduce the main actor in the following pages is to quote an eyewitness account of the most brilliant supernova observed to date. The Annales Sangallenses Maiores of the Benedictine monastery in St. Gallen for the year 1006 CE records,

"A new star of unusual size appeared, glittering in aspect and dazzling to the eyes, causing alarm. In a wonderful manner this was sometimes contracted, sometimes diffused, and moreover sometimes extinguished. It was seen likewise for three months in the inmost limits of the south, beyond all the constellations which are seen in the sky."

The spectacle provoked heated arguments among Japanese astronomers, some of whom conjectured that it might be due to a structural change in the heavens; the Arab Ali ibn Ridwan recorded that it showed an apparent disk "two and one-half to three times as large as Venus" and caused the night sky to shine; numerous accounts (Clark and Stephenson, 1977) testify that its light rivaled the full moon. The description of changes in the appearance of the star may sound less odd if one has ever looked at Sirius in a medium-sized telescope on a clear, dark night, so that it dazzles the eye. Given the proverbial taciturnity of monastic chronicles regarding astronomical prodigies, one wonders how much lies behind that mild phrase "causing alarm." The various accounts are consistent with an apparent magnitude of -9.5 at maximum, and a gradual decrease in brightness over four months or more. In 1976 Van den Bergh located the optical remnant at a distance of

roughly one kiloparsec.

Supernovae are characterized observationally by an abrupt rise in brightness to an absolute magnitude $\lesssim -16$, followed by a slow decline over a period $\gtrsim 100$ days. There seems to be two basic kinds (unfortunately, there exist two basic theoretical models, and one sometimes gets the impression the distinction between the classes is a theoretical one). Type II supernovae, which are more important for purposes of nucleosynthesis, and with which we shall be concerned, are identified by the presence of strong Balmer lines in emission and with P Cygni profiles, superimposed on a well-defined continuum. In the absence of hydrodynamic models of the light curve which are diagnostic of a particular mechanism for the explosion, there tends to be a certain disassociation between the bomb (theory) and the bang (observation), but over the past ten years a rough consensus has emerged as to how a Type II supernova occurs.

In the cores of very massive stars, the end product of thermonuclear burning is "iron" (actually a small group of nuclei with $A \approx 56$) at temperatures and densities near $T = 10^{10}$, $\rho = 10^{10}$. This matter is very nearly in thermodynamic equilibrium, except with respect to slow β -decays, and obeys the Saha equation (this situation is called "nuclear statistical equilibrium"). When the center of the star reaches this portion of the ρT plane, local energy generation ceases, because the iron group nuclei are the most tightly bound in nature, but neutrino losses do not. The response of the core, dictated by the virial theorem, is to contract to higher T and ρ , whereupon the composition of matter in nuclear statistical equilibrium

switches rather suddenly from ^{56}Fe to 13 α -particles and 4 neutrons. This transition (and the subsequent dissociation of the α 's) being endoergic by over 100 MeV per nucleus, a catastrophic refrigeration of the core removes thermal pressure support against gravitational contraction, leading to a violent implosion. During the collapse, the matter in the core neutronizes, i.e., the electron Fermi energy exceeds the endpoint energy of β -decays, so that β -unstable nuclei become stable, and matter moves to the neutron-rich side of stability as the nuclei themselves evaporate into a sea of neutrons. The collapse halts only at about three times nuclear density (if it halts at all) upon the onset of degeneracy in the nuclear matter that now comprises the core. The matter raining in from further on out in the star rebounds with the core, whose equation of state is now typical of nuclear matter and thus extremely stiff, and a reflected shock propagates out into the mantle and envelope of the star, resulting in the hydrodynamic expulsion of all of the star exterior to a "mass cut" of approximately one to two solar masses. It is this shock, which powers the optical display upon breakout from the surface of the star, that gives rise to the explosive burning of thermonuclear fuel in the deep interior, with important nucleosynthetic consequences. Neutrino transport processes, which exercised so many theoreticians for so long (Wilson, 1971, 1974; Breunn, 1975) evidently play a minor role in the explosion; the important features of the hydrodynamics seem to be adequately described by an adiabatic collapse (Van Riper, 1978; Arnett and Van Riper, 1978) at the low dimensionless entropy/nucleon of about unity, for later comparison (Bethe et al., 1978).

The supernova, together with its sequelae, is the true deus ex machina of modern astrophysics. It plays a central role in theories of nucleosynthesis, of the origin of pulsars, and possibly the origin of black holes. The phenomena thought to accompany shock breakout from the star include sudden x-ray events and primary cosmic ray generation; supernova remnants make up a goodly part of the non-thermal radio sources in the sky. Finally, supernovae have been observationally implicated in star formation.

E. Supernova-Induced Star Formation and the Solar System

In 1977, Herbst and Assousa proposed Canis Majoris R1 as a case of supernova-triggered star formation, the first of a small but growing catalog that by now includes Cepheus OB3 (Assousa et al., 1977) and possibly the Gum nebula. Canis Majoris R1, however, is perhaps the cleanest example. It consists of an expanding shell associated with a runaway star; on an edge of the shell are a number of stars whose estimated age is comparable to that inferred for the shell, interpreted as a supernova remnant.

Supernova-induced star formation also figured in a highly influential paper by Cameron and Truran (1977) that proposed on the basis of the isotropic anomalies then known in Allende that a supernova explosion simultaneously triggered the collapse of a proto-stellar cloud and contaminated it with fresh nucleosynthetic debris. On this view, anomalies in ^{16}O , ^{26}Mg , ^{40}K , ^{129}I , ^{244}Pu and other isotopes all reflect the influence of this single event. This notion rather neatly bridges the long-standing opposition between cataclysmic

theories and theories which start from the presumption that planetary formation regularly accompanies star formation by positing a catastrophic origin for the solar nebula. In this regard, the supernova has the convenient property of being a rare event (in that the probability of an outburst in any given time in the galaxy is small, $\approx 6/\text{yr}$) that is also the inevitable fate of many stars.

F. Outline of Succeeding Chapters

A reliable, quantitative model for the nucleosynthesis accompanying such an event is clearly needed in order to evaluate the hypothesis of Cameron and Truran. As no complete, quantitative theory yet exists for the nucleosynthesis which accompanies a supernova outburst, the abundance pattern to be expected from injection of matter from a single such event is problematical. The basic physical processes involved, however, are considered to be well understood (Arnett, 1973), and advances in the theory of stellar evolution provide a basis for obtaining plausible estimates of the available conditions in an explosion. It is thus possible to construct a crude model of the nucleosynthetic yields from a single massive supernova with fair confidence. The calculations to follow perform this task for a limited suite of potential anomalies, concentrating on the crucial isotopes of Mg and Al. Chapter II reviews the basic theory of element synthesis in thermonuclear burning and the numerical methods used to study it. In Chapter III, a simplified account of the hydrostatic nuclear burning that determines the initial composition of the presupernova, assumed to be very similar to the $25 M_{\odot}$ model of Weaver, Woosley and Zimmerman

(1978), at the moment of core collapse is presented. An equally simplified model of shock passage through the nuclear fuel-laden mantle of the supernova is developed in order to estimate the initial conditions for explosive nucleosynthesis in Chapter IV. Chapter V presents the results of explosive nucleosynthesis calculations performed with the network code described in Chapter II with the peak thermodynamic conditions developed in the preceding chapter. Finally, Chapter VI discusses the application of the model to the supernova trigger hypothesis.

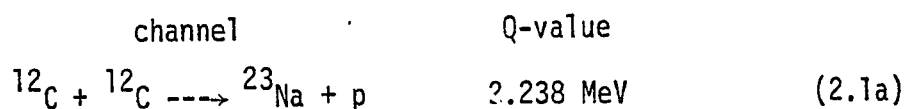
CHAPTER II

THERMONUCLEAR BURNING PROCESSES

A. General

This study will concentrate on the nucleosynthesis accompanying the advanced burning states, i.e., post-core-helium burning, of a massive star. Two basic energy-generating processes will dominate in the production of nuclei in the range $20 \leq A \leq 30$: Carbon burning, which has been extensively studied since the measurement of the $^{12}\text{C} + ^{12}\text{C}$ fusion cross-section at astrophysical energies by Patterson, Winkler and Zaidans (1969), both as a static burning stage (Arnett and Truran, 1969; Arnett, 1973; Endal, 1975; Arnett and Wefel, 1978) and as an explosive one (Arnett, 1969; Howard et al., 1972; Pardo et al., 1974; Cameron and Truran, 1977) and neon burning, which has received much less attention.

Following exhaustion of helium by the triple- α reaction in either core or shell burning, the nuclear fuel combining greatest abundance and lowest Coulomb barrier is ^{12}C , which liberates free nucleons and α -particles by the reactions





In addition, a small amount of a nucleus such as ^{22}Ne or ^{25}Mg will provide free neutrons by an (α, n) reaction under stellar conditions, in which the material has undergone a neutron enrichment because of β -decays in its prior history. The liberated nucleons (including α 's in the term henceforth) then initiate reactions upon the heavy nuclei in the plasma and upon the primary burning products. Stellar material which has undergone helium burning is liable to have a variety of nuclei between neon and silicon, as well as a large ($\geq 50\%$) amount of ^{16}O , so that the nuclear evolution is naturally complex, resulting in significant quantities of ^{20}Ne , ^{23}Na , $^{24,25,26}\text{Mg}$, ^{27}Al , and $^{28,29,30}\text{Si}$, as well as nonnegligible amounts of heavier nuclei.

Exhaustion of ^{12}C leaves ^{16}O from $^{12}\text{C}(\alpha, \gamma)^{16}\text{O}$ and as a survivor from helium burning, ^{20}Ne from $^{12}\text{C} + ^{12}\text{C}$ and $^{16}\text{O}(\alpha, \gamma)^{20}\text{Ne}$, and smaller amounts of many other nuclei, including ^{25}Mg and ^{26}Mg , which together contain most of the readily available excess neutrons. Before the next important fusion reaction, $^{16}\text{O} + ^{16}\text{O}$ ($^{12}\text{C} + ^{16}\text{O}$ never plays more than a supplementary role) can commence, ^{20}Ne , whose α -particle separation at 4.73 MeV is fairly low (compare with $S_\alpha = 7.16 \text{ MeV}$ for ^{16}O) will undergo photodisintegration in the hot ($T_9 \gtrsim 1.5$) thermal bath,



followed by



The α -capture on $^{16}_0\text{O}$ helps establish a rapid equilibrium between production and destruction of free α 's. Free neutrons and protons come from secondary reactions, chiefly



and



B. The Solution of Nuclear Reaction Networks

1. The nuclear evolution accompanying basic energy generating processes such as the above presents sufficiently many difficulties that calculations of stellar nucleosynthesis cannot, in practice, be directly included in numerical models of stellar evolution and hydrodynamics (see Hillebrandt et al., 1976 for a rare exception). The approach that comes closest to an actual coupling of nucleosynthesis to stellar evolution is called "post-processing," in which the dynamical evolution of a star is computed using a drastically simplified description of the nuclear energy generation in order to provide a

thermodynamic history for each mass element in the star, which serves as input to a program that computes the nuclear evolution in detail; Arnett and Wefel (1978) present one example of this method. However, nucleosynthesis theory has developed in large measure independently of, although in parallel with, the elaborate stellar evolutionary calculations of the past decade, so that complex nucleosynthetic processes are generally studied without direct reference to stellar models, by a parameterized method. In this approach, the thermodynamic history of a packet of stellar matter is prescribed, and the quality of agreement between the nuclear abundances produced in a major burning stage and the isotopic pattern observed in the solar system is taken to indicate what thermodynamic conditions actually occur inside stars. Studies of this sort have proven a valuable guide to developments in stellar theory, especially in the theories of stellar explosions (Arnett, 1969; Arnett and Clayton, 1970; see Arnett, 1973, for a review).

The time development of thermodynamic conditions assumed in this approach generally corresponds to one of two extremes. Static burning, appropriate for quiescent stages of nuclear burning in which the timescale for nuclear evolution is longer than that required for hydrostatic adjustment of stellar structure, assumes (naturally enough)

$$\rho \approx \text{const.} \quad (2.5a)$$

$$T \approx \text{const.} \quad (2.5b)$$

For very violent stages of nuclear burning, characterized by nuclear timescales shorter than the local dynamical, i.e., freefall, timescale of the matter,

$$\tau_{HD} \approx (24\pi G\rho)^{-1/2} \quad (2.6a)$$

$$= 446 \rho^{-1/2} (\text{gcm}^{-3}) \quad (2.6b)$$

one invokes the hydrodynamic approximation (Fowler and Hoyle, 1964), in which the temperature and density of the material rise essentially instantaneously to peak values, corresponding to the passage of a shock, and then fall off as the matter rarifies and cools by adiabatically expanding in the explosion on roughly the hydrodynamic timescale, so that

$$\rho \approx \rho_0 \exp(-t/\chi\tau_{HD}) \quad (2.7a)$$

$$\rho T^{\Gamma_3-1} \approx \text{const.} \quad (2.7b)$$

Here χ is a scaling parameter, usually assumed of order unity, and the adiabatic exponent (Clayton, 1968, p. 118)

$$\Gamma_3-1 \equiv \partial \log T / \partial \log \rho \quad (2.8)$$

is close to 3 for matter that is nearly radiation dominated;

$$\rho T^3 \approx \text{const.} \quad (2.9)$$

2. Numerical Scheme

The evolution in time of the abundances of nuclear species undergoing thermonuclear burning is described by a system of nonlinear ordinary differential equations. The abundance of nucleus i is given in terms of the mass fraction X_i (more properly, the fraction of

nucleons bound in the i^{th} species), the fractional abundance Y_i , or the number density N_i , related by

$$\begin{aligned} N_i &= \rho N_a X_i / A_i \\ &= \rho N_a Y_i \end{aligned} \quad (2.10a)$$

where N_a is Avogadro's number and A_i is the atomic weight of nucleus i . Note that

$$\sum_i X_i = 1 \quad (2.11)$$

follows from conservation of nucleons. In terms of the abundances, the time dependence of the nuclear composition obeys

$$\frac{dY_i}{dt} = - \sum_{j,k} Y_i Y_j \lambda_{jk}(i) + \sum_{\ell m} Y_\ell Y_m \lambda_{mi}(\ell) \quad (2.12)$$

where the reaction rates $\lambda_{jk}(i)$ will be discussed below.

Because of the importance of processes such as $^{12}\text{C}(^{12}\text{C},x)$ the system (2.12) is nonlinear for most astrophysically interesting problems, and thus intractable for analytic solution, even for simple networks. In general, a numerical approach is required. A fast, simple scheme, developed by Arnett and Truran (1969) and employed here, proceeds by casting eqn.(2.12) in terms of the unidirectional flows

$$f_{ij}(k) \equiv Y_i Y_j \lambda_{jk}(i) \quad (2.13)$$

so that

$$\frac{dY_i}{dt} = - \sum_j f_{ij} + \sum_{k,\ell} f_{ki}(\ell) \quad (2.14)$$

For $\Delta t = t^{n+1} - t^n$ sufficiently small (denoting quantities at time t^n by a superscript n), one may approximately write

$$f_{ij}^{n+1}(k) = \gamma_i^{n+1} \gamma_j^{n+1} \lambda_{jk}(i) \quad (2.15a)$$

$$= \left[\gamma_i^{n+1} \gamma_j^n + \gamma_j^{n+1} \gamma_i^n - \gamma_i^n \gamma_j^n \right] \lambda_{jk}^{n+1}(i) \quad (2.15b)$$

$$\approx \left[\gamma_i^n \gamma_j^n + \Delta_i \gamma_j^n + \Delta_j \gamma_i^n \right] \lambda_{jk}^{n+1}(i) \quad (2.15c)$$

where $\Delta_i = \gamma_i^{n+1} - \gamma_i^n$, and terms $O(\Delta^2)$ are discarded. Upon replacing the time derivative by

$$\frac{d\gamma_i}{dt} = \frac{\Delta_i}{\Delta t} \quad (2.16)$$

the system takes the (linearized) form

$$\begin{aligned} & \gamma_i^{n+1} \left[\frac{1}{\Delta t} + \gamma_j^n \lambda_{jk}^{n+1}(i) \right] + \gamma_j^{n+1} \left[\gamma_i^n \lambda_{jk}^{n+1}(i) \right] \\ & - \gamma_\ell^{n+1} \left[\gamma_m^n \lambda_{mk}^{n+1}(\ell) \right] - \gamma_m^{n+1} \left[\gamma_\ell^n \lambda_{mk}^{n+1}(\ell) \right] \\ & = \gamma_i^n \gamma_j^n \lambda_{jk}^{n+1}(i) - \gamma_\ell^n \gamma_m^n \lambda_{mk}^{n+1}(\ell) + \gamma_i^n \left[\frac{1}{\Delta t} \right] \end{aligned} \quad (2.17)$$

Equation (2.17) gives the updated abundances γ_i^{n+1} as the solution of a set of coupled linear equations which may be solved by Gaussian elimination for each time t^{n+1} .

C. Thermonuclear Reaction Rates

1. General Remarks

The reaction rate for a two-body process



that appears in the network equation (2.12) is related to its cross-section by

$$\lambda_{jk}(i) = \left(\frac{1}{1+\delta_{ij}} \right) \rho N_a \langle \sigma v \rangle_{jk}^i \quad (2.19)$$

where (Clayton, 1968, p. 291 ff)

$$\langle \sigma v \rangle_{jk}^i \equiv \left(\frac{8}{\pi M_r} \right)^{1/2} (kT)^{-3/2} \int_0^\infty \sigma_{jk}^i(E) E \exp(-E/kT) dE \quad (2.20)$$

is the average of σv over a maxwellian velocity distribution at temperature T , and looks very much like the Laplace transform of σE with respect to $s = 1/kT$. Here M_r is the reduced mass of the reacting pair, and δ_{ij} is the Kronecker delta. Numerically,

$$\langle \sigma v \rangle_{jk}^i = 3.732 \times 10^{10} \hat{A}_{ij}^{-1/2} T_9^{-3/2} \int_0^\infty \sigma_{jk}^i E \exp(-11.605 E/T_9) dE \quad (2.21)$$

with σ in barns, E in MeV, and \hat{A} the reduced atomic weight

$$\hat{A}_{ij} = \frac{A_i A_j}{A_i + A_j}$$

Weak-screening limit estimates of electron screening factors (Clayton, 1968, p.360; DeWitt et al., 1973) imply an enhancement of only 5% for the $^{12}\text{C} + ^{12}\text{C}$ reaction at $T_9 = 2$; Coulomb screening, of course, has negligible effect on the rate for $^{20}\text{Ne}(\gamma, \alpha)^{16}\text{O}$, and its effect on light particle-initiated reactions is quite small under the conditions of interest in this study. Therefore, screening was neglected entirely.

Knowing the rate (2.19) one can find the rate for the inverse process,



by (Fowler et al., 1967)

$$\langle \sigma v \rangle_{kj}^{\ell} = \left(\frac{g_i g_j}{g_k g_{\ell}} \right) \left(\frac{G_i}{G_{\ell}} \right) \left(\frac{A_i A_j}{A_k A_{\ell}} \right)^{3/2} \langle \sigma v \rangle_{jk}^i \exp(-11.605 Q_{jk}/T_9) \quad (2.24)$$

where

$$g_i = 2J_i + 1 \quad (2.25)$$

is the statistical weight of the ground state for species i , Q_{jk} is the energy release of the reaction in MeV (positive if exothermic), and G_i is the partition function for species i divided by the statistical weight of the ground state. Equation (2.24) holds when both j and k are nucleons. If k is a photon, then detailed balance leads to (Fowler et al., 1967)

$$\langle \sigma v \rangle_{\gamma j}^{\ell} = \left(\frac{g_i g_j}{g_{\ell}} \right) \left(\frac{G_i}{G_{\ell}} \right) \left(\frac{A_i A_j}{A_{\ell}} \right)^{3/2} \left(\frac{kT}{2\pi m_a^2} \right)^{3/2} \langle \sigma_{j\gamma}^i v \rangle \exp(-Q_{j\gamma}/kT) \quad (2.26a)$$

$$= 9.8677 \times 10^9 T_9^{3/2} \left(\frac{g_i g_j}{g_{\ell}} \right) \left(\frac{G_i}{G_{\ell}} \right) \left(\frac{A_i A_j}{A_{\ell}} \right)^{3/2} \langle \sigma_{j\gamma}^i v \rangle \exp(-11.605 Q_{j\gamma}/T_9) \quad (2.26b)$$

Inspection of tabulated partition functions in Woosley et al. (1975) reveals that for $T_9 \lesssim 3.0$ they rarely depart from unity even at the percent level (though $G(T_9 = 2.5) = 1.19$ for ^{23}Na is typical of the exceptions), so the ratio G_i/G_{ℓ} has been set to unity in computation of inverse rates.

A complication arises in applications of the inverse formulae (2.24) and (2.26) to experimentally determined rates. These formulae, properly speaking, only hold in the case of thermodynamic equilibrium of the participating species. In particular, the cross-sections in both forward and reverse channels should be those for nuclei in a mixed state with a thermal distribution of excited levels (called "true stellar" cross-sections by Woosley et al.). However, laboratory experiments rarely provide anything but cross-sections for the target in its ground state. Discussions of this ticklish point may be found in Woosley et al. (1975, pp.10-11) and Fowler et al. (1975, pp.90-91).

2. Sources for Reaction Rates

The position of a researcher seeking thermonuclear reaction rates for astrophysical calculations has improved immensely over the past decade. Not only have many new cross-sections been measured (and

many old ones remeasured), but there has also been a massive effort to provide sound theoretical cross-sections for those nuclei lacking experimental data. As a result, one could say that nucleosynthesis theory has attained the status of a quantitatively inexact science.

The majority of the reaction rates which underly these calculations come either from the experimental compendium of Fowler et al. (1975), or from a collection of Hauser-Feshbach calculations by Woosley et al. (1975). These two sources provide virtually all the rates needed for calculations of explosive carbon and oxygen burning. A small number of strong rates come from Howard (private communication) or from the older compilation of Wagoner (1969); these last are known to be less reliable, but none are employed for crucial reactions. Weak interaction rates come from Wagoner and from fitting formulae given in Hansen (1966).

A significant departure from this practice occurs for the branching ratios used for $^{12}\text{C} + ^{12}\text{C}$; we use the branchings given by Endal (1975):

$$\lambda_{\alpha}/\lambda_{\text{tot}} = 0.300 + 0.108 T_9^{3/2} \quad (2.27a)$$

$$\lambda_p/\lambda_{\text{tot}} = 0.752 - 0.159 T_9^{3/2} \quad T_9 \geq 1.12 \quad (2.27b)$$

$$= 0.700 - 0.108 T_9^{3/2} \quad T_9 < 1.12 \quad (2.27c)$$

$$\lambda_n/\lambda_{\text{tot}} = 1 - \lambda_{\alpha}/\lambda_{\text{tot}} - \lambda_p/\lambda_{\text{tot}} \quad (2.27d)$$

in preference to the recommendations for Fowler et al. (1975), which give a poor presentation of the opening of the neutron channel as

reported by Patterson et al. (1969). The fusion rate for $^{12}\text{C} + ^{12}\text{C}$ still comes from Fowler et al. (1975), however.

Fowler et al. (1967) give fitting formulae for their rates which represent the best experimental data to \lesssim 25% accuracy for $10^{-3} \leq T_9 \leq 10$. The reliability of the experiments is difficult to judge, but uncertainties of at least 10% and at most a factor of three bracket the range, with 50% cited as a typical value. These formulae are based on laboratory cross-sections, but include "stellar" corrections where the difference is likely to be important; however, no attempt was made in their implementation to follow Fowler et al.'s (1967) recommendations for the use of partition functions in the inverse ratios for these cases.

The Hauser-Feshbach calculations are more uncertain, largely because of the vexed problem of estimating γ -emission widths; Woosley et al. quote an uncertainty of about a factor of two. In addition, some (n,γ) rates are suspect at low temperatures because a combination of small effective energy and thermal spread for the bombarding neutrons (both $\approx kT$ because of the lack of a Coulomb barrier) and small Q-value for radiative capture leads to a small level density in the compound nucleus at the effective range of excitation, so that the requirements of the method may not be met (cf. Woosley et al., 1975, pp.26-27). Woosley et al. provide both "stellar" rates and "laboratory" rates based on the ground state only; in the case of $^{23}\text{Na}(\alpha,n)^{26}\text{Al}$, in which both target and product nuclei have excited states below half an MeV, the ratio of stellar to laboratory rates varies between 1.96 and 1.59

as T_9 goes from 1.0 to 2.5, so the difference could conceivably be of importance.

"Stellar" reaction rates presented in tabular form by Woosley et al. were interpolated using a fitting formula based on a modification of a form suggested by Michaud and Fowler (1970), who observed that charged particle thermonuclear reaction rates based on Hauser-Feshbach cross-sections at high temperature could often be approximated by the simple formula

$$\log\langle\sigma v\rangle_{T_9} = B_1 + B_2(1/4 - 1/T_9). \quad (2.28)$$

Experimentation revealed that making $B_2 = B_2(T_9)$ a linear function of temperature generally allowed an accurate ($\lesssim 1\%$ mismatch) fit to the tabulated rates over a range of $\Delta T_9 = 2\text{--}3$ about the fitting point, even though the rate might vary by tens of decades in that range. The interesting regime of temperature for this study, $1.0 \leq T_9 \leq 2.5$, falls well inside this interval. Therefore, eqn.(2.28) was cast in the form

$$\log\langle\sigma v\rangle_{T_9} = \log\langle\sigma v\rangle_{T_0} + (mT_9+b)(1/T_0-1/T_9) \quad (2.29)$$

where the constants m and b are determined by a linear least squares match to the tabulated rate; the correlation coefficient automatically provides a convenient figure of merit. $T_0 = 2\text{--}3$ for most fits. This method applied successfully to a few neutron capture rates, as well; however, most (n,γ) rates taken from Woosley et al. were fitted to a quadratic in $T_9^{1/2}$ (Clayton, 1968, p.552). A constant value estimated from Allen et al. (1971) was employed for $^{56}\text{Fe}(n,\gamma)^{57}\text{Fe}$.

D. Description of the Network Code

1. General

A computer code, named BRUNO, was written for the numerical solution of parameterized nucleosynthetic network problems as described in Sections A-C above, and performed all nucleosynthetic calculations used in this study. The course of a typical calculation runs as follows. BRUNO first accepts input from three files, which may reside on disk or come through the card reader. These include a "restart deck," containing the initial abundances and parameters for the current job -- starting values for the temperature and density, printing and punching frequencies for new restart files, and other information; a deck specifying the parameters for the calculation, such as the peak thermodynamic conditions, hydrodynamic scaling parameter, stepsize selection prescriptions, and a table heading for the printed output; and a deck which defines the nuclear reaction network. This last contains a card image for every reaction in the network, which bears a character identifier such as MG24(A,G)SI28 for $^{24}\text{Mg}(\alpha,\gamma)^{28}\text{Si}$, for example, and numerical indices which label the species linked by the reaction. BRUNO dynamically allocates workspace, and storage for the restart data and the network deck, which is used to initialize part of a reaction rate structure. The calculation proper commences when the main program selects an initial timestep and calls the reaction routine RATEACE, which calculates $N_a\langle\sigma v\rangle$ at the updated time t^{n+1} and stores the values in the appropriate location of the rate structure. The routine STEPPER then constructs the linearized difference equations(2.17) and passes

them to the Gaussian elimination routine MLSQ from the IBM 7L/1 Scientific Subroutine Package, which solves for the abundances at t^{n+1} . If the maximum fractional change falls within a predetermined limit, the new abundances are stored, a new increment is selected, and the process repeats. The calculation may terminate either at the end of a specified number of steps, or when the temperature falls below a specified value. Intermediate results periodically go into the restart file, or appear as printed output, along with the forward and net flows

$$f_{ij}^{n+1}(k) \approx Y_i^{n+1} Y_j^{n+1} \lambda_{jk}^{n+1}(i) - \Delta_i \Delta_j \lambda_{jk}^{n+1}(i) \quad (2.30a)$$

$$f_{ij}^{n+1(\text{net})}(k) = f_{ij}^{n+1}(k) - f_{kl}^{n+1}(i) \quad (2.30b)$$

which are the partial rates of change of a species caused by an individual reaction. The sum of mass fractions also appears as a measure of roundoff error, which is generally quite small. For 185 steps with a 17-species network, the accumulated error in nucleon conservation lay in the fourteenth decimal place.

2. Additional Features

For many purposes, information concerning nuclear energy generation or thermal neutrino energy losses is valuable. BRUNO includes a routine that computes the energy loss rate per unit mass due to neutrinos according to the rates of Beaudet, Petrosian and Salpeter (1967), and a routine that computes the local nuclear energy generation

accompanying nucleosynthesis. If these are desired, a flag in the restart deck enables the energetics routines and causes the local energy production and neutrino losses to appear on the printed output.

The rate per unit mass at which nuclear reactions liberate energy inside a parcel of stellar material maintained at a given temperature and density by the change in nuclear binding energy resulting from the rearrangement of nucleons is

$$\epsilon_{\text{nuc}} = - N_a \sum_i B_i \frac{dY_i}{dt} \text{ erg g}^{-1} \text{ s}^{-1} \quad (2.31)$$

where B_i is the nuclear binding energy of species i . The accompanying change in internal kinetic energy of the gas is

$$\epsilon_{\text{thermal}} = \frac{-3}{2} N_a kT \sum_i \frac{dY_i}{dt} \text{ erg g}^{-1} \text{ s}^{-1} \quad (2.32)$$

These may be approximated by finite differences and combined to yield

$$\epsilon_{\text{tot}} \approx - N_a \sum_i \left(B_i + \frac{3}{2} kT \right) \Delta_i / \Delta_t \text{ erg g}^{-1} \text{ s}^{-1} \quad (2.33)$$

for the total rate of energy liberation or consumption.

E. A Network for Carbon and Neon Burning

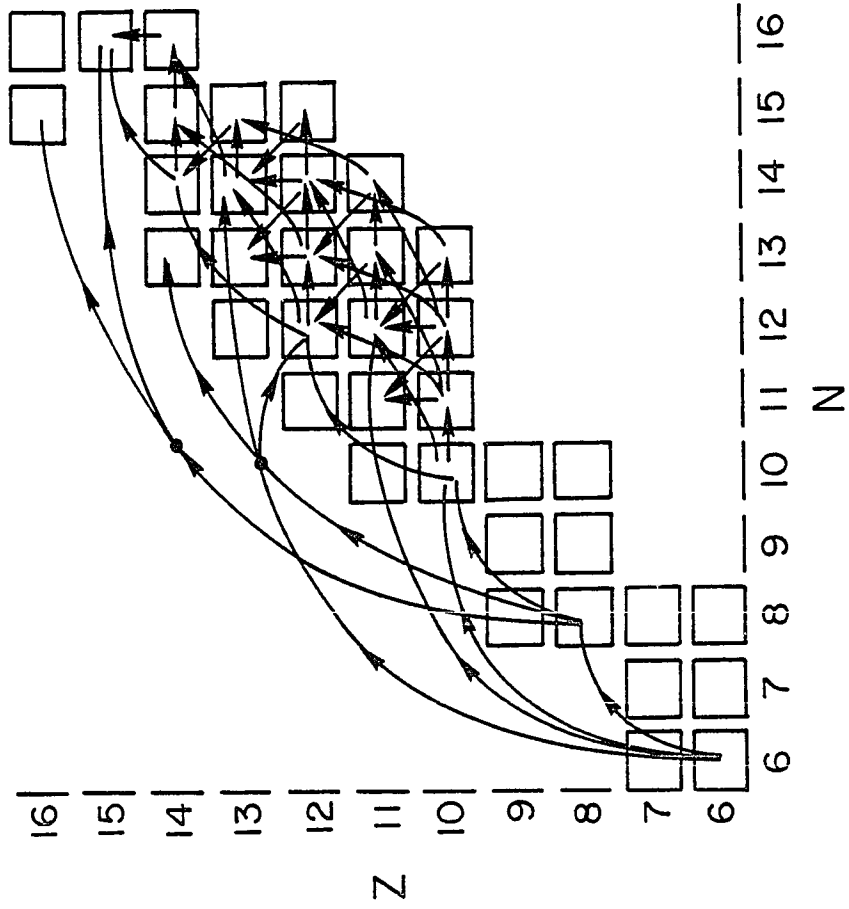
The basic nuclear reaction network used for the numerical calculations in this study appears in Table (1) and in more graphic form in Figure (1). The starting point for its development is the "short code" of Pardo et al. (1974), which approximates carbon burning with only 17 species plus heavy seed, and 37 reaction links. Experimentation and

TABLE 1
Nuclear Reaction Network

$^{12}\text{C}(\alpha, \gamma)^{16}\text{O}$	$^{25}\text{Mg}(\alpha, n)^{28}\text{Si}$	$^{27}\text{Mg}(p, n)^{27}\text{Al}$
$^{16}\text{O}(\alpha, \gamma)^{20}\text{Ne}$	$^{25}\text{Mg}(p, \gamma)^{26}\text{Al}$	$^{22}\text{Ne}(n, \gamma)^{23}\text{Ne}$
$^{20}\text{Ne}(\alpha, \gamma)^{24}\text{Mg}$	$^{28}\text{Si}(\alpha, p)^{31}\text{P}$	$^{24}\text{Na}(n, \gamma)^{25}\text{Na}$
$^{24}\text{Mg}(\alpha, \gamma)^{128}\text{S}$	$^{30}\text{Si}(p, \gamma)^{31}\text{P}$	$^{22}\text{Ne}(\alpha, p)^{25}\text{Na}$
$^{20}\text{Ne}(\alpha, p)^{23}\text{Na}$	$^{20}\text{Ne}(n, \gamma)^{21}\text{Ne}$	$^{56}\text{Fe}(n, \gamma)^{57}\text{Fe}$
$^{22}\text{Ne}(p, \gamma)^{23}\text{Na}$	$^{21}\text{Ne}(p, \gamma)^{22}\text{Na}$	$^{26}\text{Al}(\beta + \nu)^{26}\text{Mg}$
$^{24}\text{Mg}(n, \gamma)^{25}\text{Mg}$	$^{21}\text{Ne}(\alpha, n)^{24}\text{Mg}$	$^{27}\text{Mg}(\beta - \nu)^{27}\text{Al}$
$^{22}\text{Ne}(\alpha, n)^{25}\text{Mg}$	$^{21}\text{Ne}(n, \gamma)^{22}\text{Ne}$	$^{22}\text{Na}(\beta + \nu)^{22}\text{Ne}$
$^{25}\text{Mg}(n, \gamma)^{26}\text{Mg}$	$^{21}\text{Ne}(\alpha, p)^{24}\text{Na}$	$^{24}\text{Na}(\beta - \nu)^{24}\text{Mg}$
$^{26}\text{Mg}(p, n)^{26}\text{Al}$	$^{22}\text{Ne}(p, n)^{22}\text{Na}$	$^{28}\text{Al}(\beta - \nu)^{28}\text{Si}$
$^{23}\text{Na}(\alpha, p)^{26}\text{Mg}$	$^{24}\text{Na}(p, n)^{24}\text{Mg}$	$^{12}\text{C}(^{12}\text{C}, \alpha)^{20}\text{Ne}$
$^{23}\text{Na}(\alpha, n)^{26}\text{Al}$	$^{24}\text{Na}(\alpha, n)^{27}\text{Al}$	$^{12}\text{C}(^{12}\text{C}, p)^{23}\text{Na}$
$^{26}\text{Mg}(p, \gamma)^{27}\text{Al}$	$^{23}\text{Na}(n, \gamma)^{24}\text{Na}$	$^{12}\text{C}(^{12}\text{C}, n)^{23}\text{Mg}$
$^{27}\text{Al}(p, \gamma)^{28}\text{Si}$	$^{28}\text{Al}(p, n)^{28}\text{Si}$	$^{16}\text{O}(^{12}\text{C}, n)^{27}\text{Si}$
$^{28}\text{Si}(n, \gamma)^{29}\text{Si}$	$^{27}\text{Al}(n, \gamma)^{28}\text{Al}$	$^{16}\text{O}(^{12}\text{C}, p)^{27}\text{Al}$
$^{26}\text{Mg}(\alpha, n)^{29}\text{Si}$	$^{26}\text{Mg}(n, \gamma)^{27}\text{Mg}$	$^{16}\text{O}(^{12}\text{C}, \alpha)^{24}\text{Mg}$
$^{29}\text{Si}(n, \gamma)^{30}\text{Si}$	$^{23}\text{Na}(\alpha, \gamma)^{27}\text{Al}$	$^{16}\text{O}(^{16}\text{O}, n)^{31}\text{S}$
$^{27}\text{Al}(\alpha, p)^{30}\text{Si}$	$^{26}\text{Mg}(\alpha, \gamma)^{30}\text{Si}$	$^{16}\text{O}(^{16}\text{O}, p)^{31}\text{P}$
$^{24}\text{Mg}(\alpha, p)^{27}\text{Al}$		

FIGURE 1

The nuclear reaction network.



comparison with a standard explosion run with a complete network kindly supplied by M. Howard indicated that greater detail in the treatment of minor burning products was needed in order to guarantee a faithful simulation of the larger network for the major burning products between neon and silicon: ^{20}Ne , ^{23}Na , $^{24,25,26}\text{Mg}$, ^{27}Al and $^{28,29,30}\text{Si}$. Also, a reliable estimate of ^{26}Al production is of great concern for this problem. These desiderata governed the choice of additional links and minor species. An attempt was made to include all species whose reaction flows directly contributed to the production of major products at the percent level or higher, with enough additional detail to allow a fair approximation of the production of minor nuclei with major products as immediate daughters. The resultant network, with 27 species plus heavy seed, and 55 reactions, is very sparse for $A < 20$, including only the principal heavy-ion reactions on ^{12}C and ^{16}O and (α, γ) links, and essentially terminates at the silicon isotopes. Sulfur and phosphorus appear only as terminal sinks. No especial effort went towards faithful treatment of minor products of reactions on the major isotopes, so that ^{25}Na , for example, has no destructive reactions in the network, and is thus unphysically over-represented in the final abundance. In general, neglecting these refinements causes little distortion of the pattern of burning products, for the chief effect of such minor constituents is upon the free nucleon abundances, and the vast majority of nuclei in the network play a numerically minor role as individuals in maintaining the free nucleons.

By contrast, the (n,γ) reaction on ^{56}Fe very approximately simulates the collective effect of heavy nuclei not included in the network on the free neutron abundance. This reaction appears in the network with ^{57}Fe represented in the rate indices as ^{56}Fe , causing the destructive terms in the difference equation for ^{56}Fe to cancel. This dodge causes a slight defect in nucleon conservation, which is used as an estimate of the integrated loss to heavy seed. Typically, inclusion of heavy seed at the level 10^{-3} by mass depresses the free neutron abundance by a factor of two to four relative to the case with no seed (Pardo et al., 1974), but has little effect on the final abundance of major nuclei.

A slightly modified version of the network served for static burning in which β -unstable species with short half-lives were deleted from the network.

CHAPTER III

PRESUPERNOVA NUCLEAR EVOLUTION

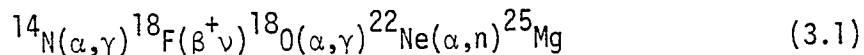
A. Gross Features

For many purposes, one can think of the course of the advanced stages of stellar evolution primarily in terms of the successive stages of nuclear burning in the hydrogen-exhausted core whose formation marks the end of the main-sequence life of a star (that is, provided one does not need to know anything of the star's external appearance!). The sequence of core helium burning, then core carbon burning and shell helium burning, then core neon burning, shell carbon and helium burning, then core oxygen burning, etc. leads to a stratified composition, immortalized in the "onion skin" model; peeling the onion, so to speak, reveals products of progressively more advanced burning stages. Moreover, the composition profile for the most part takes on a piecewise constant appearance, caused by convective instability above nuclear shell sources. The actual evolution belies an oversimple view, however. For example, Arnett (1974a) has found that transient mixing following core flashes during oxygen burning can incorporate ^{20}Ne into the (neon-exhausted) oxygen burning regions for α -core masses of 4 and 8 M_{\odot} . Nevertheless, it is possible to think of the presupernova star as possessing several "zones" in which the composition is dominated by the

products of a shell burning stage occurring at the base of a convectively mixed region, with rare exceptions (Arnett, 1977).

A parcel of matter in the carbon- or neon-burning zones of a massive star will bear traces not only of carbon or neon burning, but also of its entire previous history of nuclear burning. The important parts of this legacy fall into two categories. Firstly, succeeding stages of nuclear burning will tend to modify, rather than obliterate, the major products of earlier stages; ^{16}O , which is doubly magic and thus a difficult nucleus to erode, originates by $^{12}\text{C}(\alpha, \gamma)^{16}\text{O}$ during core helium burning, and survives both carbon and neon burning with little modification. Secondly, a slow neutron-enrichment by weak interactions occurs systematically throughout nuclear burning. This latter process has important nucleosynthetic consequences, for it provides the excess neutrons without which synthesis of neutron-rich nuclei cannot subsequently occur, in particular that of the heaviest nuclei formed by the r-process.

Neutron enrichment during core helium burning has been investigated in detail by Couch, Schmiedekamp and Arnett (1974) and by Lamb et al. (1977), who find that it proceeds in conjunction with a mild s-process. The most effective source of excess neutrons in massive stars is the sequence



The last step in the chain is endothermic by -0.480 MeV and thus exhausts ^{22}Ne during static helium burning only if the star is fairly

massive ($\gtrsim 30 M_{\odot}$), but significant enhancement of light nuclei such as ^{25}Mg and ^{26}Mg as well as medium ($A < 90$) nuclei can accompany the partial burnout of ^{22}Ne in cores of lower mass stars.

The matter that commences carbon burning will therefore start out with nonnegligible mass fractions of the heavier isotopes of Mg and other "carbon burning" products. Carbon burning itself erodes the heavy Mg isotopes, while making large amounts of ^{20}Ne , ^{23}Na and ^{24}Mg , along with smaller amounts of ^{27}Al and the isotopes of silicon as it destroys ^{12}C and ^{22}Ne . ^{16}O suffers a slight diminution. The final pre-explosion suite of abundances will consequently resemble the products of "standard" explosive carbon burning rather than the starting abundances usually taken to characterize the standard case (Arnett, 1969; Pardo *et al.*, 1974). These trends will be accentuated in the matter which undergoes carbon exhaustion and early neon burning beneath the carbon-burning shell source that marks the boundary between "neon" and "carbon" zones in the presupernova star.

The manifold and subtle nuclear burning history sketched above that precedes the final, violent events of shock passage and disruption of the star has been simulated for the purposes of these calculations by static burning in a single zone. It is not immediately clear that this is a good approximation. In a convectively unstable shell source inside a real star, material will experience a distribution of burning conditions. The very strong ($\propto T^{40}$) temperature sensitivity of $^{12}\text{C} + ^{12}\text{C}$ means that burning products will be produced near the base of the convecting layer and continuously diluted with unburned matter, so that the enrichment of burning products will occur much more slowly than in

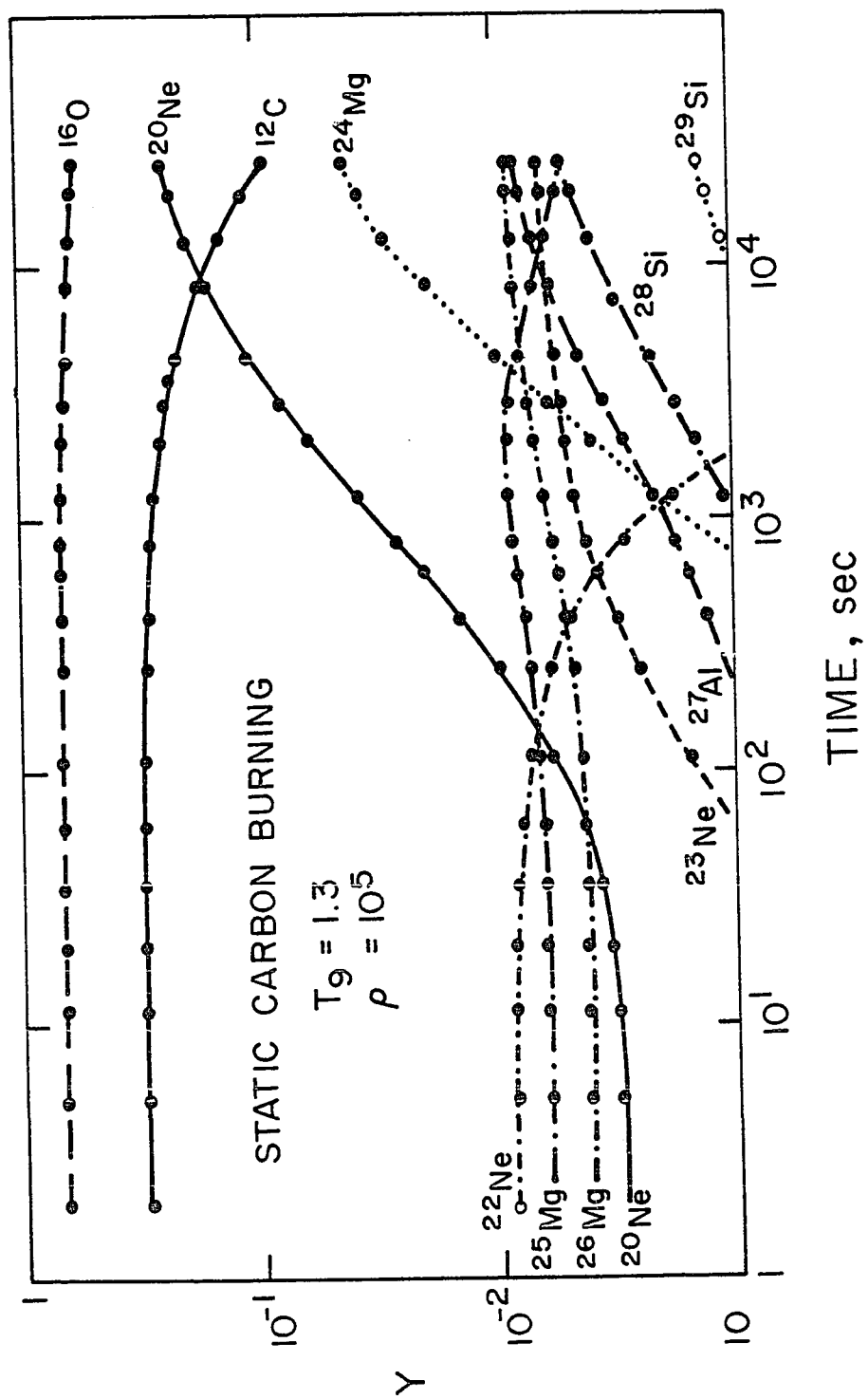
a single-zone calculation. This point is of particular importance with regard to ^{26}Al production, and will be discussed further in the next section. However, comparison of single-zone burning at suitably chosen effective burning temperature and density with multizone models of burning in the presence of convection (Arnett, 1973; Endal, 1975) suggests that the end result of the nuclear evolution is very similar for the major products (cf. especially Figure 2 in Endal, 1975).

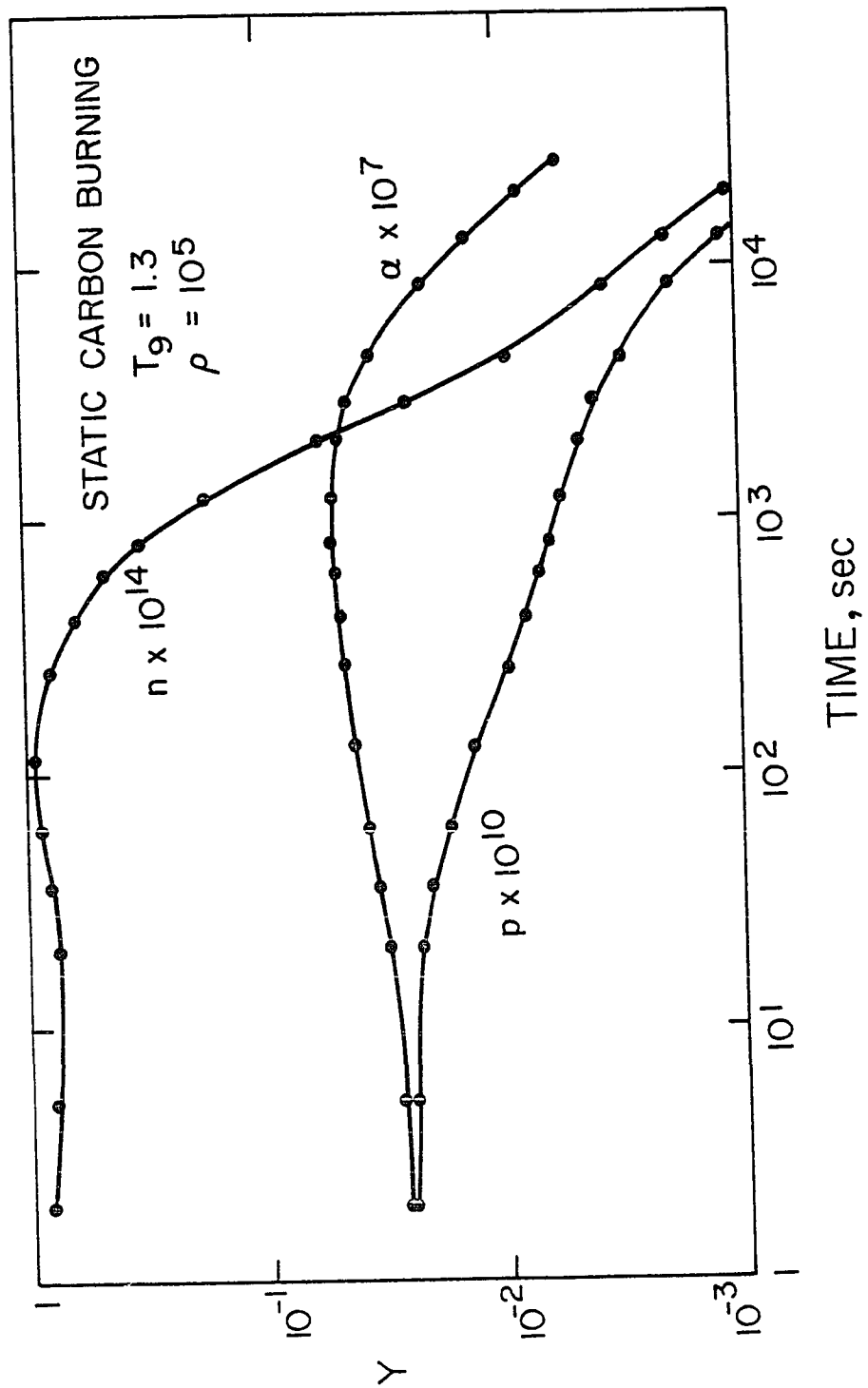
The initial abundances used for static carbon burning are products of a helium-burning-cum-s-process computation kindly supplied by W. D. Arnett (reproduced in Table 9), with initial $X(^{12}\text{C}) = 0.304$, $X(^{16}\text{O}) = 0.671$, and $X(^{22}\text{Ne}) = 8.62 \times 10^{-3}$. $^{25/26}\text{Mg}$ already occur at the level 6.2×10^{-3} and 4.2×10^{-3} , respectively. The post-helium burning composition underwent carbon burning at $T_9 = 1.3$ and $\rho_5 = 1.0$; this choice of effective temperature and density reproduced fairly well both high-temperature static carbon burning as described by Arnett and Truran (1969) and the results of a more elaborate "post-processing" treatment utilizing time-dependent burning conditions from a stellar model sequence (Arnett, private communication). When carbon is exhausted to $X(^{12}\text{C}) \approx 4\%$, the mass fractions of the important α -particle nuclei ^{16}O , ^{20}Ne , ^{24}Mg and ^{28}Si agree to within a few percent with the composition of the carbon zone of the $25 M_\odot$ presupernova model of Weaver et al. (1978, Figure 2a), indicating that the nucleosynthetic history of the matter in this zone may be adequately represented by the results of such a single-zone calculation, at least in the first

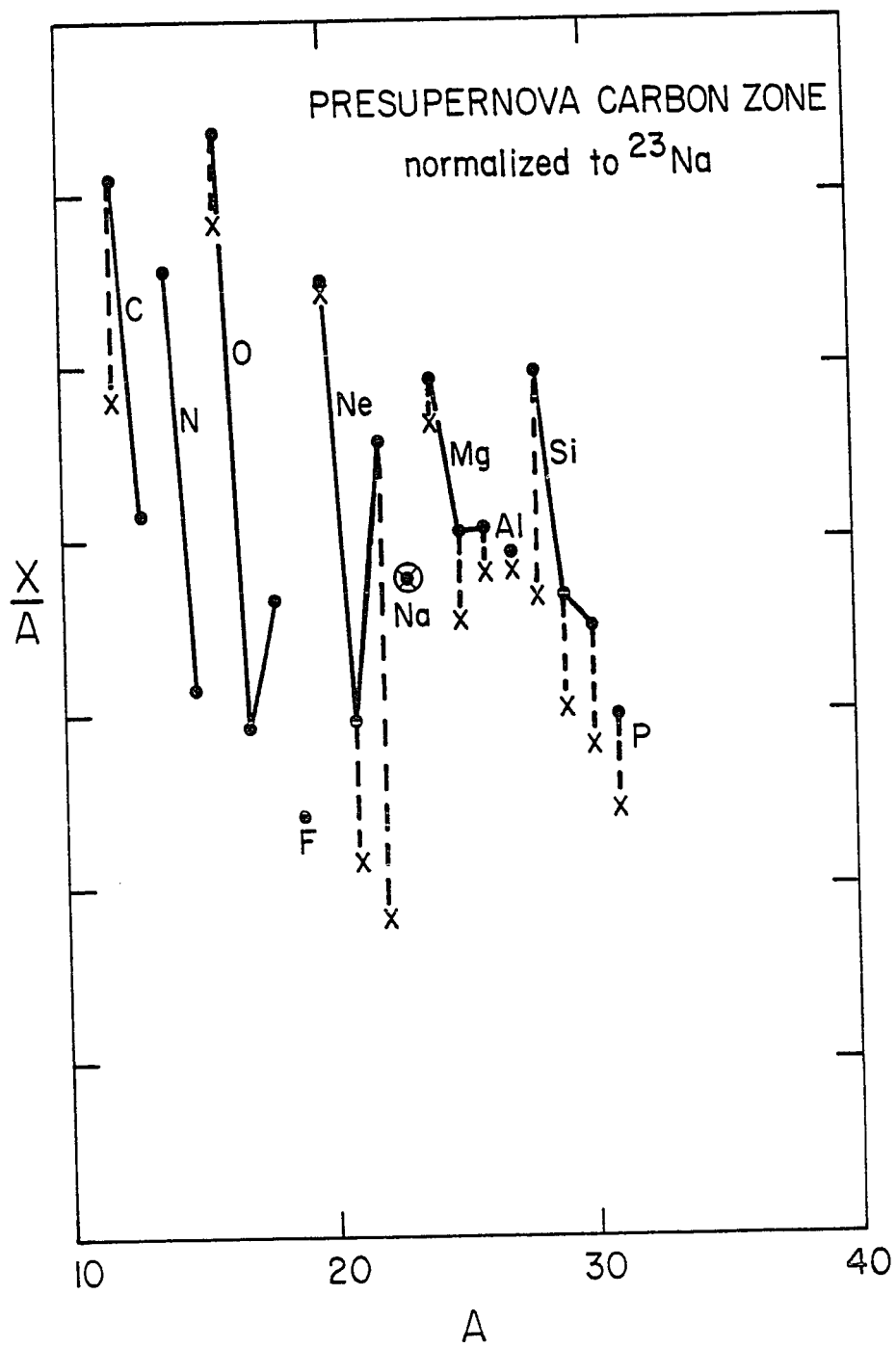
FIGURE 2 The time evolution of important nuclear species during static carbon burning at $\rho_5 = 1.0$, $T_9 = 1.3$. Initially, $X(^{12}\text{C}) = 0.304$ and $X(^{22}\text{Ne}) = 8.62 \times 10^{-3}$.

FIGURE 3 Free nucleon history for the same calculations as Figure 1.

FIGURE 4 Presupernova abundances for the carbon zone, obtained by exhausting carbon to $\approx 4\%$ by mass, normalized to $X/A(^{23}\text{Na}) = \text{solar}$.







approximation. Figures (2), (3) and (4) display the important features of the nuclear evolution.

The initial abundances for the neon-zone were taken from a calculation in which carbon exhausted at $T_9 = 1.5$, $\rho_5 = 2.0$. The slightly more extreme burning conditions are taken as representative of the higher mean temperature and density which the last of the carbon experiences in the shell source as it is quantitatively burnt out; these figures also approximate the makeup of Weaver *et al.*'s neon-zone.

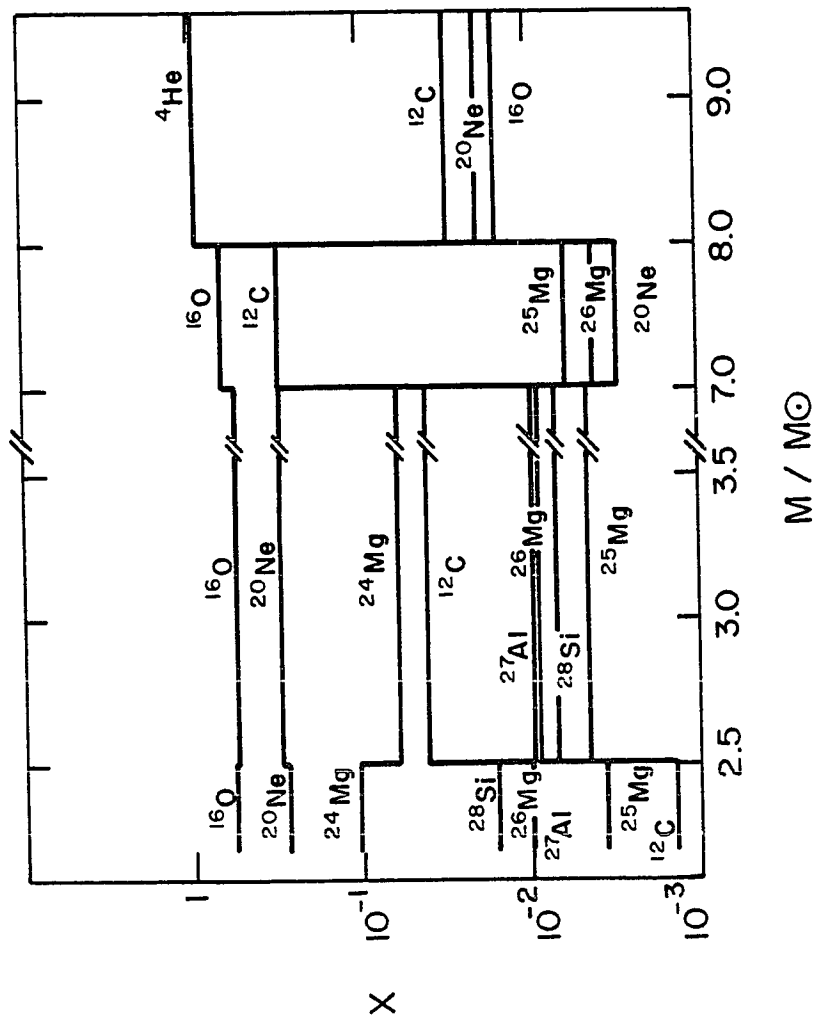
The post-static burning abundances so obtained were used to model the composition structure of the carbon and neon zones of Weaver *et al.*'s $25 M_\odot$ presupernova star as shown in Figure (5). For the sake of simplicity, the composition gradients in Mg and Si present in the radiative neon zone of the actual model are represented by estimated average values, so that the composition profile appears as a series of step functions. The neon zone lies between 2.3 and $2.6 M_\odot$, the carbon zone between 2.6 and $7.0 M_\odot$, and the region between the edge of the convective carbon zone and the base of the helium shell source goes from 7.0 to $8.0 M_\odot$ in this idealized picture.

B. ^{26}Al

Calculations of the production of ^{26}Al , whose possible role in the origin of meteoritic ^{26}Mg excesses has caused so much furor since 1974, present a number of difficulties. An evaluation of the $^{26,27}\text{Al}$ ratio present in a massive star at the time of its explosion must involve considerations of time-dependent convection as well as of some

FIGURE 5

Presupernova composition structure for the neon,
carbon, and post-helium-burning zones.



unusual nuclear physics questions; the discussion to follow attempts to convey an appreciation of the peculiarities of the problem, and to justify the approximations that will enter into (and influence) the final answer to the question: How much ^{26}Al comes from the explosion of a massive star?

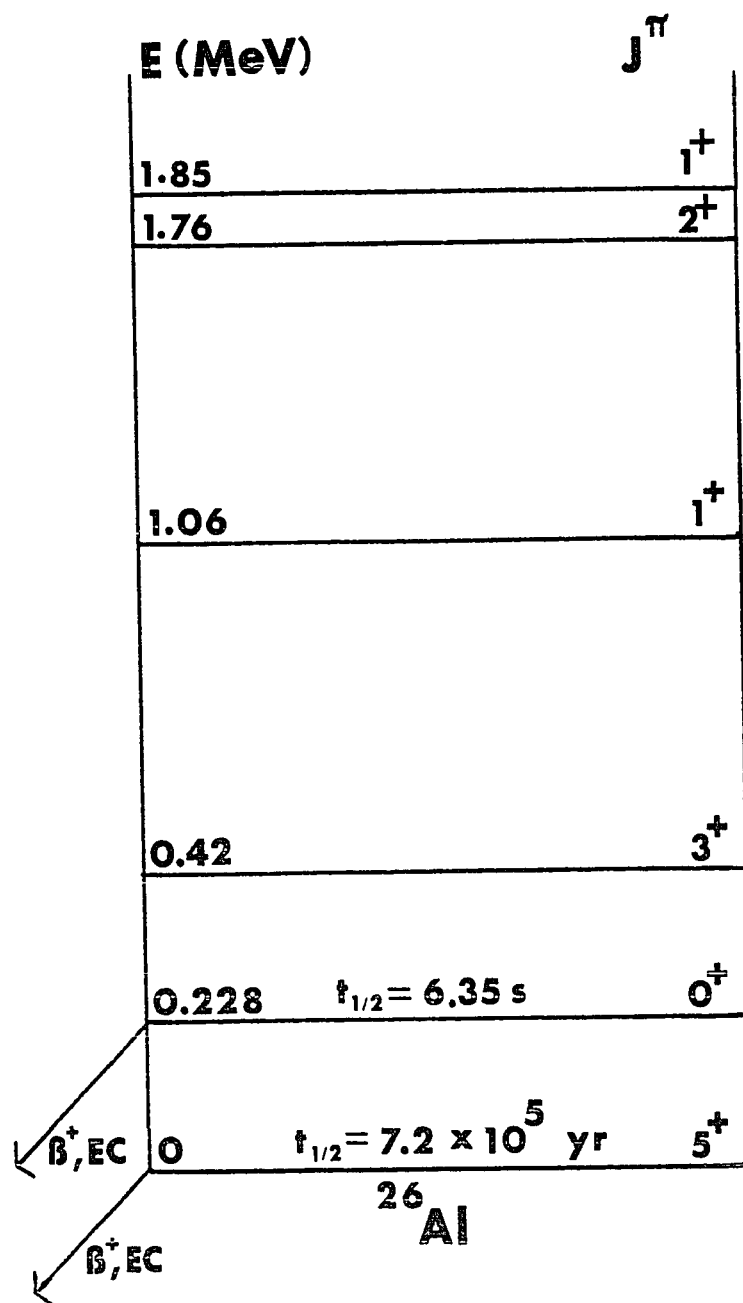
1. Equilibration

^{26}Al , whose nuclear level scheme appears in Figure (6), has a ground state with $J^\pi = 5^+$, and an 0^+ isomer at the unusually low energy (for such a light nucleus) of 0.228 MeV. Both ground state and isomer β -decay to states in ^{26}Mg by a competition between positron emission and electron capture. Under terrestrial conditions, the ground state half-life is 7.2×10^5 yr, and that of the isomer, 6.35 sec. At the high temperatures and densities of a stellar interior, the lifetime of an ^{26}Al nucleus will be modified by complete ionization of the nucleus, which eliminates bound-state candidates for electron capture; enhanced availability of continuum electrons at the nuclear surface; and thermal excitation of the short-lived isomer. Of these effects, the last causes the greatest variability of the lifetime for the conditions liable to obtain during the synthesis of ^{26}Al in a massive star. The fitting formulae from Hansen become inaccurate for $T_9 < 1$, so that for $m \geq 3.5 M_\odot$ the lifetimes become seriously underestimated, but for the purposes of discussion, an adequate approximation is to write

$$\lambda_\beta(^{26}\text{Al}) \approx (2.2 \times 10^{13} \text{ s})^{-1} + \frac{1}{11} \exp \left(\frac{-0.228 \text{ MeV}}{kT} \right) \left(\frac{1}{6.35 \text{ s}} \right) \quad (3.2)$$

FIGURE 6

Nuclear level scheme for ^{26}Al .



This form ignores stellar enhancement of electron capture, which turns out to have a small effect on the overall rate.

The weak decay rates summarized above only hold if the ^{26}Al system is in thermal equilibrium. A great oddity of this nucleus is that it is not immediately obvious this is the case under stellar conditions. The ground and first excited states differ by 5 units of angular momentum, and have the same parity; no transition connecting the two has ever been seen in the laboratory. All excited states below 4.20 MeV have even parity, so that the fastest transitions going through likely higher-energy intermediates will be at best magnetic dipole (i.e., first forbidden).

In order to resolve this question, one must examine the approach of the ^{26}Al system to equilibrium in a thermal bath by solving the master equation,

$$\frac{dP_i}{dt} = - \sum_j W_{ji} P_i + \sum_k W_{ik} P_k \quad (3.3)$$

where the P_i are the occupation numbers for the various states, and the upward and downward transition probabilities are related by the Boltzman factor,

$$W_{ji} = \left(\frac{2J_i+1}{2J_j+1} \right) \exp \left(\frac{E_i - E_j}{kT} \right) W_{ij} \quad (3.4)$$

(Reif, 1965, pp.551-553). Once the relaxation of the system has been followed numerically by solving eqn.(3.3), it is possible to deduce a characteristic timescale for equilibration. This problem has been

examined by Ward (private communication) and Nørgaard (1978), and by this author, although it did not prove possible to include any results in this thesis. The studies of Ward and Nørgaard, however, indicate that an ^{26}Al nucleus exposed to a thermal bath at $T_9 = 2$ (explosive carbon burning conditions) will thermalize in $\lesssim 10^{-6}$ sec due to photon-induced transitions alone. Coulomb excitation should enhance the rate of relaxation. For comparison, an estimate of the lifetime of an ^{26}Al nucleus under these conditions is $\approx 10^{-5}$ sec, determined by the rate for $^{26}\text{Al}(n,p)^{26}\text{Mg}$. One concludes that ^{26}Al may be regarded as thermally equilibrated under these conditions. The equilibration time becomes of order 10^{-3} sec for $T_9 = 1$, appropriate for static burning; the lifetime against (n,p) then becomes of order 10^3 sec; here the β -lifetime is comparable to or shorter than that for strong interactions. These estimates make it plausible to assume ^{26}Al is always thermally equilibrated during the nucleosynthetic processes of concern for this study; the question of its survival following the "freezeout" of equilibrating transitions that will occur during postshock expansion and cooling has yet to be addressed.

2. Distribution of ^{26}Al in the Carbon Zone of a Massive Presupernova

If we therefore accept the weak lifetimes given by eqn.(3.2) or Hansen (1966), as appropriate, and the stellar reaction rates discussed earlier as applicable, the important contributor to ^{26}Al production during static carbon burning is $^{25}\text{Mg}(p,\gamma)^{26}\text{Al}$, while $^{26}\text{Al}(n,p)^{26}\text{Mg}$ and $^{26}\text{Al}(\beta^+ \nu)^{26}\text{Mg}$ account for its destruction.

$^{23}\text{Na}(\alpha, n)^{26}\text{Al}$ was omitted from the static network, as ^{23}Na is a product of the static burning and thus present in low concentration throughout most of the burning. It is, however, an important source of ^{26}Al during explosive carbon burning. As ^{12}C becomes exhausted in the convective shell which occupies some $4.5 M_{\odot}$ of the $25 M_{\odot}$ presupernova model of Weaver et al., the free neutrons fall off to the point that the destruction of ^{26}Al becomes dominated by its weak decays.

Now consider the simplified view of static carbon burning in a convective region discussed by Endal (1975). In this model, a single zone calculation performed with "average" burning conditions is replaced by several mass zones with burning conditions taken from a sequence of stellar models. After each timestep, the abundances of all stable species are averaged ("instantaneous mixing") over the convective zone, while the unstable species such as neutrons, protons, α 's, and short-lived radioactivities which do not live long enough for individuals to migrate convectively, retain the abundances dictated by local equilibrium at the burning conditions of each mass zone. As remarked earlier, such calculations give results generally similar to, though not identical with, the final abundances predicted by the simpler single-zone approximation.

How is ^{26}Al to be treated in this picture? Its "stability" may be assessed by comparing its lifetime as given by eqn.(3.2) with the time required to transport it convectively through the carbon zone. Following Despain (1977) and Weaver et al. (1978) we assume that time-dependent convective mixing is described by a diffusion approximation,

$$\frac{\partial Y}{\partial t} = \frac{1}{4\pi r^2 \rho} \frac{\partial}{\partial r} \left(4\pi r^2 \rho D_c \frac{\partial Y}{\partial r} \right) + q(r,t) - \lambda_\beta Y \quad (3.5)$$

where Y is the abundance of ^{26}Al by number, $q(r,t)$ is its local production in s^{-1} from nuclear reactions, and λ_β is the appropriate β -decay rate. The turbulent diffusivity is estimated using the mixing-length theory of convection,

$$D_c = \Lambda v_c / 3 \quad (3.6)$$

where the mixing length Λ is assumed $\approx H_\rho$, the density scale height, and v_c is the convective velocity, given by (Endal, 1975; Clayton, 1968, pp.256-257)

$$v_c = \left[\left(\frac{1}{c_p \rho} \right) \left(\frac{GM}{r^2} \right) \left(\frac{1}{T} \right) \left(\frac{L}{4\pi r^2} \right) \frac{\Lambda}{2} \right]^{1/3} \quad (3.7)$$

where L is the local value of the internal luminosity, c_p is the specific heat at constant pressure of the stellar plasma (including radiation), and the other symbols have their usual meanings. The specific heat is given by (Clayton, 1968, p.120)

$$c_p = \frac{(32/3 - 8\beta - \beta^2)}{\beta^2} c_v \quad (3.8)$$

where the specific heat at constant volume for the particles alone is

$$c_v = \frac{3}{2} \left(\frac{N_a k}{\mu} \right) \quad (3.9)$$

and

$$\beta = P_{\text{gas}} / P_{\text{tot}} \approx 0.5 \quad (3.10)$$

One can estimate a convective timescale

$$\tau_c \approx \Lambda/v_c \quad (3.11)$$

which may be thought of as the time required by mass motions to transport material over the mixing length. Using the following values to estimate this time,

$$\rho = 1.297 \times 10^5 \text{ g cm}^{-3} \quad (3.12a)$$

$$T = 1.346 \times 10^9 \text{ }^\circ\text{K} \quad (3.12b)$$

$$C_p = 5.14 \times 10^9 \text{ erg g}^{-1} \text{ }^\circ\text{K}^{-1} \quad (3.12c)$$

$$r = 1.219 \times 10^9 \text{ cm} \quad (3.12d)$$

$$L \approx 1/2 L_{\text{phot}} = 5.75 \times 10^{38} \text{ erg s}^{-1} \quad (3.12e)$$

$$M = 3.0 M_\odot \quad (3.12f)$$

$$\Lambda = 7.797 \times 10^8 \text{ cm} \quad (3.12g)$$

where the numbers chosen correspond roughly to the interior of Weaver et al.'s $25 M_\odot$ presupernova, eqn.(3.7) yields

$$v_c \approx 1.423 \times 10^4 \text{ cm s}^{-1} \quad (3.13)$$

which in turn gives

$$\tau_c = 5.478 \times 10^4 \text{ s} \quad (3.14)$$

The lifetime of an ^{26}Al nucleus, on the other hand, is, from eqn.(3.2),

$$\tau_\beta = 371.6 \text{ s} \quad (3.15)$$

approximately 1% of τ_c . It therefore appears that ^{26}Al will decay

long before convection has a chance to mix it throughout the carbon zone, and that ^{26}Al should be treated as an unstable species in local equilibrium with its parents and daughters. In fact, convection should smear out the ^{26}Al distribution over distances of order

$$\delta \approx \sqrt{D_c \tau_\beta} \quad (3.16)$$

by analogy with the notion of a "flame front thickness" from the theory of combustion (Landau and Lifshitz, 1958, p.475). For the example considered above,

$$D_c \approx 3.698 \times 10^{12} \text{cm}^2 \text{s}^{-1} \quad (3.17)$$

and

$$\delta \approx 3.707 \times 10^7 \text{cm} , \quad (3.18)$$

much less than a scale height.

It is possible to construct an analytical solution to the diffusion eqn.(3.5) under simplifying assumptions which may have heuristic value in assessing the meaning of some of the dimensional quantities introduced above and the importance of the "tail" of the ^{26}Al distribution in the presupernova star resulting from nuclei which survive decay to be mixed convectively to cooler parts of the carbon zone where their lifetime against decay is much longer than in the deep interior. Consider the solution of eqn.(3.5) for the somewhat artificial case of steady state convection in an interior with constant scale height and diffusivity, and $q = 0$ (no production of ^{26}Al):

$$\frac{1}{\rho r^2} \frac{\partial}{\partial r} \left(\rho r^2 \frac{\partial Y}{\partial r} \right) - \left(\frac{\lambda_\beta}{D_c} \right) Y = 0 \quad (3.19)$$

Expanding the Laplacian yields

$$\frac{\partial^2 Y}{\partial r^2} + \left(\frac{2}{r} + \frac{1}{H_\rho} \right) \frac{\partial Y}{\partial r} - \left(\frac{1}{\delta^2} \right) Y = 0 \quad (3.20)$$

Use of the integrating factor

$$v(r) = \frac{1}{r} \exp(-r/2H_\rho) \quad (3.21)$$

converts eqn.(3.20) into

$$\frac{d^2 u}{dr^2} - \left| \frac{1}{\delta^2} + \left(\frac{1}{2H_\rho} \right)^2 + \left(\frac{1}{H_\rho} \right) \left(\frac{1}{r} \right) \right| u = 0 \quad (3.22a)$$

$$Y(r) = u(r) v(r) \quad (3.22b)$$

which is of the form

$$u'' - \phi(r) u \quad (3.23)$$

and may be treated with the WKB approximation if

$$|\phi'| \ll |\phi|^{3/2} \quad (3.24)$$

(Mathews and Walker, 1970, p.27). Numerical estimates indicate that this condition will hold for values of r , δ , and H_ρ characteristic of the carbon zone of Weaver et al.'s 25 M_\odot presupernova. If

$$a \equiv \frac{1}{\delta^2} + \left(\frac{1}{2H_\rho} \right)^2 \quad (3.25)$$

and

$$b \equiv \frac{1}{H_\rho}$$

then

$$u \approx \frac{(\sqrt{ar} + \sqrt{ar+b})^{b/\sqrt{a}}}{(a+b/r)^{1/4}} C_{\pm} \exp \pm \sqrt{ar^2+br} \quad (3.27)$$

The argument in the exponential is larger in absolute magnitude than than in eqn.(3.21), so that in order to ensure $Y < \infty$ as $r \rightarrow \infty$ (a somewhat artificial choice of boundary condition, but a convenient one for illustrative purposes) we must take the negative sign in eqn.(3.27). If we fix the remaining boundary condition by specifying the value of Y at a fiducial radius, we have

$$Y(r) \approx Y(r_0) F(r)/F(r_0) \quad (3.28a)$$

where

$$F(r) = \frac{(\sqrt{ar} + \sqrt{ar+b})^{b/\sqrt{a}}}{(a+b/r)^{1/4}} \left[\frac{1}{r} \right] \exp - \left[\sqrt{ar^2+br} + \frac{br}{2} \right] \quad (3.28b)$$

Note that, as $H_p \gg \delta$, so that $a \gg b$, and $b/\sqrt{a} \ll 1$, the leading dependence of F is roughly Yukawian,

$$F(r) \approx f(r) \left(\frac{1}{r} \right) \exp (-r/\delta) \quad (3.29)$$

where $f(r)$ is slowly varying. This would be the sole dependence in the case $H_p \rightarrow \infty$ (i.e., $\rho = \text{const.}$) for which eqn.(3.20) would reduce to

$$\nabla^2 Y - (1/\delta^2) Y = 0 \quad (3.30)$$

Thus δ plays the role of a kind of "skin depth" for the convected ^{26}Al .

Insertion of appropriate values for δ , H_ρ , and r indicates that, indeed, little ^{26}Al survives decay to be washed "downstream" by convection. For the deep interior of Weaver et al.'s carbon zone, the values of H_ρ near $3.0 M_\odot$ cited above and $\delta = 6.069 \times 10^7$ cm yield the solid line in Figure (7); the choice for δ (corresponding to $\tau_\beta = 996$ sec at $4.0 M_\odot$) gives an upper limit to the convectively mixed abundance. For comparison, the ^{26}Al abundances predicted by local equilibrium (see below) are marked with circles (the dashed line connecting them has no other significance than as a guide to the eye). Assuming the ^{26}Al at $3.0 M_\odot$ is maintained at the local value, the local abundance at $4.0 M_\odot$ exceeds what convection from deeper in the zone can supply by a factor of 285, even though the two locations in the star are separated by slightly less than a scale height. Further out in the carbon zone, the situation is not so clear, as Figure (8) shows; the same quantities as in Figure (7) are plotted for parameters corresponding to the region between $5.0 M_\odot$ and $6.0 M_\odot$:

$$H_\rho = 1.344 \times 10^9 \text{ cm} \quad (3.31a)$$

$$\delta = \begin{cases} 1.233 \times 10^8 \text{ cm} \\ 1.873 \times 10^8 \text{ cm} \end{cases} \quad (3.31b)$$

$$(3.31c)$$

where values of δ using D_c and τ_β as estimated near $5 M_\odot$ and $6 M_\odot$, respectively, have been used. For the second of these choices, convection is capable of slightly exceeding local production, so that there may be a steady-state ^{26}Al level maintained by convection in the outermost regions of the carbon zone, although this will contribute a

FIGURE 7 Comparison of convectively mixed ^{26}Al concentration for the example worked in the text with local steady-state concentration near $3.0 M_{\odot}$ in the presupernova star.

FIGURE 8 Same as for Figure 7, near $5.0 M_{\odot}$, for two values of δ .

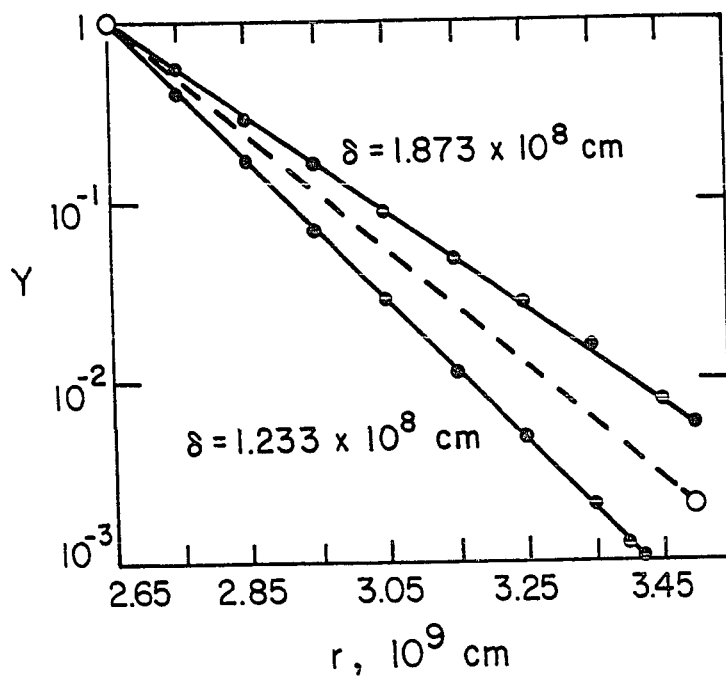
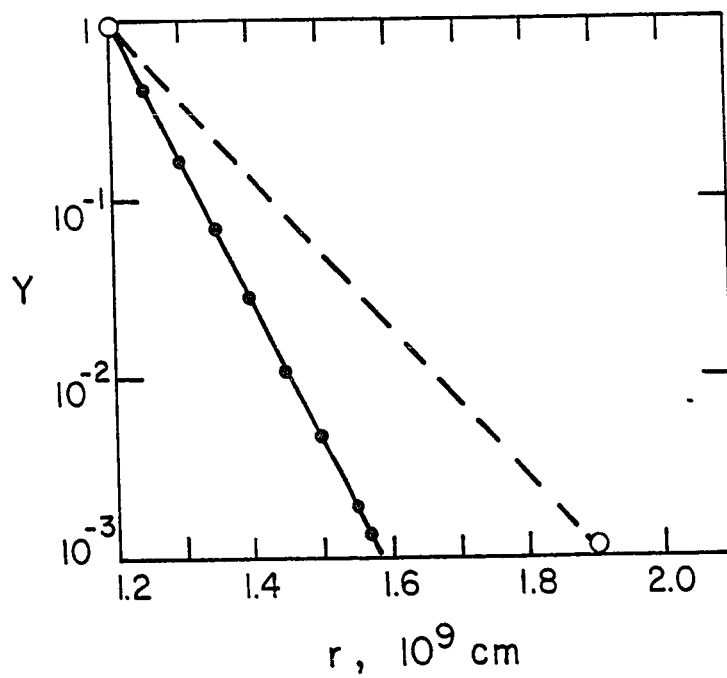


TABLE 2

Equilibrium ^{26}Al Concentrations in the Presupernova Star

M/M_{\odot}	$Y_{\text{eq}}(^{26}\text{Al})$
2.6	2.55×10^{-6}
2.8	2.90×10^{-6}
3.0	2.68×10^{-7}
3.5	5.81×10^{-9}
4.0	3.04×10^{-10}
5.0	4.19×10^{-13}
6.0	8.50×10^{-16}

small amount to the total production.

The considerations outlined above dictated the assumption for this study that all ^{26}Al in the presupernova star was in local equilibrium; the values used for the abundances were obtained by running the static network with the final static abundances for a small number of steps with the thermodynamic variables appropriate for each mass location in the model, in order to force the free nucleon abundances to equilibrate under these conditions. The equilibrium ^{26}Al abundance is then given by

$$Y_{\text{eq}} = \frac{\sum(\text{productive flows})}{\lambda_{\beta}} \quad (3.32)$$

where the flows and the (unequilibrated) abundance $Y(^{26}\text{Al})$ may be read directly from the printed output. The resulting abundances, which complete the requirements of our nucleosynthetic model for the presupernova composition of the carbon and neon zones, appear in Table (2).

CHAPTER IV

STRONG SHOCKS IN THE MANTLE OF A SUPERNOVA

A. General Remarks

1. Statement of the Problem

We want to find a way to relate parameterized nucleosynthetic calculations to the hydrodynamics of mass ejection in a supernova outburst, because the bulk yields of interesting isotopes will depend on the systematics of the peak thermodynamic conditions endured by nuclear fuel-bearing regions during the course of shock passage, e.g., the yield of ^{26}Al from a single star. In contrast, bulk elemental yields, which are primarily determined by the history of static nuclear burning prior to the final outburst, depend much less sensitively on the details of the explosion -- so much so that Arnett (1978) neglects the effects of explosive processing altogether in his discussion of the bulk yields of nucleosynthesis for the elements between carbon and iron.

Unfortunately, the hydrodynamics of mass ejection from believable supernova models is as yet ill-understood; most theoretical attention has focused to date on the problems of getting collapse in the core to result in mass ejection plus a condensed remnant. As a result, most hydrodynamical models which include those regions of the star with

potentially explosive nuclear fuel -- Colgate and White (1966) and Imenshik et al. (1973) are two examples -- do not give useful conditions for nucleosynthesis (when they result in mass ejection), while the more realistic models of Wilson (1971,1974) or Bruenn (1975) do not extend into these regions at all. Only in the recent dynamical r-process calculations of Hillebrandt et al. (1976) is there a published account of a calculation in which the shock following core collapse is followed far enough into the outlying regions of the model to predict conditions for nucleosynthesis.

Inspection of the models of Wilson reveals another problem. Prior to 1976, stellar evolutionary models of advanced burning stages generally lacked the external hydrogen envelope of the star for reasons of economy. Arnett (1972a,b,c;1973;1974a,b;1977) has conducted an exhaustive survey of the evolution of helium stars, also called α -cores, while the work of Hyashi's group in Japan (Ikeuchi et al. 1971) and the older study of Rakavy, Shaiviv and Zinamon (1967) took as their starting point stars composed of carbon and oxygen. Now, while these calculations seem to reproduce quite well the evolution to be expected during the late stages of stellar evolution, which depends almost exclusively on conditions near the star's center once neutrino losses become important, and give plausible composition structures, their density structure must necessarily depart from that in a real star. As an example, Arnett (1978) estimates that his $8 M_{\odot}$ α -core corresponds to the interior of a star of $22 M_{\odot}$, so that the weight of $14 M_{\odot}$ exterior to the hydrogen-exhausted core is neglected.

The evolution of numerical models of massive stars from the hydrogen-burning main sequence all the way to advanced burning stages in the core has been calculated recently by Endal (1975a) and Iben, Lamb and Howard (1976) through core carbon burning, and by Weaver, Woosley and Zimmerman (1978) through core silicon burning and on into early core collapse. This last calculation agrees substantially with Arnett's $8 M_{\odot}$ α -core history as far as composition and evolution of central conditions are concerned, but the density profiles of the two models differ by as much as two orders of magnitude in the fuel-rich "mantle" region, with which this study is concerned.

So there is not much help to be found in existing hydrodynamic calculations. However, the availability of "whole star" evolutionary calculations with final models teetering on the edge of collapse encourages one to estimate peak burning conditions following shock passage by approximate, semi-quantitative methods. In these, the Rankine-Hugoniot relations will naturally play a primary role. The preshock temperature and density at a point in the star can be estimated from the static presupernova structure, at least for those parts of the star for which preshock infall will not greatly compress the material. Given an estimate of the postshock fluid velocity, the Rankine-Hugoniot relations will provide the postshock thermodynamic variables, which may be taken over without further ado as peak burning conditions for a parameterized network calculation. Since (as will appear later) the local energy generation exceeds energy losses from neutrino processes by many orders of magnitude, ensuring approximate adiabaticity, one

might suppose that Bernoulli's equation could be used to estimate the postshock velocity (Howard (1971) used essentially this method). We can see the failure of such an approach in the present situation as follows: Consider Euler's equation in Lagrangian form:

$$\frac{dv}{dt} = -4\pi r^2 \frac{\partial P}{\partial m} - \frac{Gm}{r^2} \quad (4.1)$$

Upon multiplication by v , this becomes

$$\frac{d}{dt} \left[\frac{1}{2} v^2 - \frac{Gm}{r} \right] = -4\pi r^2 v \frac{\partial P}{\partial m} \quad (4.2a)$$

$$= \frac{\partial}{\partial m} [4\pi r^2 v P] + P \frac{\partial}{\partial m} (4\pi r^2 v) \quad (4.2b)$$

Use of the equation of continuity

$$\frac{\partial \rho}{\partial t} + \rho \operatorname{div} \mathbf{w} = 0 \quad (4.3)$$

($\frac{\partial}{\partial t} = \frac{D}{Dt}$ in Lagrangian coordinates) where

$$\operatorname{div} \mathbf{w} = \frac{1}{r^2} \frac{\partial}{\partial r} r^2 v \quad (4.4a)$$

$$= 4\pi \rho \frac{\partial}{\partial m} r^2 v \quad (4.4b)$$

so that

$$\frac{\partial V}{\partial t} = \frac{\partial}{\partial t} \left(\frac{1}{\rho} \right) = \frac{\partial}{\partial m} (4\pi r^2 v) \quad (4.5)$$

yields

$$\frac{d}{dt} \left[\frac{1}{2} v^2 - \frac{Gm}{r} \right] = - \frac{\partial}{\partial m} (4\pi r^2 v P) + P \frac{\partial V}{\partial t} \quad (4.6)$$

By the first law of thermodynamics, which for our purposes takes the form

$$T \frac{\partial s}{\partial t} = \frac{\partial u}{\partial t} + p \frac{\partial V}{\partial t} \quad (4.7)$$

we have

$$\frac{d}{dt} \left[\frac{1}{2} v^2 + u - \frac{Gm}{r} \right] = - \frac{\partial}{\partial m} (4\pi r^2 v p) \quad (4.8)$$

If the right hand side vanishes, we recover Bernoulli's equation; only if it is very small will Bernoulli's equation be a useful approximation. To aid in estimating whether this is the case, convert (4.8) to the integral form

$$\frac{d}{dt} \int_{m_1}^{m_2} dm \left[\frac{1}{2} v^2 + u - \frac{Gm}{r} \right] = -4\pi r^2 v p \Big|_{m_1}^{m_2} \quad (4.9)$$

and approximate the left hand side by

$$\Delta m \frac{d}{dt} \left[\frac{1}{2} v^2 + u - \frac{Gm}{r} \right] \approx -4\pi r^2 v p \Big|_{m_1}^{m_2} \quad (4.10)$$

where v , E and r are taken to be values at a suitably chosen "representative" Lagrangian coordinate m in the mass interval (m_1, m_2) , in the sense of the mean value theorem for integrals. Letting

$$u = \frac{3}{2} \frac{N_a}{\mu} kT + \frac{1}{\rho} aT^4 \quad (4.11)$$

and using the following "reasonable" estimates for postshock variables in the range $m_1 = 3 M_\odot$, $m_2 = 5 M_\odot$ (taken from shock profiles developed below, at $m = 4 M_\odot$) in the $25 M_\odot$ model of Weaver et al. (1978):

$$T = 1.5 \times 10^9 \text{ }^\circ\text{K} \quad (4.12a)$$

$$P = 1.46 \times 10^5 \text{ gcm}^{-3} \quad (4.12b)$$

$$v = 4.63 \times 10^8 \text{ cm s}^{-1} \quad (4.12c)$$

one finds

$$\frac{1}{2} v^2 + - \frac{Gm}{r} = 1.88 \times 10^{17} \text{ erg g}^{-1} \quad (4.13)$$

Using $\rho_5 = 3.16$, $T_9 = 1.9$ at $3 M_\odot$ and $\rho_5 = 0.94$, $T_9 = 1.5$ at $5 M_\odot$, also taken from the Hugoniot to be presented below, gives

$$4\pi r^2 v P \bigg|_{m_1}^{m_2} = 1.12 \times 10^{50} \text{ erg s}^{-1} \quad (4.14)$$

for the right-hand side of (4.10). Multiplying (4.13) by $2 M_\odot = 4 \times 10^{33} \text{ g}$, and dividing this by (4.14) gives a quantity with dimensions of time

$$\tau \approx 6.7 \text{ s} \quad (4.15)$$

which can be thought of as a characteristic timescale for hydrodynamics to change the internal energy of a parcel of gas in this part of the star by PdV work during the explosion. However, the radius of the star $\approx 7 \times 10^{13} \text{ cm}$, so that even at an average velocity of 10^9 cm/s for the shocked matter (an overestimate) it requires on the order of 10 hr for it to disperse sufficiently to be thought of as unbound from the star. Therefore, Bernoulli's equation cannot be used to relate post-shock conditions in the mantle to the asymptotic velocity of ejected matter. As we shall see, this is a great pity.

2. Approach

The approach taken in these calculations will start with the Hugoniot curves which can be constructed at each point in the pre-supernova model, estimating the preshock conditions from the $25 M_{\odot}$ model of Weaver et al. (1978) at the start of core collapse. Table 3 shows the temperature and density at a number of representative locations in the star as estimated from Figure 2b of Weaver et al. These appear plotted in the ρT plane as Figure 9.

One can estimate the effect of preshock compression due to infall of the inner regions of the star during collapse with the aid of Figure 3 of Weaver et al., which shows infall velocities during the early stages of core collapse. At $2.5 M_{\odot}$, for example,

$$v \approx 1.5 \times 10^7 \text{ cm s}^{-1} \quad (4.16)$$

From numerical integration of

$$\frac{4}{3} \pi r^3 = \int \frac{dm}{\rho} \quad (4.17)$$

one finds

$$r(2.5 M_{\odot}) \approx 7.7 \times 10^8 \text{ cm} \quad (4.18)$$

from which comes the freefall timescale

$$\tau_{\text{ff}} \approx \frac{r}{v_{\text{esc}}} = \sqrt{\frac{r^3}{2Gm}} \quad (4.19)$$

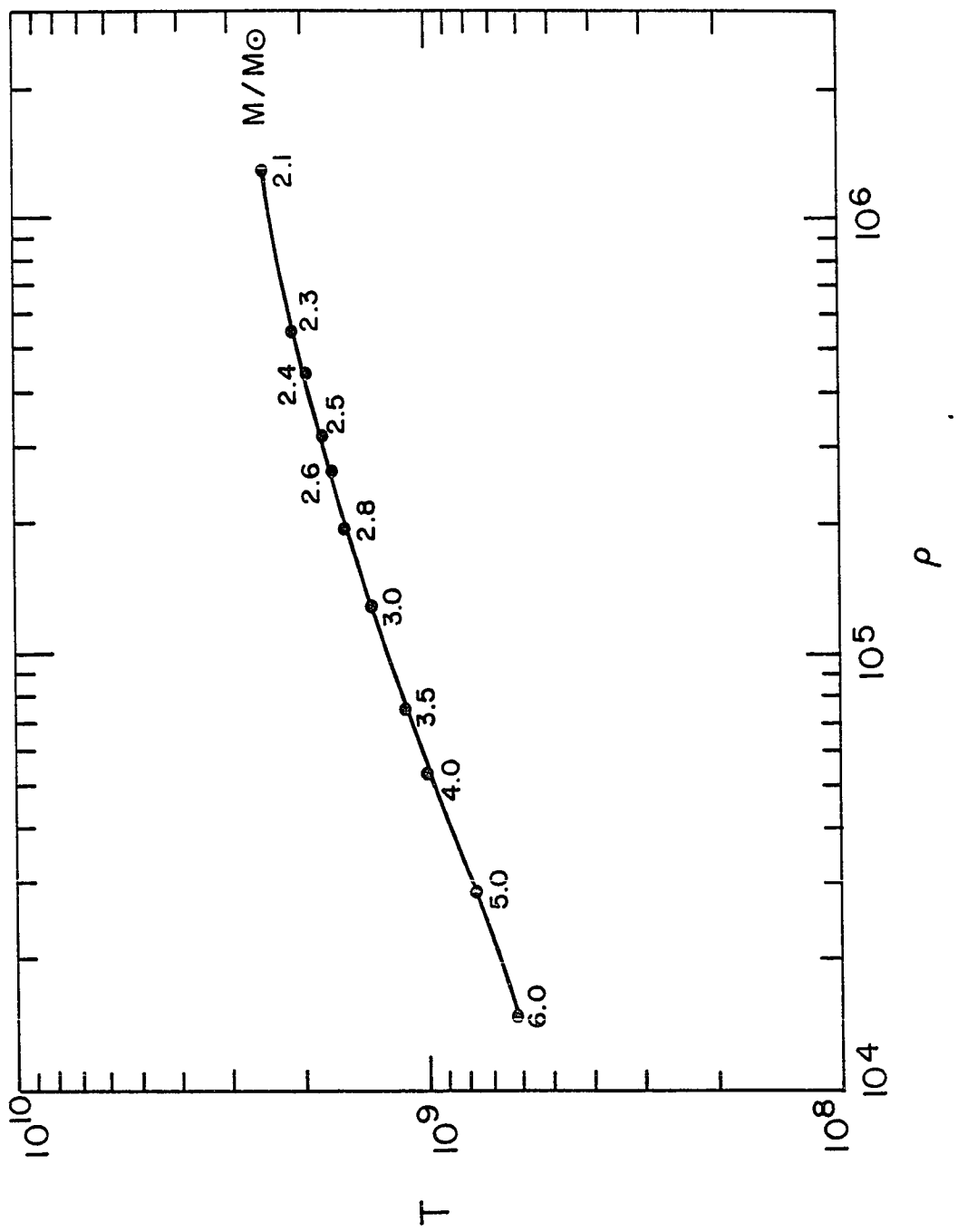
During this time a mass element at Lagrangian coordinate $m = 2.5 M_{\odot}$ will move a distance

TABLE 3
Thermodynamic Variables for Selected
Locations in the Presupernova Star

M/M_{\odot}	ρ_5	T_9
2.1	12.87	2.438
2.3	5.52	2.102
2.4	4.417	1.951
2.5	3.162	1.767
2.6	2.626	1.682
2.8	1.951	1.562
3.0	1.297	1.346
4.0	0.5319	1.00
5.0	0.2829	0.771
6.0	0.1493	0.6171

FIGURE 9

Presupernova thermodynamic structure plotted
in the $\log \rho - \log T$ plane.



$$\Delta r \approx 1.24 \times 10^7 \text{ cm} \quad (4.20)$$

Thus,

$$\Delta P/\rho \approx 3 \Delta r/v \lesssim 4.8 \times 10^{-2} \quad (4.21)$$

This change is smaller than the uncertainty involved in estimating the densities from the figures, and its neglect will affect none of the results of this study. Mass points lying further out in the star will experience even smaller compression.

Given the thermodynamic state of the material prior to shock passage, its postshock state must correspond to a point on the Hugoniot curve passing through the preshock variables in the pT plane. Thus, originating from each point in Figure 9 will be a continuous curve which is the locus of possible postshock conditions of the matter at that point in the star. Once these are known, a profile for the shock must be chosen, i.e., which set of postshock conditions corresponds to a supernova shock resulting in mass ejection? In the absence of numerical results from hydrodynamical calculations, one can only constrain the possible profiles by crude, essentially qualitative arguments, and attempt a sort of parameterized approach. A powerful aid in this version of Hobb's choice is provided by a knowledge of the change in entropy suffered by the material as it is shocked to various points on the Hugoniot, especially when combined with the requirement that "reasonable" nucleosynthetic conditions result.

B. Hugoniots

1. Rankine-Hugoniot Relations

Perhaps the most concise illustration of the problem of shock formation and propagation in hydrodynamics emerges from an observation made by von Neumann (1943). If one considers the boundary value problem posed by the hydrodynamic equations for an ideal classical fluid (i.e., one for which viscosity and heat conductivity may be ignored) confined to a box, whose shape may change with time, with prescribed values for the fluid variables throughout the box at an initial time, then a solution exists only so long as the motion of the boundary does not compress the fluid. If the boundary does advance into the fluid (no matter how regular the motion), there is no solution; the fluid variables become discontinuous on a surface after a finite time, in exactly the same way shocks are observed to form experimentally. (Characteristically, this paraphrase conveys little of the force or brevity of von Neumann's remarks.) Of course, the experimentally observed situation is that the fluid description breaks down on length scales much smaller than those characteristic of the bulk flow, and that dissipative processes of microscopic origin dominate the transition to another regime of continuous flow.

The key point is that shock formation has its origin in the macroscopic description of fluid motion. It then follows that flow discontinuities cannot violate the basic conservation laws that apply to the bulk fluid. These include mass, energy, and momentum conservation, embodied in the Rankine-Hugoniot relations connecting the flow

variables on either side of a shock. In addition, the realization that the basic features of shocks occur independently of any assumptions regarding the microscopic properties or dissipative length scales of the fluid* underlies the successful use of an arbitrary but conveniently chosen "artificial viscosity" in numerical schemes to spread the discontinuity over several mesh points while very nearly reproducing the correct jumps in the flow variables (von Neumann and Richtmeyer, 1950).

Consider the relation between fluid variables on either side of a shock, as viewed in the shock's rest frame (Figure 10). If we limit ourselves to a case where the fluid velocity is normal to the shock, the requirements of continuity in mass, energy, and momentum across the shock result in the following equations (Landau and Lifshitz, 1958, p.319):

$$\text{mass continuity:} \quad \rho_1 v_1 = \rho_2 v_2 \quad (4.22a)$$

$$\text{momentum balance:} \quad p_1 + \rho_1 v_1^2 = p_2 + \rho_2 v_2^2 \quad (4.22b)$$

$$\text{energy conservation:} \quad w_1 + \frac{1}{2} v_1^2 = w_2 + \frac{1}{2} v_2^2 \quad (4.22c)$$

where w is the fluid enthalpy:

$$w = u + P/\rho \quad (4.23)$$

in terms of energy, pressure and density.

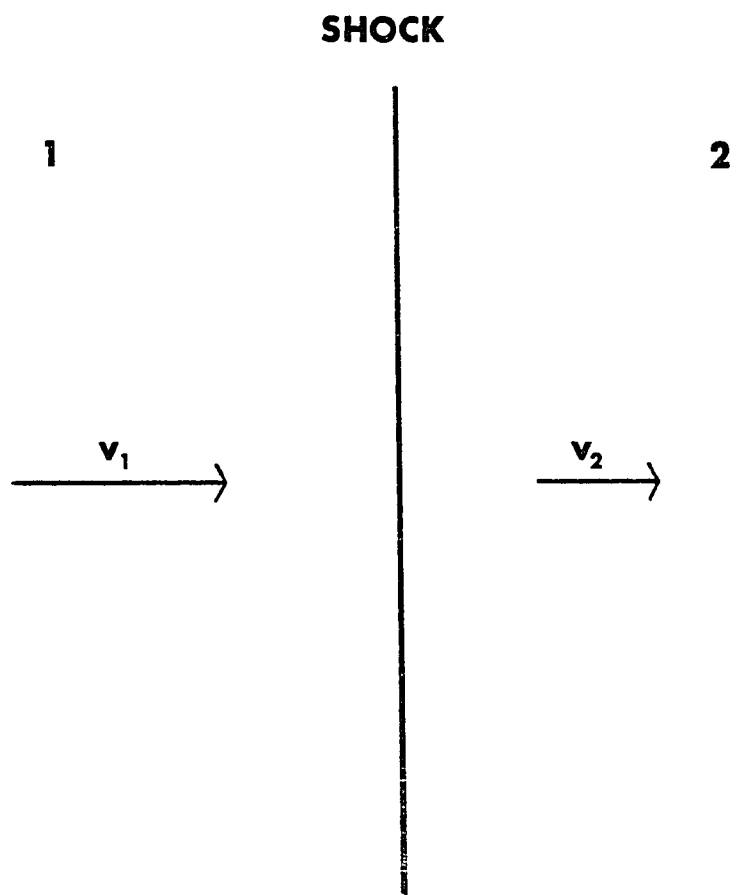
These are the Rankine-Hugoniot relations; they are simple, general, and exact. The requirement that the entropy (which, like

* With the exception of radiating shock fronts, which involve additional boundary conditions on the heat flow.

•

FIGURE 10

Relation between shock and fluid motions
in equations (4.22).



the other state variables, suffers a discontinuity at the shock)
increase

$$s_2 > s_1 \quad (4.24)$$

can be shown to imply that the fluid is both compressed and decelerated in passing through the shock (Landau and Lifshitz, 1958, p.325):

$$\rho_2/\rho_1 > 1 \quad (4.25a)$$

$$v_2/v_1 < 1 \quad (4.25b)$$

Before describing the equation of state to be used in constructing shock profiles, we quote the solution of eqns.(4.22) for a useful special case, that of a shock in an ideal gas with a constant ratio of specific heats, for which the R-H relations become (Zel'dovic and Razier, 1966, p.50)

$$\frac{\rho_2}{\rho_1} = \frac{(\gamma+1)p_2 + (\gamma-1)p_1}{(\gamma-1)p_2 + (\gamma+1)p_1} \quad (4.26)$$

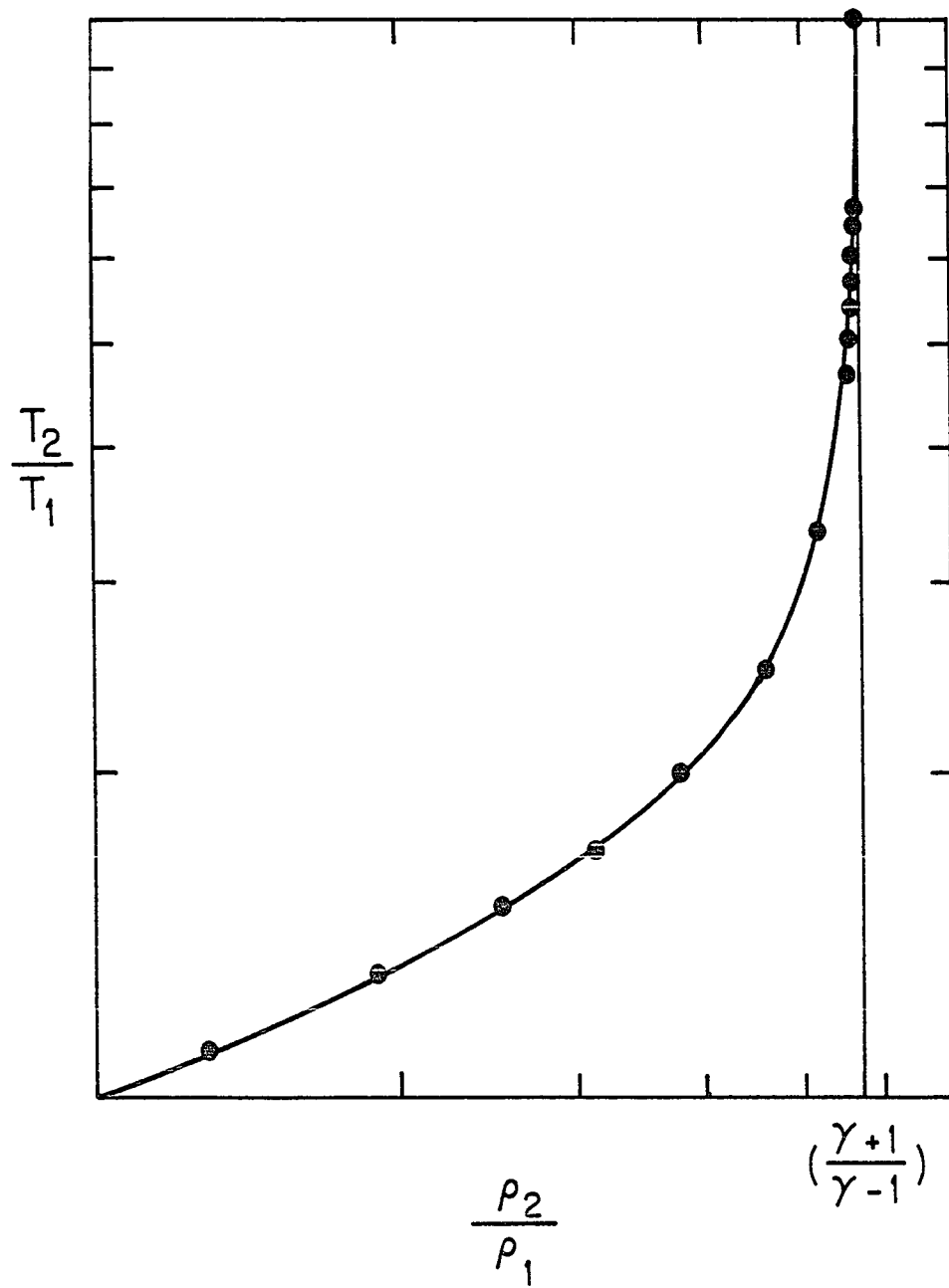
$$\frac{p_2}{p_1} = \frac{(\gamma+1)/\rho_1 - (\gamma-1)/\rho_2}{(\gamma+1)/\rho_2 - (\gamma-1)/\rho_1} \quad (4.26b)$$

If we limit ourselves to $\rho_2/\rho_1 > 1$, the relation between ρ and T appears as in Figure 11; the postshock temperature (or pressure) may increase without bound, but the postshock compression tends to the limit

$$\frac{\rho_2}{\rho_1} \longrightarrow \frac{(\gamma+1)}{(\gamma-1)} \quad (4.27)$$

FIGURE 11

Hugoniot curve in a gas with constant
ratio of specific heats.



for very strong shocks. The fluid velocities on either side of the shock are given by

$$v_1^2 = \frac{1}{2}[(\gamma-1)P_1 + (\gamma+1)P_2]/\rho_1 \quad (4.28a)$$

$$v_2^2 = \frac{1}{2} \frac{[(\gamma+1)P_1 + (\gamma-1)P_2]^2}{[(\gamma-1)P_1 + (\gamma+1)P_2]} \quad (4.28b)$$

2. Equation of State

The stellar plasma is assumed to consist of completely ionized matter and radiation. The matter portion may be divided further into ions and electrons. The equation of state therefore has three parts:

$$P(\rho, T) = P_i + P_e + P_r \quad (4.29)$$

Similarly, the energy density is

$$u = u_i + u_e + u_r \quad (4.30)$$

The entropy for a collection of weakly interacting systems is given by the sum of the individual entropies (Wehr1, 1978), so that

$$S = S_i + S_e + S_r$$

It will be convenient to work in terms of a dimensionless entropy per nucleon,

$$\sigma \equiv S/\rho N_a k \quad (4.32)$$

The contribution of each constituent will now be discussed in turn.

(1) Ions. The ions are assumed to form an ideal Boltzman gas, for which

$$P_i = N_i kT \quad (4.33a)$$

$$u_i = \frac{3}{2} N_i kT \quad (4.33b)$$

The number density of ions is related to the density by

$$N_i = \rho N_a / \mu_i \quad (4.34)$$

where the mean molecular weight per ion

$$\frac{1}{\mu_i} \approx \sum_z \frac{X_z}{A_z} \equiv \langle \frac{1}{A} \rangle \quad (4.35)$$

is related to the mean molecular weight,

$$\frac{1}{\mu} = \sum_z \frac{X_z}{A_z} (Z + 1) \quad (4.36)$$

and the mean molecular weight per electron,

$$\frac{1}{\mu_e} = \sum_z \frac{ZX_z}{A_z} \quad (4.37)$$

by

$$\frac{1}{\mu} = \frac{1}{\mu_i} + \frac{1}{\mu_e} \quad (4.38)$$

(Clayton, 1968, pp.82-83).

The entropy per particle for an ideal Boltzman gas is given by the Sackur-Tetrode formula

$$\frac{S_i}{N_i k} = \frac{5}{2} - \log \left[\frac{N_i}{V} \left(\frac{2\pi m^2}{\mu_i k T} \right)^{3/2} \right] \quad (4.39)$$

which, by (4.34), may be written

$$\sigma_i = \frac{1}{\mu_i} (S_i / N_i k) . \quad (4.40)$$

Note that while (4.39) does not satisfy the Third Law upon substitution of $T = 0$, only differences in S_i between states of high temperature will occur in its application, a situation for which (4.39) is a reliable expression (Huang, 1968).

(2) Radiation. The pressure, energy density, and entropy of a photon gas are given by the well-known expressions

$$P_r = \frac{1}{3} u_r \quad (4.41a)$$

$$u_r = aT^4 \quad (4.41b)$$

$$\sigma_r = \frac{S_r}{\rho N_a k} = \frac{4}{3} \frac{aT^4}{\rho N_a k} . \quad (4.41c)$$

(3) Electrons. The equation of state of an ideal Fermi gas is given in parametric form as averages over a Fermi-Dirac distribution of momentum states. If

$$t(p) = \sqrt{p^2 c^2 + m^2 c^4} - mc^2 \quad (4.42)$$

is the particle kinetic energy in terms of its 3-momentum p , and the chemical potential is related to the conventional degeneracy parameter η by

$$\mu = \eta kT \quad (4.43)$$

and the statistical weight is

$$g = 2J + 1 \quad (4.44)$$

(equals 2 for an electron), the number density per unit volume is

$$n_e = \frac{g}{2\pi^2 \hbar^3} \int_0^\infty p^2 dp \left[\exp \left(\frac{t-\mu}{kT} \right) + 1 \right]^{-1} \quad (4.45a)$$

and the specific energy density is

$$u_e = \frac{g}{\pi^2 \hbar^3} \int_0^\infty p^2 dp \, t(p) \left[\exp \left(\frac{t-\mu}{kT} \right) + 1 \right]^{-1} \quad (4.45b)$$

The pressure is given by the average of the momentum transfer through a surface element $d\vec{\Sigma}$ averaged over all directions; in the isotropic case it is

$$p_e = \frac{g}{6\pi^2 \hbar^3} \int_0^\infty p^2 dp \, p v \left[\exp \left(\frac{t-\mu}{kT} \right) + 1 \right]^{-1} \quad (4.45c)$$

$$= \frac{g}{6\pi^2 \hbar^3} \int_0^\infty p^3 dp \, \frac{\partial t}{\partial p} \left[\exp \left(\frac{t-\mu}{kT} \right) + 1 \right]^{-1} \quad (4.45d)$$

by the use of one of Hamilton's equations, as in the limit of statistical equilibrium the particle interactions may be ignored (Cox and Giuli, 1968). The entropy per unit volume comes from the identity

(Cox and Giuli, 1968, eqn.24.76b)

$$S_e = \frac{u_e + p_e}{T} - \eta n_e k . \quad (4.45e)$$

For a nonrelativistic electron gas, the equation of state can be cast in terms of the Fermi-Dirac integrals (McDougall and Stoner, 1938)

$$F_k(\eta) \equiv \int_0^\infty Z^k dZ [\exp(Z-\eta) + 1]^{-1} \quad (4.46)$$

upon a change of variable from p to $t(p)/kT$. Making the same transformation and introducing a "relativity" parameter

$$\beta \equiv kT/mc^2 \quad (4.47)$$

yields (Cox and Giuli, 1968,p.808)

$$n_e = 8\pi\sqrt{2} \left(\frac{mc^2}{\hbar}\right)^3 \beta^{3/2} \int_0^\infty dZ Z^{1/2} (1 + \frac{1}{2} \beta Z)^{1/2} (1 + \beta Z) [\exp(Z-\eta)+1]^{-1} \quad (4.48a)$$

$$u_e = 8\pi\sqrt{2} \left(\frac{mc^2}{\hbar}\right)^3 mc^2 \beta^{5/2} \int_0^\infty dZ Z^{3/2} (1 + \frac{1}{2} \beta Z)^{1/2} (1 + \beta Z) [\exp(Z-\eta)+1]^{-1} \quad (4.48b)$$

$$p_e = \frac{16\pi\sqrt{2}}{3} \left(\frac{mc^2}{\hbar}\right)^3 mc^2 \beta^{5/2} \int_0^\infty dZ Z^{3/2} (1 + \frac{1}{2} \beta Z)^{3/2} [\exp(Z-\eta)+1]^{-1} \quad (4.48c)$$

By defining

$$F_k(\eta, \beta) \equiv \int_0^\infty Z^k dZ (1 + \frac{1}{2} \beta Z)^{1/2} [\exp(Z-\eta)+1]^{-1} \quad (4.49)$$

as a generalization of the FD integrals (4.46) one can write (Bludman and Van Riper, 1977)

$$n_e = 8\pi\sqrt{2} \left(\frac{mc^2}{\hbar}\right)^3 \beta^{3/2} \left[F_{1/2}(\eta, \beta) + \beta F_{3/2}(\eta, \beta) \right] \quad (4.50a)$$

$$u_e = 8\pi\sqrt{2} \left(\frac{mc^2}{\hbar}\right)^3 mc^2 \beta^{5/2} \left[F_{3/2}(\eta, \beta) + \beta F_{5/2}(\eta, \beta) \right] \quad (4.50b)$$

$$p_e = \frac{16\pi\sqrt{2}}{3} \left(\frac{mc^2}{\hbar}\right)^3 mc^2 \beta^{5/2} \left[F_{3/2}(\eta, \beta) + \frac{1}{2} \beta F_{5/2}(\eta, \beta) \right] \quad (4.50c)$$

However, for the numerical evaluations used in this study, an alternative, approximate set of expressions was used, which requires only the ordinary FD integrals previously defined (Divine, 1966; Chiu, 1968). To start, define

$$f(u, \beta) = (1 + u\beta)(1 + \frac{1}{2} u\beta)^{1/2} \quad (4.51)$$

and

$$g(u, \beta) = (1 + \frac{1}{2} u\beta)^{1/2} \quad (4.52)$$

Then, if

$$u_{1/2}(\eta) = (F_2(\eta)/F_{3/2}(\eta))^2 \quad (4.53)$$

and

$$u_{3/2}(\eta) = (F_3(\eta)/F_{5/2}(\eta))^2 \quad (4.54)$$

Equations (4.50) are closely approximated by

$$n_e = \frac{\sqrt{2}}{\pi} \left(\frac{mc^2}{\hbar}\right)^3 \beta^{1/2} \left[F_{1/2}(\eta) + F_{3/2}(\eta) \left[\frac{f(u_{1/2}, \beta) - 1}{u_{1/2}} \right] \right] \quad (4.55a)$$

$$u_e = \frac{\sqrt{2}}{\pi} \left(\frac{mc^2}{\hbar}\right)^3 mc^2 \beta^{5/2} \left[F_{3/2}(\eta) + F_{5/2}(\eta) \left[\frac{f(u_{3/2}, \beta) - 1}{u_{3/2}} \right] \right] \quad (4.55b)$$

$$p_e = \frac{2^{3/2}}{3\pi^2} \left(\frac{mc^2}{\hbar} \right)^3 mc^2 \beta^{5/2} \left[F_{3/2}(\eta) + F_{5/2}(\eta) \left[\frac{g(u_{3/2}, \beta) - 1}{u_{3/2}} \right] \right] \quad (4.55c)$$

Equations (4.55) are exact in the four limiting cases (extreme degenerate/extreme relativistic, extreme nondegenerate/extreme relativistic, extreme degenerate/nonrelativistic, and nondegenerate/nonrelativistic) and cause an error of less than 3×10^{-3} in the worst intermediate case (Chiu, unpublished).

For $\eta < 0$, the ordinary FD integrals have the series expansion (McDougall and Stoner, 1938)

$$F_k(\eta) = \Gamma(k+1) \sum_{r=1}^{\infty} (-)^{r-1} \frac{\exp(r\eta)}{r^{k+1}} \quad (4.56)$$

Since this series consists of a monotonically decreasing sequence of terms which alternate in sign, the first term neglected automatically provides an upper limit to the truncation error caused by taking only a finite number of terms. For $\eta < -1.5$, including four terms in the expansion for $k = 2, 5/2$, and 3, and five terms for $k = 1/2$ and $3/2$ gives the FD integrals to an accuracy of better than one part in 10^5 . For $-1.5 \leq \eta \leq 0$, the low-order McLaurin expansions given by Bludman and Van Riper (1977) are reliable to about half a percent.

Equations (4.51) - (4.55) and the expansions from Bludman and Van Riper (1977) were used to construct equation of state tables for $-6 \leq \eta \leq 0$, $0.5 \leq T_9 \leq 4.0$, with a spacing of 0.05 in both T_9 and ρ . Values of the thermodynamic variables P_e and S_e are obtained by

interpolation between entries in the tables which bracket the desired temperature and density. It is an annoying procedure.

Empirically,

$$P_e/n_e kT - 1 \lesssim 5\% \quad (4.57)$$

for $\eta \leq -1$, which holds for all situations encountered in this study. Ordinarily, the departure from ideal gas behavior proved rather smaller than this limit. As the plasma in the deep interior of Weaver et al.'s massive star is borderline radiation dominated, the error caused in the total pressure by neglecting degeneracy will be $\lesssim 2.5\%$. Degeneracy effects must be watched more closely in the electron contribution to the entropy, by (4.45e).

The electron energy density and pressure are related by

$$P_e = \left(\frac{2}{3}\right) u_e \quad (4.58)$$

in the extreme nonrelativistic limit and by

$$P_e = \left(\frac{1}{3}\right) u_e \quad (4.59)$$

in the extreme relativistic limit. In the intermediate regime, one can write, after Cox and Giuli (1968)

$$P_e = \left(\frac{\bar{\alpha}}{3}\right) u_e \quad (4.60)$$

where $\bar{\alpha}$ does not depend on the degree of degeneracy. For computational purposes, $\bar{\alpha}$ was obtained as a function of temperature by Lagrangian interpolation between values of P_e and u_e selected from the equation of state tables.

3. Construction of Hugoniot

The numerical solution of the Hugoniot relations (4.22) with the equation of state (4.29) begins with the preshock temperature and density, a prescribed value for the postshock temperature, and a starting guess for the postshock compression ratio. This latter, upon iteration a few times in eqn.(4.26a), may be substituted into eqns.(4.28) to give initial guesses for the pre- and post-shock fluid velocities. The starting values so obtained prove sufficiently accurate for a Newton-Raphson solution for ρ_2 , v_1 and v_2 , performed on eqns.(4.22) modified by the substitution of (4.22a) into (4.22b) to get

$$P_2 + \rho_2 v_2^2 = P_1 + \rho_1 \left(\frac{\rho_2 v_2}{\rho_1} \right)^2, \quad (4.61)$$

reducing the system from three to two simultaneous equations. Without this modification, the Newton-Raphson method fails to converge.

When repeated for an interesting range of postshock temperatures, this procedure yields the attainable postshock conditions summarized in Figure 12. Table 4 presents the data for $4.0 M_\odot$ numerically, and also contains the change in dimensionless entropy per nucleon, $\Delta\sigma$, for each entry, where

$$\sigma = \sigma_i + \sigma_r + S_e / \rho N_a k \quad (4.62)$$

The quantity

$$v_{ps} = v_1 - v_2 \quad (4.63)$$

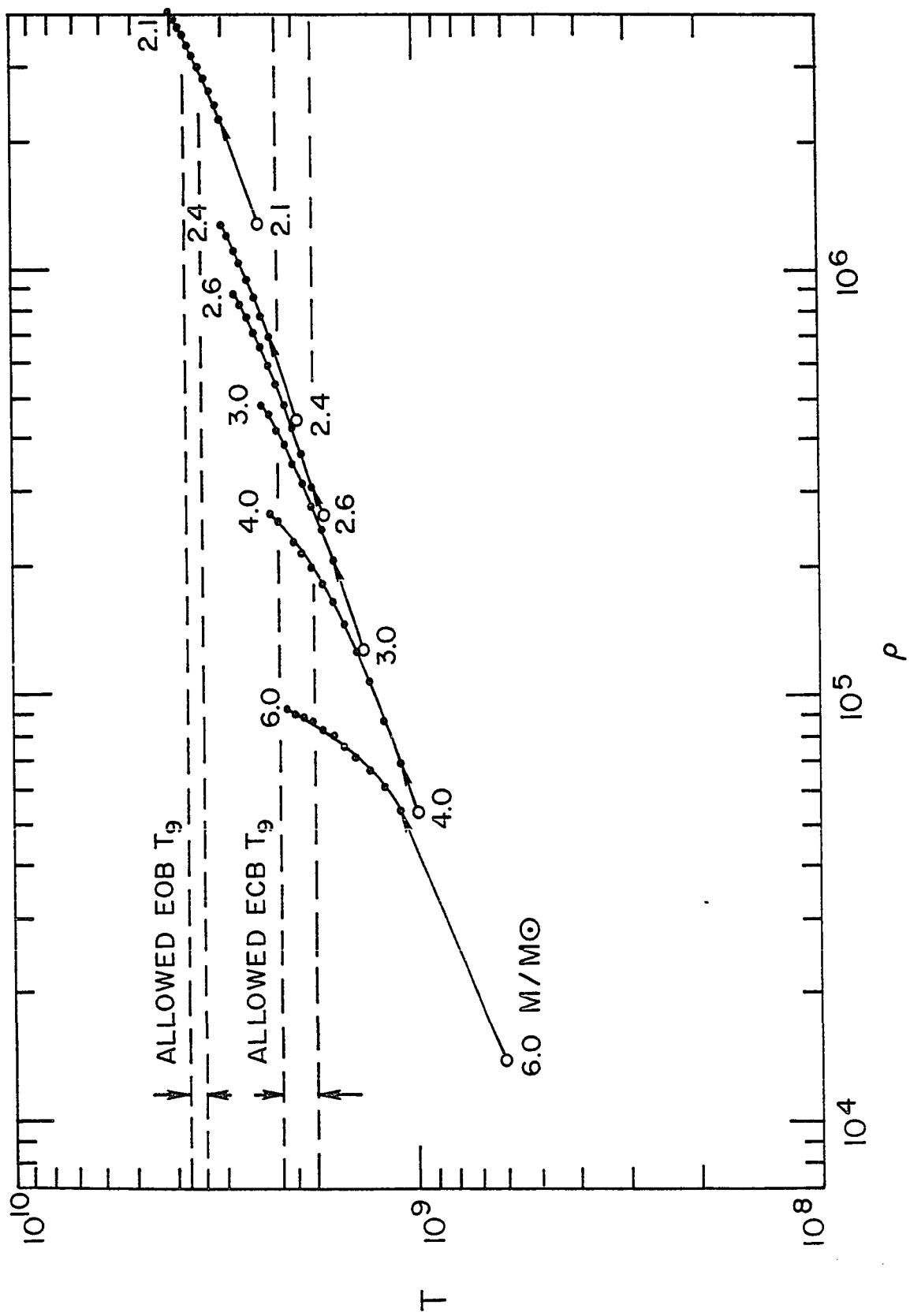
TABLE 4
Postshock Conditions for 4.0 M_{\odot}

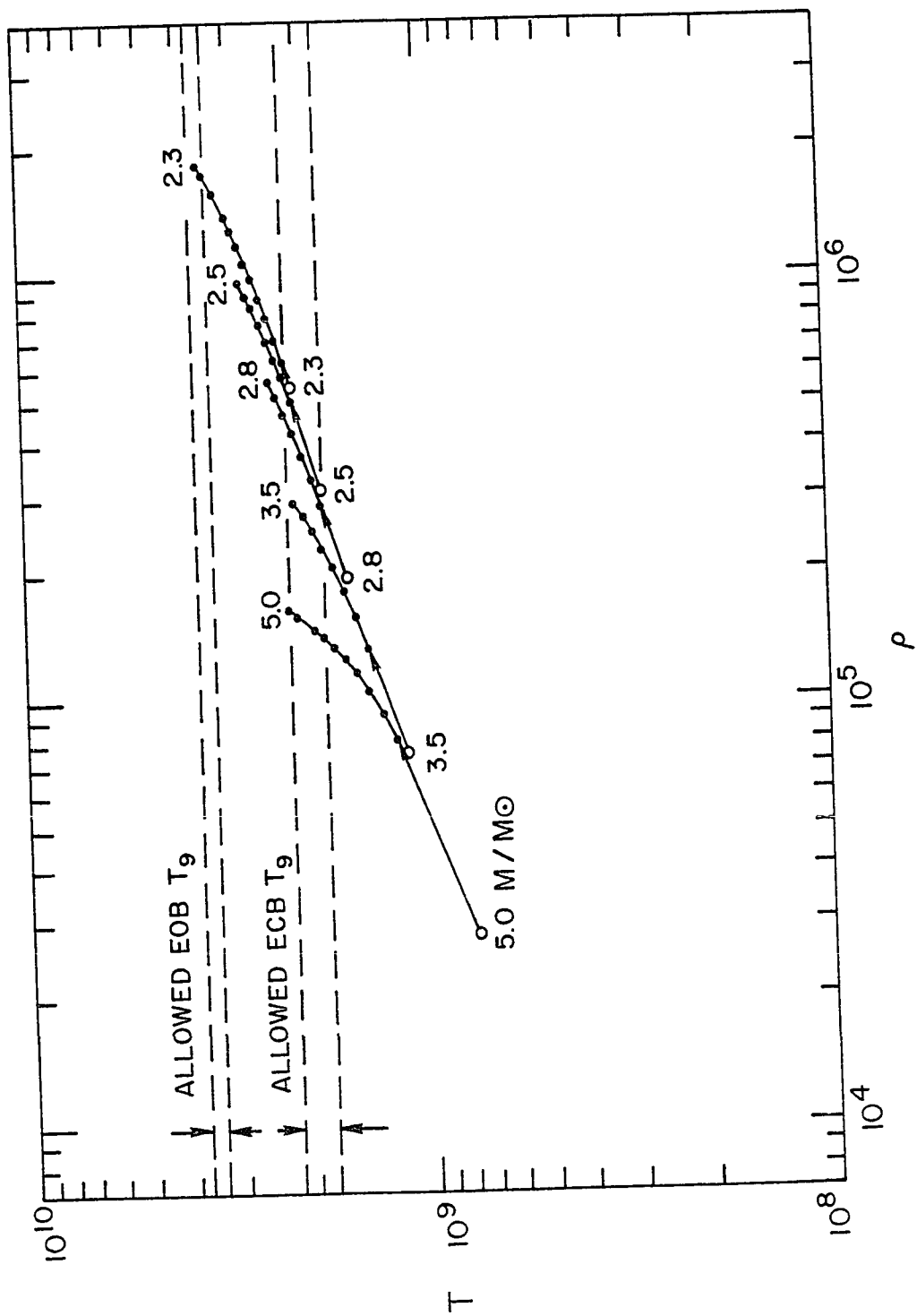
ρ_5	T_9	$\Delta\sigma$	v_{ps}	
2.663	2.3	3.333	1.188×10^9	
2.553	2.2	2.817	1.092×10^9	
2.299	2.0	1.920	9.047×10^8	
2.155	1.9	1.532	8.141×10^8	
1.998	1.8	1.189	7.253×10^8	
1.829	1.7	0.8875	6.374×10^8	
1.650	1.6	0.6245	5.501×10^8	
1.461	1.5	0.4073	4.628×10^8	
1.265	1.4	0.2359	3.757×10^8	
0.8741	1.2	0.0388	1.938×10^8	
0.6929	1.1	noise	0.989×10^8	
0.5319	1.0	0	0	← pre SN

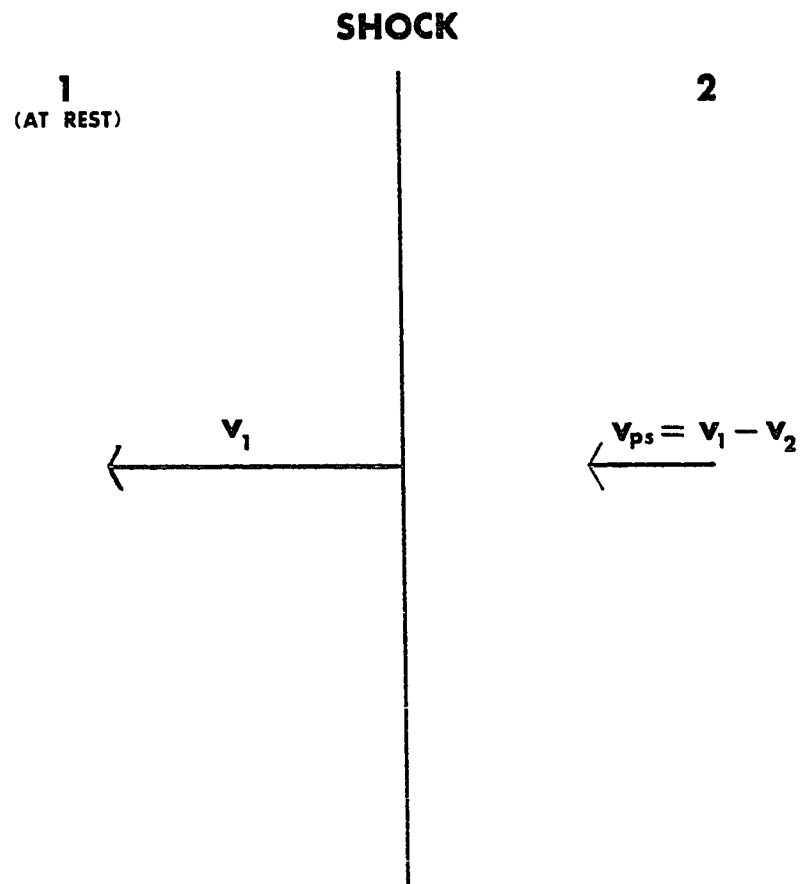
FIGURE 12a. Hugoniot curves originating from ρ_1, T_1 in the presupernova star for 2.1, 2.4, 2.6, 3.0, 4.0 and 6.0 M_\odot .

FIGURE 12b. Same as Figure 12a, but for 2.3, 2.5, 2.8, 3.5 and 5.0 M_\odot .

FIGURE 13. Relation between shock and fluid motions in the supernova mantle.







is the postshock fluid velocity as viewed in a frame in which the pre-shock fluid lies at rest. In this frame, the shock moves with $v = v_1$ into the fluid, and the material behind the front moves with $v = v_{ps}$. For $v_1 < 2 \times 10^9$ cm/s the transformation between this frame (Figure 13) and that pictured in Figure 10 is Galilean to better than 2×10^{-3} .

C. Shock Profiles

Given the Hugoniot curves for a suite of points in the star, one must still select from them a locus of postshock conditions to fix a model of the shock. In the absence of any sure knowledge of the hydrodynamic behavior of shock propagation in the mantles of supernovae, one must fall back upon indirect arguments to justify a choice of shock profile. It is reasonable to suppose that the change in specific entropy across the shock will vary in some smooth manner (save perhaps in the case of a discontinuity in composition) as the shock propagates down the density gradient of the mantle. Therefore, a natural starting point for the construction of plausible shock profiles is an understanding of the systematics of dissipation by a shock in a density gradient.

However, the simple requirement of smoothness itself places strong limitations on "reasonable" shock behavior, when considered in light of the requirements of nucleosynthesis. Since the mass-weighted average contributor to galactic nucleosynthesis lies at approximately $22\text{--}25 M_\odot$ for the progenitor mass, one expects that, of all places in the universe, the canonical explosive nucleosynthetic

processes should operate in a star of roughly $25 M_{\odot}$. In particular, the demand that a "reasonable" shock profile result in good nucleosynthetic conditions for oxygen burning in the oxygen shell, and for carbon burning in the carbon shell, with a smooth transition (in terms of $\Delta\sigma$ vs. m) in the intervening neon shell, allows one to circumscribe the interesting range of shock profile variation fairly sharply, so that the exact form of $\Delta\sigma$ has little influence on nucleosynthesis, to first order.

Parametric studies of explosive oxygen burning reveal that reasonable agreement between burning products and solar system abundances will not obtain unless the peak burning temperature lies in the range

$$3.1 \leq T_9 \leq 3.9 \quad (4.64)$$

and the peak density in the range

$$10^5 \leq \rho \leq 10^7 \quad (4.65)$$

Woosley et al. (1973, Fig. 13) have further shown that for $X(^{16}\text{O}) = 0.8$ (approximately true in the oxygen-bearing zones of Weaver et al.'s $25 M_{\odot}$ star) oxygen burning with peak temperatures of

$$3.4 \leq T_9 \leq 3.7 \quad (4.66a)$$

and peak densities

$$10^6 \leq \rho \leq 7 \times 10^6 \quad (4.66b)$$

will result in agreement with solar system abundances of the major burning products to within a factor of two. Good agreement with solar system values for the products of explosive carbon burning, on the

other hand, requires that

$$1.8 \leq T_g \leq 2.2 \quad (4.67a)$$

and

$$10^4 \leq \rho \leq 10^7 \quad (4.67b)$$

(Pardo et al. 1974). Examination of tabulated Hugoniot reveals that at the point

$$T_g = 3.60 \quad (4.68a)$$

$$\rho_s = 33.87 \quad (4.67b)$$

on the Hugoniot for $m = 2.1 M_\odot$, which lies near the base of the oxygen zone and thus should be shocked to conditions near the upper end of the allowed range (4.66), the change in entropy/nucleon is

$$\Delta\sigma = 0.286 \quad (4.69)$$

On the other hand, the conditions

$$T_g = 2.20 \quad (4.20a)$$

$$\rho_s = 4.76 \quad (4.70b)$$

which lie on the Hugoniot for $2.8 M_\odot$, near the base of the carbon zone, have

$$\Delta\sigma = 0.266 \quad (4.71)$$

-- the same, within numerical errors ca. 0.02, as for $2.1 M_\odot$. One can thus construct a shock profile connecting these two points in the ρT plane for which

$$\Delta\sigma \approx \text{const.} \quad (4.72)$$

as the shock sweeps out in mass; this appears as model A in Table 5.

Although this model seems a reasonable one in terms of nucleosynthetic requirements, it has been obtained by an arbitrary choice for the systematics of $\Delta\sigma$ with m . It would be helpful to know if the choice is a plausible one, even if only in a qualitative sense. For this purpose, an analytic model is an invaluable guide. The only simple analytic solutions of the hydrodynamic equations for shock propagation down a density gradient are the similarity blast waves of Sedov (1959); these concern shock motion in a polytropic gas with an initial power law for the density:

$$\rho_1 = A r^{-\omega} \quad (4.73)$$

In this case, the shock front motion with time follows

$$r_s = \text{const. } t^{2/(5-\omega)} \quad (4.74)$$

For $\omega = 0$, eqn.(4.74) reduces to the celebrated Taylor-Sedov solution (Taylor 1950; see also von Neumann, 1943a). The entropy behind the shock, for adiabatic index γ , is proportional to

$$P/\rho^\gamma = \text{const. } r^{(\gamma\omega-3)} \quad (4.75)$$

Since the initial pressure is ignored in this solution, the postshock entropy is also the change in entropy. If the power-law index is greater than (less than)

$$\omega = 3/\gamma \quad (4.76)$$

the postshock entropy increases (decreases).

The shock front moves with velocity

$$\frac{dr_s}{dt} = \left(\frac{2}{(5-\omega)} \right) \left(\frac{r_s}{t} \right) \propto r^{(\omega-3)/2} \quad (4.77)$$

so that for ω greater than (less than) 3, the shock accelerates (decelerates).

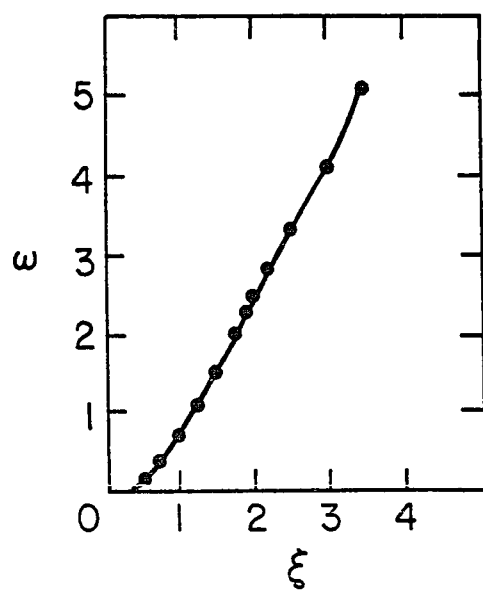
To apply these results to the problem at hand, regard the actual density profile in the presupernova star as defining a variable power-law index $\omega(r)$; as long as dissipation length scales for the shock are much smaller than a scale height, this should be a good approximation. By plotting $-d \log \rho / d \log r$ for an $n = 3$ polytrope (say), one gets Figure 14 for $\omega(r)$, which grows approximately linearly with radius because of the increasingly rapid fall-off in density as the outer regions of the polytrope are approached. Thus one expects on the basis of this analogy that both the shock velocity and postshock entropy will initially decrease, then increase. Numerical studies of shock propagation in exponential density distributions indeed display this qualitative behavior for the postshock fluid velocity (Grover and Hardy, 1966). Curiously enough, shocks in planar and cylindrical geometry reflect the same behavior as the spherical case.

However, the Sedov solution applies to a different physical situation than the one in question; there is neither preshock pressure nor entropy, and gravitation is neglected. Comparison of the Sedov solution with examples of shock propagation in polytropic stellar models indicates that the qualitative features should in fact appear in the more complicated setting of a stellar explosion. Sakurai (1956)



FIGURE 14

$\omega = - d \log \rho / d \log \xi$, where ξ is a normalized radial coordinate, for a polytrope with $n = 3$.



has used power-series expansions to solve for the propagation of a blast wave in the deep interior of an $n = 2.5$ polytrope; the quantity P/ρ^γ decreases as the shock moves out, but the radius of convergence of the expansions is too small to follow the shock to a point where a turnover might be expected. The supernova models of Ono et al. (1961) show an accelerating shock in the outer regions of the star in their Figure 7. Indeed, it seems intuitively reasonable that a shock resulting in mass ejection should accelerate in the outer, steeper regions of the mantle.

In addition to the nucleosynthetic constraints on the shock profile, we will therefore impose the qualitative requirement that $\Delta\sigma$ vs. m have a minimum, with the turning point corresponding roughly to the radius at which $\omega = 3/\gamma \approx 2.1$. A crude fit of Table 1 to an $n = 3$ polytrope indicates that this occurs near $m = 3 M_\odot$.

Finally, it is possible to place a crude limit on $\Delta\sigma$ for a reasonable profile by applying simple energetics to the outer reaches of the mantle, for which $\omega > 3$, and thus for which the shock velocity and postshock fluid velocity increase, until the shock encounters the steep density gradient which marks the edge of the α -core, at which point the similarity solutions lose even an approximate applicability. For this part of the star, $\frac{1}{2} v_{ps}^2(r)(m_\alpha - m(r))$ is a lower limit to the kinetic energy imparted to the remaining mass in the original α -core. Clearly, a reasonable shock will not deposit more than a fraction of the total energy release of the explosion $\approx 10^{51}$ ergs in this part of the mantle; this requirement places an upper limit on $\Delta\sigma$ in the outer ($\omega > 3/\gamma$) part of the mantle.

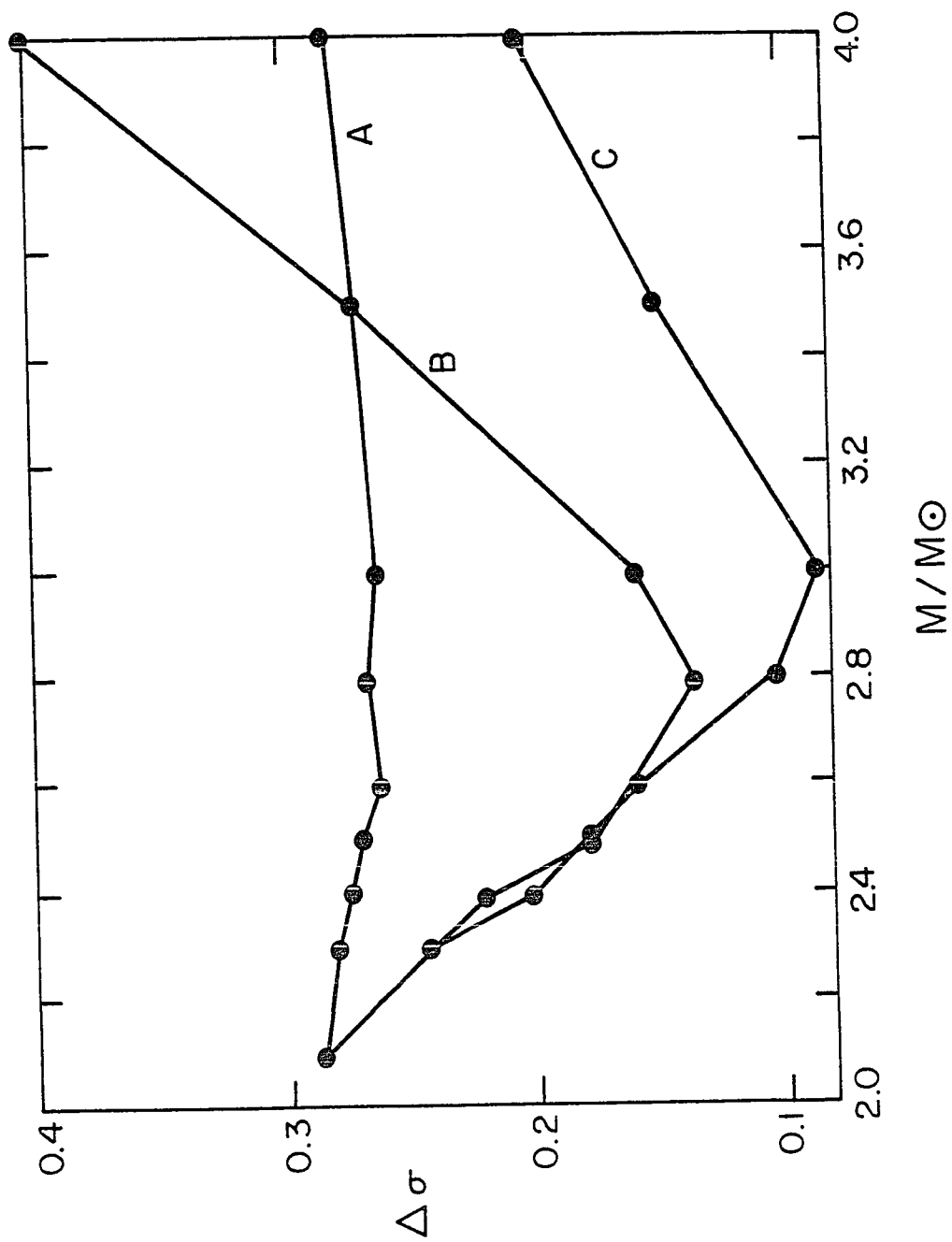
Table 5 displays three shock profiles selected on the basis of the foregoing considerations; Figure 15 shows $\Delta\sigma$ for these cases. Model A is the profile mentioned previously with $\Delta\sigma \approx \text{const.}$; Models B and C each have a minimum in $\Delta\sigma$ near $m = 3 M_{\odot}$, but Model B has systematically higher postshock entropy than Model C. These models should give an idea of the sensitivity of postshock conditions to the detailed variation of $\Delta\sigma$ vs. m within the qualitative guidelines advanced. The three profiles correspond to generally similar nucleosynthetic conditions. For comparison, the locus of peak burning conditions obtained from a hydrodynamic calculation of Arnett (private communication) appears in Figure 16 along with the other profiles; it runs approximately parallel to the peak conditions of Model A, but lower by some 5% in T_9 . Clearly, for purposes of nucleosynthesis the two are nearly identical, as a slight systematic difference in the run of postshock density for Model A, corresponding to a minor change in the mass-weighting of the products, will cause them to coincide. It is especially encouraging that different shock profiles selected within the range of variation allowed by the criteria developed in this section give thermodynamic conditions comparable to those found in hydrodynamic calculations. Evidently the main features of the model (from the point of view of a parameterized network study) are fixed by the "endpoints" of $\Delta\sigma$ vs. m , and do not depend very sensitively on the manner of variation assumed for the intermediate region.

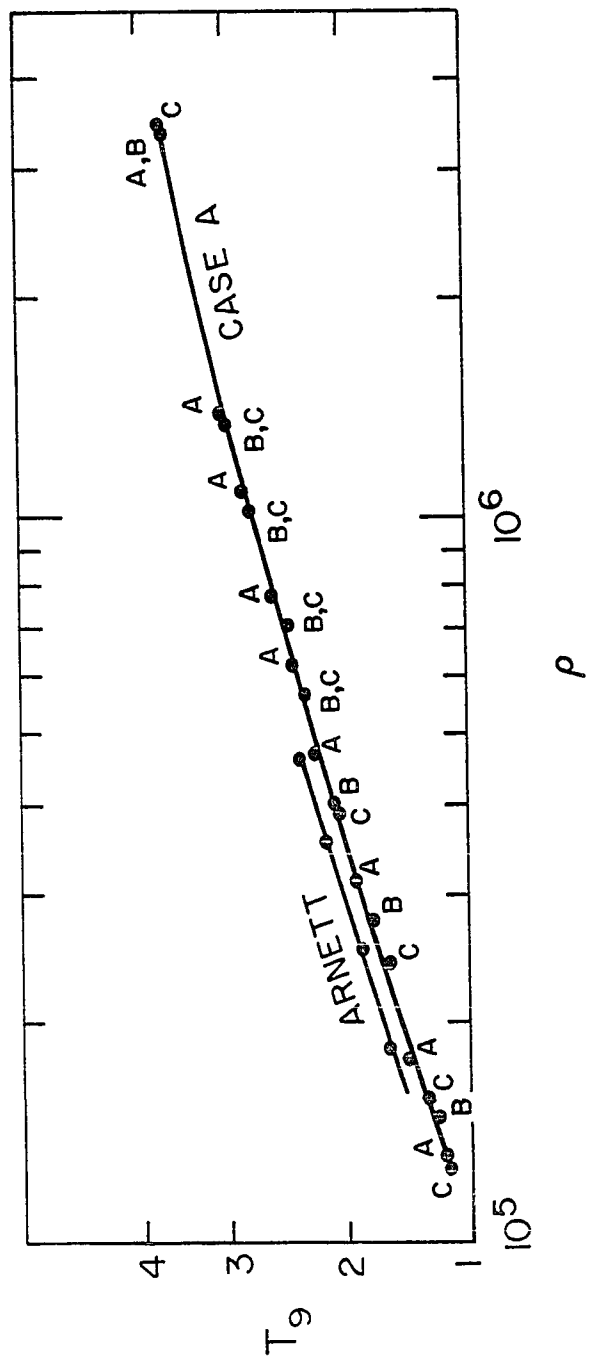
TABLE 5
Shock Profiles

M/M_{\odot}	A		B		C	
	ρ_5	T_9	ρ_5	T_9	ρ_5	T_9
2.1	33.87	3.60	33.87	3.60	34.782	3.65
2.3	13.856	3.00	13.362	2.95	13.362	2.95
2.4	10.984	2.775	10.346	2.7	10.346	2.7
2.5	7.855	2.512	7.096	2.4	7.096	2.4
2.6	6.43	2.375	5.692	2.25	5.69	2.25
2.8	4.761	2.20	4.048	2.05	3.882	2.0
3.0	3.162	1.90	2.799	1.8	2.439	1.7
3.5	1.813	1.60	1.813	1.6	1.569	1.5
4.0	1.314	1.425	1.461	1.5	1.265	1.4
5.0	---	---	---	---	---	---
6.0	---	---	---	---	---	---

FIGURE 15 $\Delta\sigma$ vs. M/M_\odot for shock profiles A, B and C from Table 3.

FIGURE 16 Peak burning conditions from shock passage for Models A, B and C in the ρT plane. The solid line is for Model A, and shock loci from a hydrodynamic model of shock passage by Arnett appears for comparison.





CHAPTER V

A NUCLEOSYNTHETIC MODEL FOR THE EXPLOSION OF A MASSIVE STAR

A. General Remarks

1. Overview

The presupernova abundances obtained in Chapter III and the peak thermodynamic conditions following shock passage obtained in Chapter IV form the basis for a model of the nucleosynthetic yields of the nuclei with $20 \leq A \leq 30$ from the explosion of a massive star. The picture to bear in mind is the following: A reflected shock from core collapse passes through each mass zone in the model in turn, depositing heat in each layer according to $\Delta\sigma$ vs. m for the model. The effect of the shock on the nuclear fuel in each zone is to instantly move the material to its peak thermodynamic conditions in the ρT plane, whereupon it expands and cools on a hydrodynamic timescale. The freezeout (at $T_9 \leq 1.0$) abundances of the resultant explosive nucleosynthesis provide the bulk isotopic yields of the model. As the shock velocity is large (of order 10^9 cm s⁻¹) and the nuclear burning time of order 0.1 s, the fuel deflagrates gently, with a flame front thickness approaching a density scale height in the presupernova (10^8 cm vs. 4×10^8 cm), rather than detonating violently, and thus should have

little effect on the course of nuclear burning, although it may affect the postshock expansion.

Input to the explosive network code consisted of neon-zone abundances for 2.4, 2.5 and 2.6 M_{\odot} peak conditions, and carbon zone abundances for 2.6, 2.8, 3.0 and 3.5 M_{\odot} conditions. Postshock temperatures for $m \geq 4.0 M_{\odot}$ were too low for any appreciable ^{12}C consumption; indeed the 3.5 M_{\odot} explosions showed virtually no departure from the pre-explosion abundances, so that explosive processing of these seven zones represents the modification of the mantle composition exterior to the oxygen shell that accompanies disruption of the star.

An attempt was made to survey the sensitivity of the explosive yields to variations of explosion parameters by running Model A with $\chi = 2$ and selected zones of Models B and C with $\chi = 1$. These alterations generally produced small differences from the final abundances of Model A with $\chi = 1$. Therefore, the discussion to follow will concentrate largely on a detailed examination of Model A.

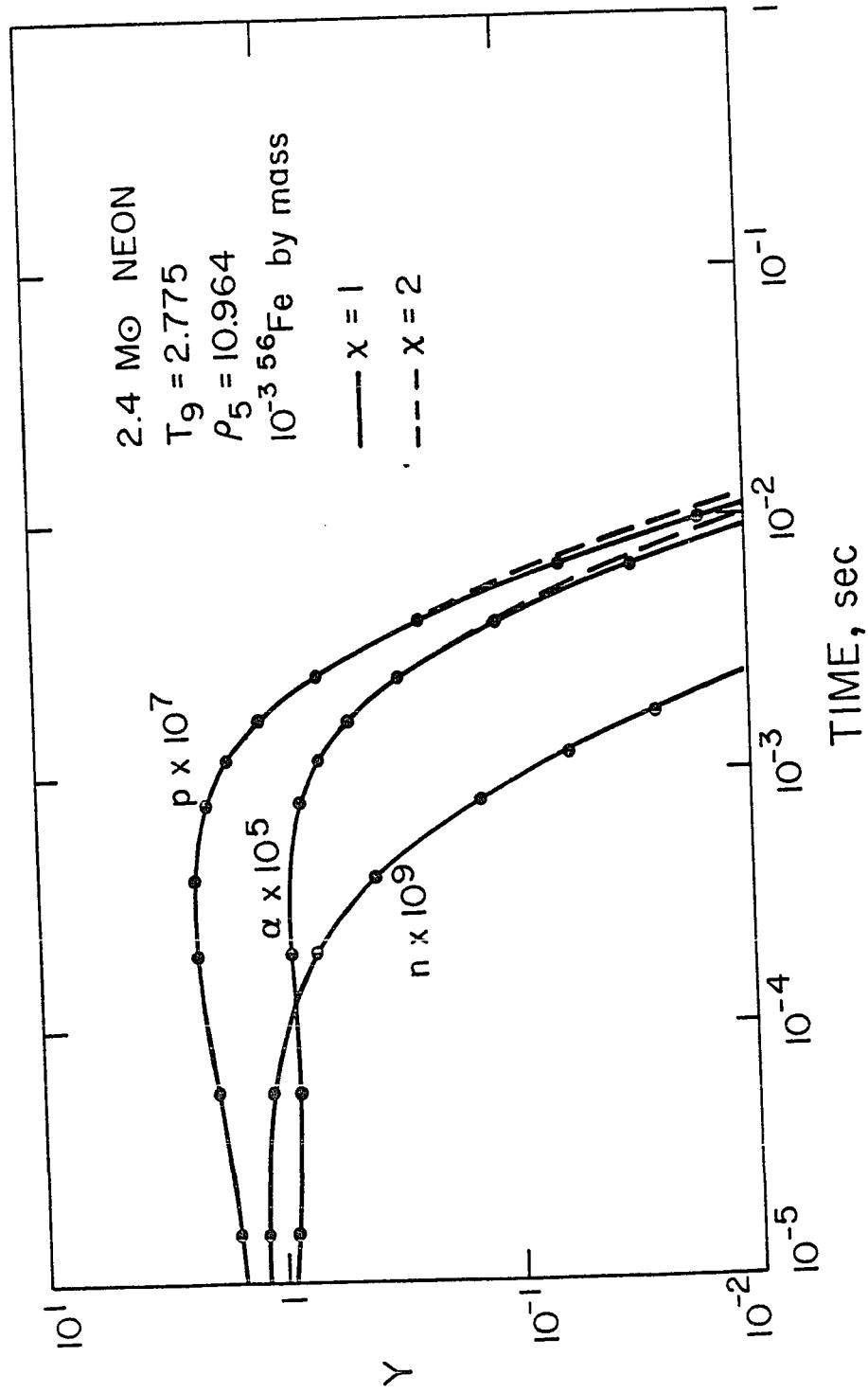
2. Explosive Processing of the Neon and Carbon Zones

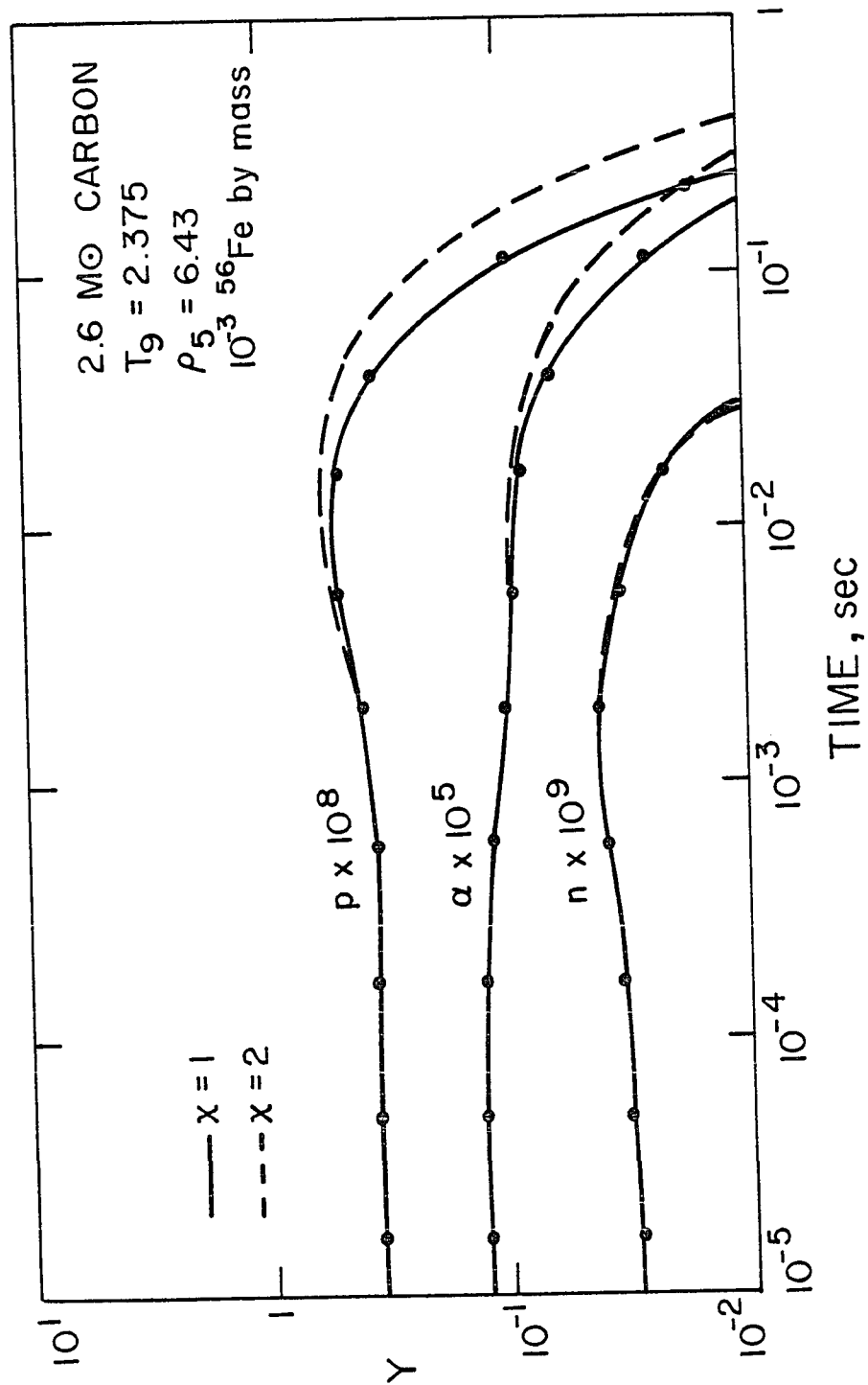
It is instructive to examine briefly the salient features of explosive carbon and neon burning in this model; explosive neon burning has not been investigated in any detail to date, and carbon burning at high temperatures ($T_9 \geq 2.2$) and low ^{12}C concentrations ($\approx 4\%$) can be expected to differ considerably from the standard case in some respects. Figures 17 and 18 show the free nucleon histories of the explosions at 2.4 M_{\odot} in the neon zone and 2.6 M_{\odot} in the carbon

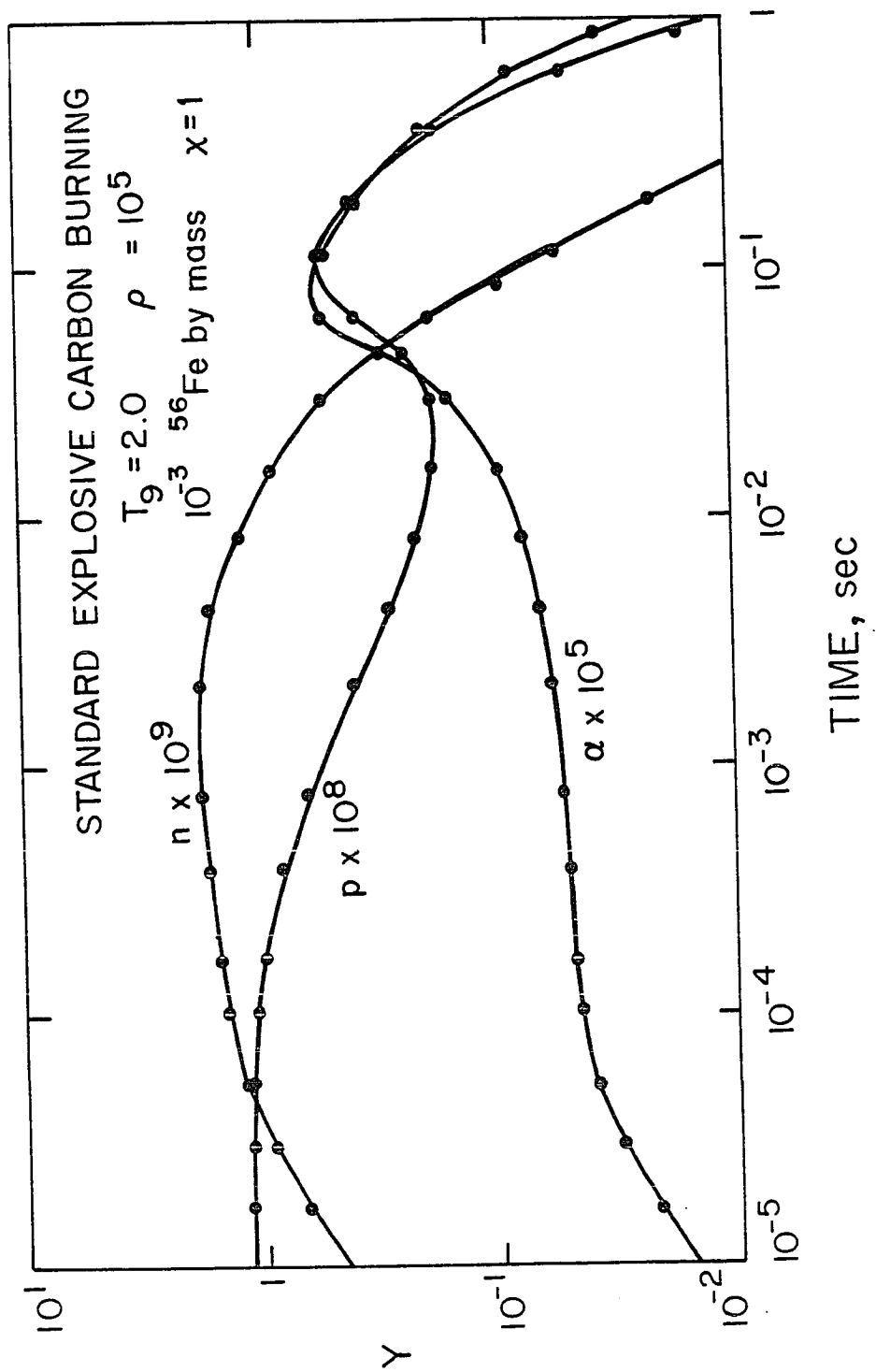
FIGURE 17 Free nucleon histories for explosive neon burning at $2.4 M_{\odot}$.

FIGURE 18 Free nucleon histories for explosive carbon burning at $2.6 M_{\odot}$.

FIGURE 19 Free nucleon histories for "standard" explosive carbon burning.





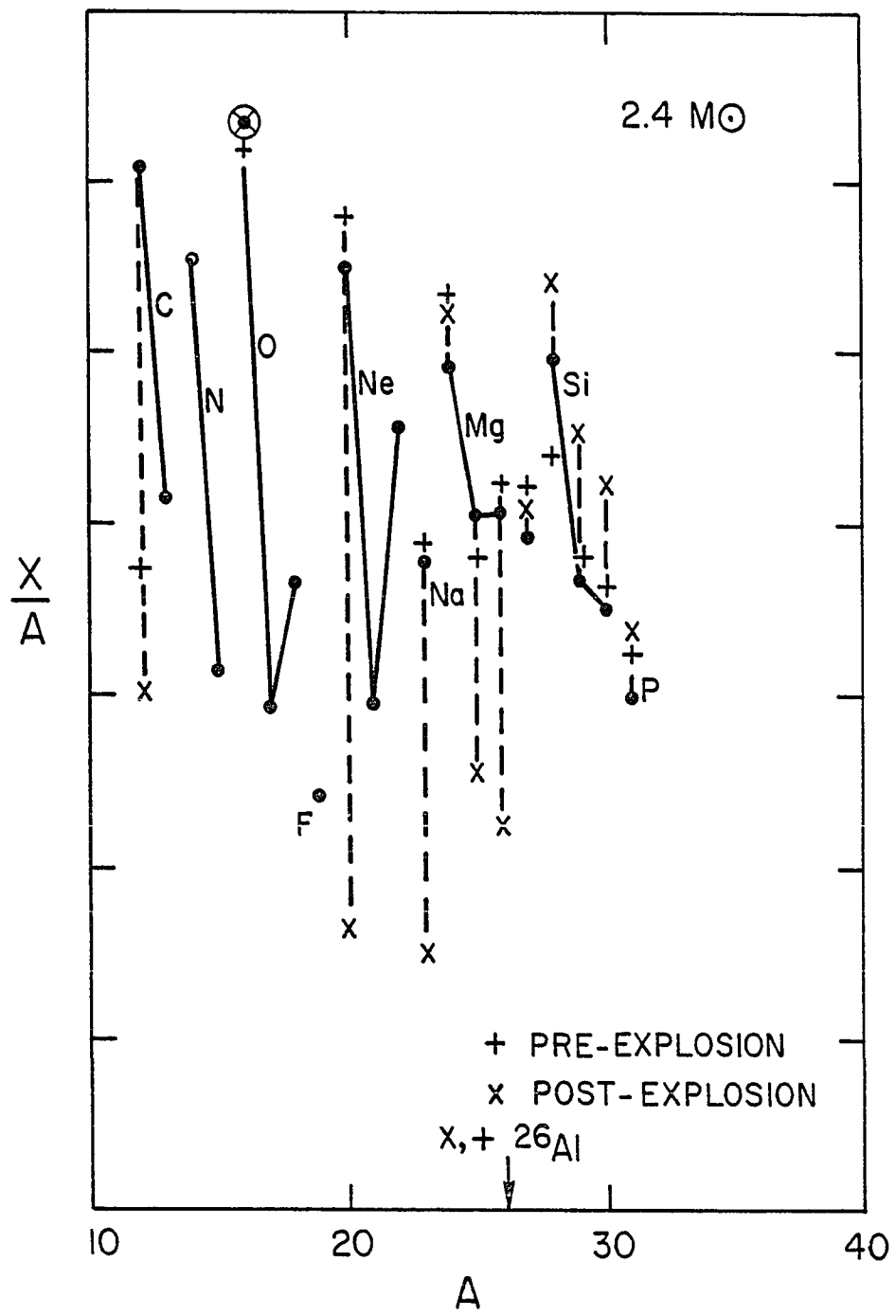


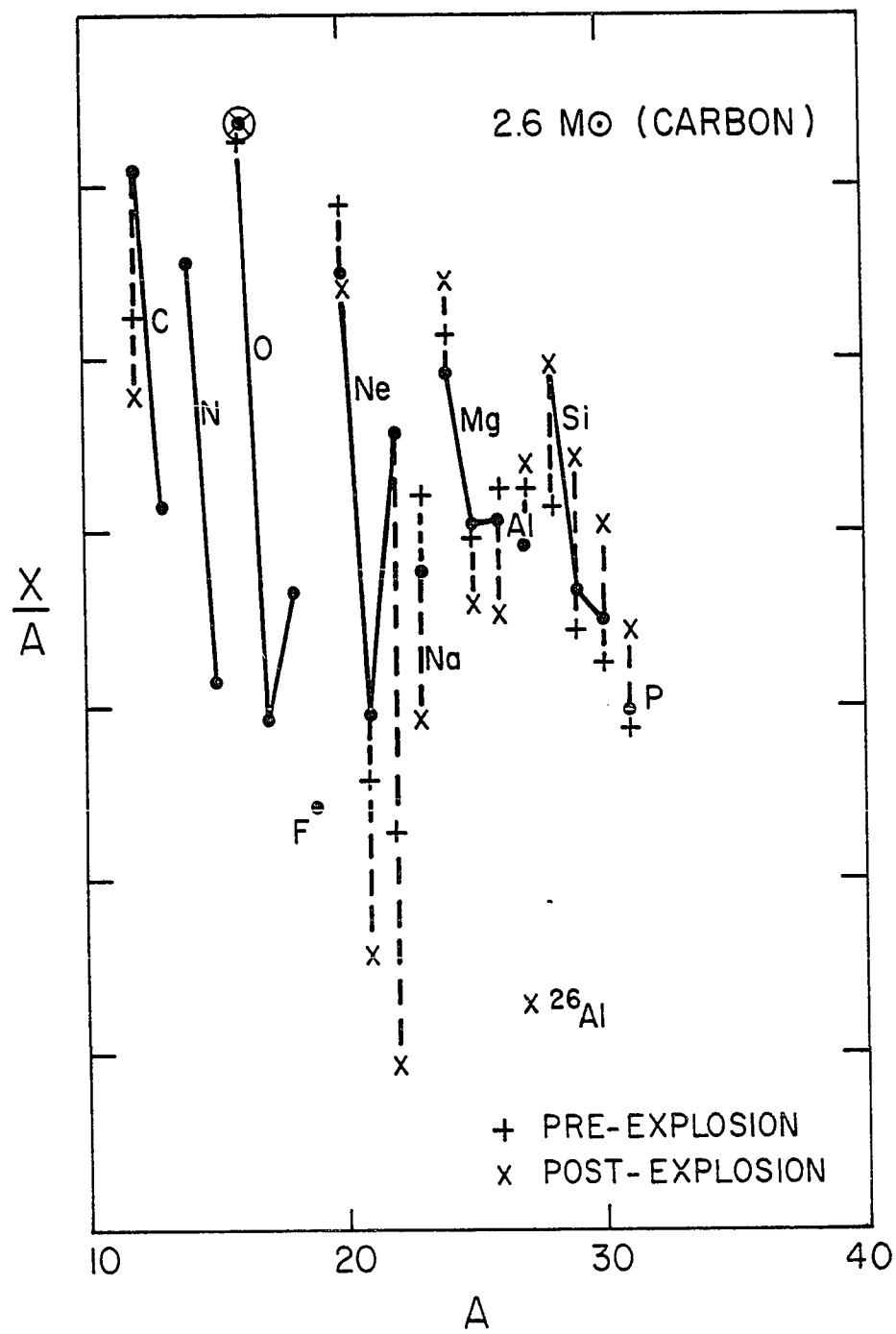
zone, respectively. Histories for explosions with $\chi = 1$ and $\chi = 2$ are plotted. For comparison, Figure 19 shows the nucleon history for "standard" explosive carbon burning, where initially $X(^{12}\text{C}) = 50\%$, $T_9 = 2.0$, and $\rho_5 = 1.0$. Although neon burning is characterized by systematically lower free neutron abundances than carbon burning, partly because the primary reaction $^{20}\text{Ne}(\gamma, \alpha)^{16}\text{O}$ liberates no neutrons, and partly because the excess neutrons (by this stage of nuclear evolution processed from ^{22}Ne into the heavy isotopes of Mg and other neutron-rich carbon burning products whose (α, n) cross-sections are much lower) are much less accessible, Figure 12 shows that at high temperatures the free neutrons from neon burning can briefly approach the level found in standard carbon burning. However, rapid exhaustion of the primary fuel truncates this burst at $\approx 10^{-3}$ s, so that the integrated neutron exposure is much smaller. The free proton and free α numbers are both substantially larger than in standard ECB, but they too fall off at much earlier times. Explosive processing of the carbon zone near $2.6 M_\odot$ liberates protons at a slightly lower level, and α 's at a slightly higher level than standard ECB, but the free neutron abundance is two orders of magnitude lower at any given time; again, the free nucleon burst does not last as long in the case with higher initial T_9 and ρ_5 .

Pre- and post-explosive abundances for these zones appear in Figures 20 and 21, normalized to the final ^{16}O abundance. One can think of these patterns as the extremes of the explosive modification of the final presupernova abundances that will occur in their respective regions of the star; in the case of carbon, at least, the other

FIGURE 20 Pre- and post-explosive abundances compared with solar system values (Cameron, 1973) for $2.4 M_{\odot}$ explosive neon burning, normalized to final $\frac{X}{A} (^{16}\text{O}) = \text{solar}$.

FIGURE 21 Pre- and post-explosive abundances for $2.6 M_{\odot}$ explosive carbon burning, normalized to ^{16}O .





extreme will grade into no modification at all. A few points of interest about the yields are: Both neon and carbon burning under these conditions deplete the heavy Mg isotopes and enhance the silicon isotopes, leaving ^{24}Mg and ^{27}Al little altered. ^{23}Na diminishes sharply; for carbon burning this is noteworthy, as ^{23}Na is ordinarily the carbon burning product par excellence, and the requirement that it be correctly reproduced relative to the major carbon burning products is used to delimit "allowed" carbon burning conditions. Indeed, $2.6 M_{\odot}$ in Model A experiences peak burning conditions outside the "allowed" range, but its effect on the bulk ^{23}Na production will not prove an embarrassment because of the small range of mass in the star involved.

B. Course of the Explosion

1. Systematics of Nuclear Burning

Tabulated yields of nuclei from the explosive network calculations for Model A, which will form the basis of discussion for most of this chapter, appear in Table (6). The various zones of the model experience drastically differing amounts of nucleosynthesis. For the carbon zone, the final initial ratio for ^{12}C varies from unity (for $m \geq 3.5 M_{\odot}$) to 0.354 for $2.6 M_{\odot}$. The burning in the neon zones was systematically more complete, ranging from final/initial $^{20}\text{Ne} = 0.336$ for $m = 2.6 M_{\odot}$ to 6.564×10^{-5} for $2.4 M_{\odot}$. The shock thus causes extensive nuclear processing throughout the neon zone, and in the inner regions of the carbon zone, and essentially no modification of the remaining, exterior portions of the helium-exhausted core.

TABLE 6

Model A, $X = 1$ Mass Fraction

Species	2.4 M_{\odot}	2.5 M_{\odot}	neon 2.6 M_{\odot}	carbon 2.6 M_{\odot}	2.8 M_{\odot}	3.0 M_{\odot}	3.5 M_{\odot}
^{12}C	2.674×10^{-4}	1.090×10^{-3}	1.311×10^{-3}	1.418×10^{-2}	2.953×10^{-2}	3.948×10^{-2}	4.006×10^{-2}
^{16}O	7.255×10^{-1}	7.149×10^{-1}	6.635×10^{-1}	6.561×10^{-1}	5.765×10^{-1}	5.590×10^{-1}	5.590×10^{-1}
^{20}Ne	1.774×10^{-5}	8.314×10^{-3}	9.092×10^{-2}	1.024×10^{-1}	2.632×10^{-1}	2.986×10^{-1}	2.987×10^{-1}
^{22}Ne	4.897×10^{-8}	3.044×10^{-9}	2.068×10^{-6}	3.739×10^{-6}	6.710×10^{-5}	7.167×10^{-5}	7.850×10^{-5}
^{23}Na	1.527×10^{-5}	1.905×10^{-5}	1.045×10^{-4}	3.746×10^{-4}	1.302×10^{-3}	7.017×10^{-3}	7.255×10^{-3}
^{24}Mg	8.880×10^{-2}	1.193×10^{-1}	1.489×10^{-1}	1.368×10^{-1}	8.502×10^{-2}	6.181×10^{-2}	6.129×10^{-2}
^{25}Mg	1.883×10^{-4}	1.394×10^{-4}	1.702×10^{-3}	1.910×10^{-3}	5.021×10^{-3}	4.433×10^{-3}	4.428×10^{-3}
^{26}Mg	8.468×10^{-5}	1.244×10^{-4}	1.229×10^{-3}	1.634×10^{-3}	8.963×10^{-3}	8.969×10^{-3}	8.873×10^{-3}
^{26}Al	3.139×10^{-7}	3.685×10^{-5}	9.642×10^{-5}	9.235×10^{-5}	4.349×10^{-5}	1.318×10^{-5}	2.128×10^{-7}
^{27}Al	7.490×10^{-3}	1.215×10^{-2}	1.382×10^{-2}	1.212×10^{-2}	1.044×10^{-2}	9.553×10^{-3}	9.553×10^{-3}
^{28}Si	1.441×10^{-1}	1.136×10^{-1}	5.351×10^{-2}	4.906×10^{-2}	1.113×10^{-2}	7.067×10^{-3}	7.016×10^{-3}
^{29}Si	2.086×10^{-2}	1.877×10^{-2}	1.463×10^{-2}	1.537×10^{-2}	4.757×10^{-3}	1.628×10^{-3}	1.594×10^{-3}
^{30}Si	1.014×10^{-2}	8.160×10^{-3}	7.455×10^{-3}	6.540×10^{-3}	2.268×10^{-3}	1.010×10^{-3}	9.975×10^{-4}
^{31}P	1.503×10^{-3}	2.545×10^{-3}	1.961×10^{-3}	1.757×10^{-3}	4.938×10^{-4}	4.468×10^{-4}	4.472×10^{-4}

TABLE 6, continued:

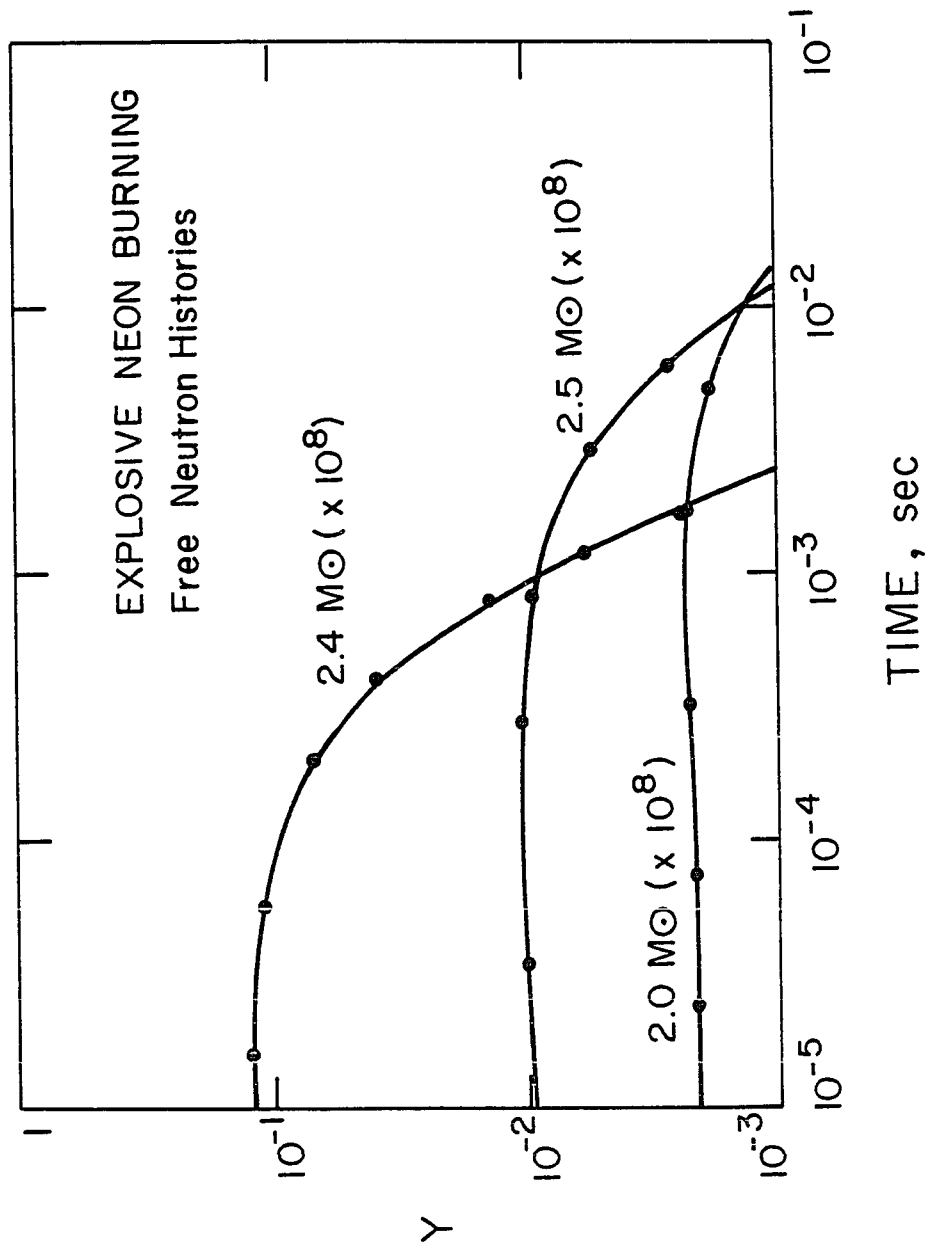
Species	$2.4 M_{\odot}$	$2.5 M_{\odot}$	neon $2.6 M_{\odot}$	carbon $2.6 M_{\odot}$	$2.8 M_{\odot}$	$3.0 M_{\odot}$	$3.5 M_{\odot}$
peak ρ_5	10.98	7.86	6.43	6.43	4.76	3.16	1.81
peak T_9	2.775	2.512	2.375	2.375	2.20	1.90	1.60
σ_1	5.54	5.69	5.81	5.81	6.06	6.02	6.22
$\Delta\sigma$	0.275	0.280	0.262	0.262	0.266	0.263	0.272

The two zones discussed in the previous section represent an upper limit to the free neutron production in their respective zones, as Figures (22) and (23) show. These graphs display the free neutron histories of the six zones of the model which liberated nonnegligible numbers of neutrons during the explosion. The rapidity with which the peak neutron abundance falls off as the shock moves out in mass is dramatic: four orders of magnitude from the base of the neon shell at $2.4 M_{\odot}$ to $3.0 M_{\odot}$ in the carbon zone. This decline in peak neutron density is not quite compensated by the lengthening time scale for neutron production which accompanies it, so that the integrated neutron exposures decrease as a function of mass within each burning zone. One therefore expects that the neutron burst accompanying the explosive processing of the neon and carbon zones will not play as important a role in the synthesis of rare light nuclei as suggested by Howard et al. (1972) on the basis of standard ECB.

Table (7) presents the final abundances for Model A with $\chi = 2$. Comparison with Table (6) indicates that the qualitative trends of the nucleosynthesis with mass remain despite quantitative alteration of individual abundances. Examination of Figure (24), which depicts ejecta as a function of mass in the presupernova for both $\chi = 1$ and $\chi = 2$ reveals: (1) Little change in the shape of the distribution, and (2) Little alteration of the area under each abundance profile. In effect, the additional processing in the $\chi = 2$ case results in significantly different final abundances for each mass $m < 3.0$, but approximately preserves the abundance gradient, so that the distribution of an isotope is shifted in mass, but otherwise little altered,

FIGURE 22 Free neutron histories for explosive neon burning
at 2.4, 2.5 and 2.6 M_{\odot} .

FIGURE 23 Free neutron histories for explosive carbon burning
at 2.6, 2.8 and 3.0 M_{\odot} .



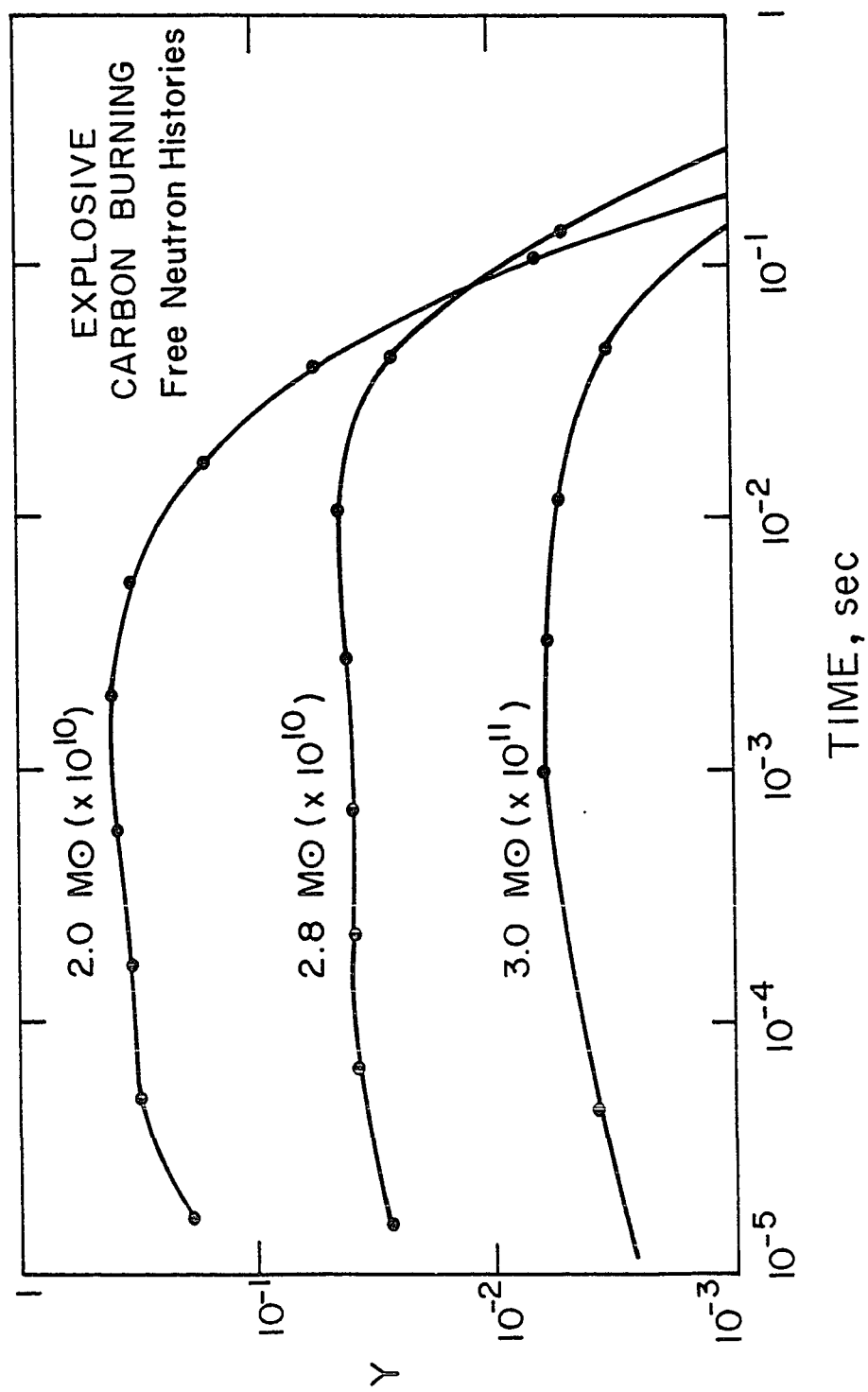


TABLE 7

Model A, X = 2 Mass Fraction

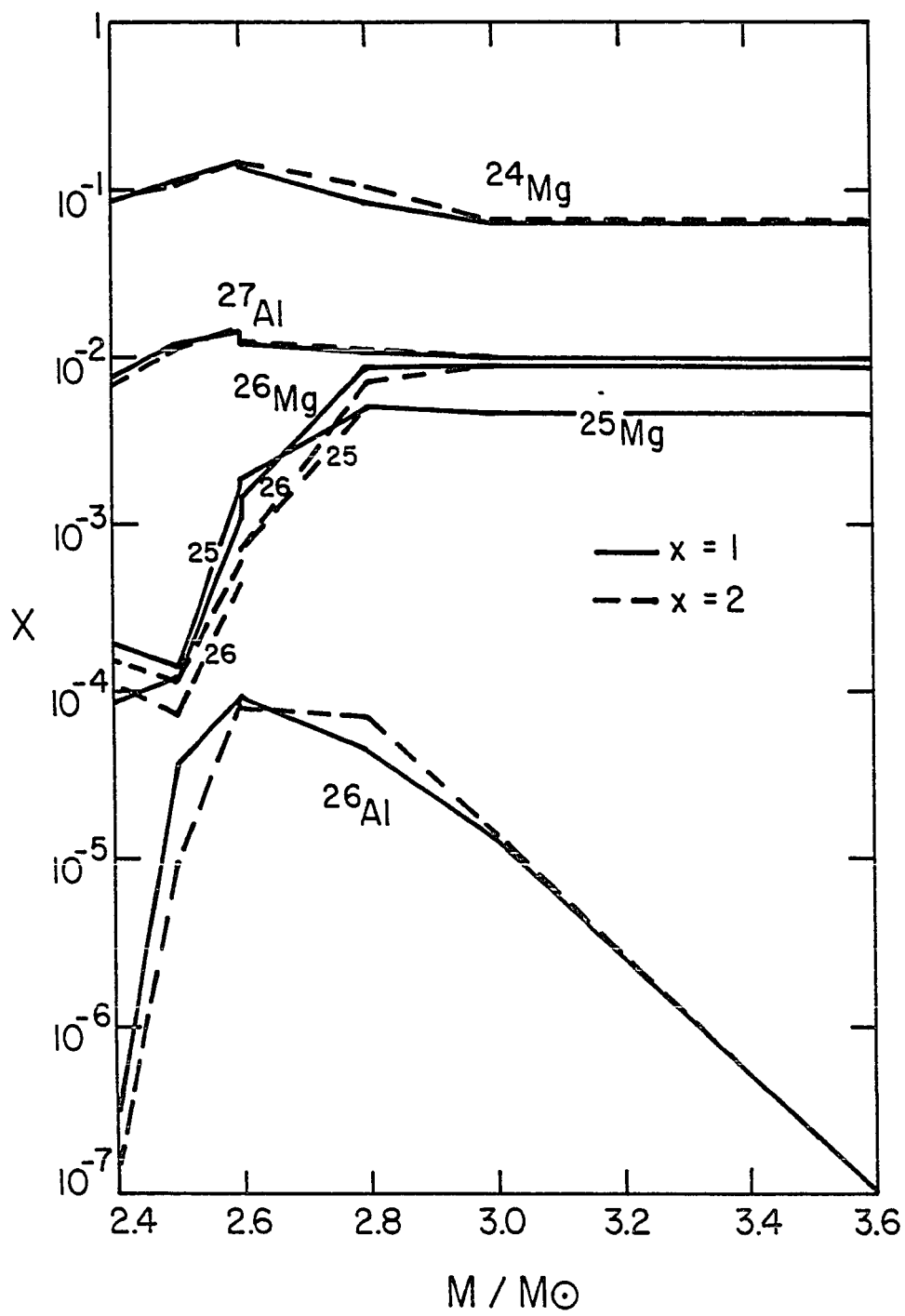
Species	2.4 M_{\odot}	2.5 M_{\odot}	Neon 2.6 M_{\odot}	Carbon 2.6 M_{\odot}	2.8 M_{\odot}	3.0 M_{\odot}	3.5 M_{\odot}
^{12}C	8.480×10^{-5}	8.701×10^{-4}	1.215×10^{-3}	8.557×10^{-3}	2.341×10^{-2}	3.890×10^{-2}	4.006×10^{-2}
^{16}O	7.251×10^{-1}	7.206×10^{-1}	6.917×10^{-1}	6.870×10^{-1}	5.918×10^{-1}	5.591×10^{-1}	5.590×10^{-1}
^{20}Ne	6.098×10^{-6}	1.081×10^{-3}	4.007×10^{-2}	4.671×10^{-2}	2.309×10^{-1}	2.986×10^{-1}	2.987×10^{-1}
^{22}Ne	9.040×10^{-8}	3.489×10^{-10}	2.415×10^{-7}	5.477×10^{-7}	4.201×10^{-5}	6.650×10^{-5}	7.850×10^{-5}
^{23}Na	4.389×10^{-6}	1.902×10^{-5}	4.935×10^{-5}	2.304×10^{-4}	9.899×10^{-4}	6.796×10^{-3}	7.255×10^{-3}
^{24}Mg	8.880×10^{-2}	1.108×10^{-1}	1.458×10^{-1}	1.376×10^{-1}	1.019×10^{-1}	6.232×10^{-2}	6.129×10^{-2}
^{25}Mg	1.657×10^{-4}	1.134×10^{-4}	5.936×10^{-4}	6.588×10^{-4}	5.110×10^{-3}	4.437×10^{-3}	4.428×10^{-3}
^{26}Mg	1.105×10^{-4}	7.099×10^{-5}	4.565×10^{-4}	6.946×10^{-4}	7.048×10^{-3}	9.057×10^{-3}	8.873×10^{-3}
^{26}Al	1.303×10^{-7}	9.641×10^{-6}	8.833×10^{-5}	7.919×10^{-5}	6.491×10^{-5}	1.374×10^{-5}	2.128×10^{-7}
^{27}Al	6.561×10^{-3}	1.158×10^{-2}	1.389×10^{-2}	1.247×10^{-2}	1.094×10^{-2}	9.564×10^{-3}	9.553×10^{-3}
^{28}Si	1.459×10^{-1}	1.239×10^{-1}	7.865×10^{-2}	7.719×10^{-2}	1.551×10^{-2}	7.117×10^{-3}	7.016×10^{-3}
^{29}Si	1.951×10^{-2}	1.899×10^{-2}	1.643×10^{-2}	1.800×10^{-2}	7.057×10^{-3}	1.662×10^{-3}	1.594×10^{-3}
^{30}Si	1.151×10^{-2}	8.414×10^{-3}	7.887×10^{-3}	6.878×10^{-3}	3.248×10^{-3}	1.022×10^{-3}	9.975×10^{-4}
^{31}P	1.120×10^{-3}	2.614×10^{-3}	2.309×10^{-3}	2.083×10^{-3}	6.882×10^{-4}	4.465×10^{-4}	4.472×10^{-4}

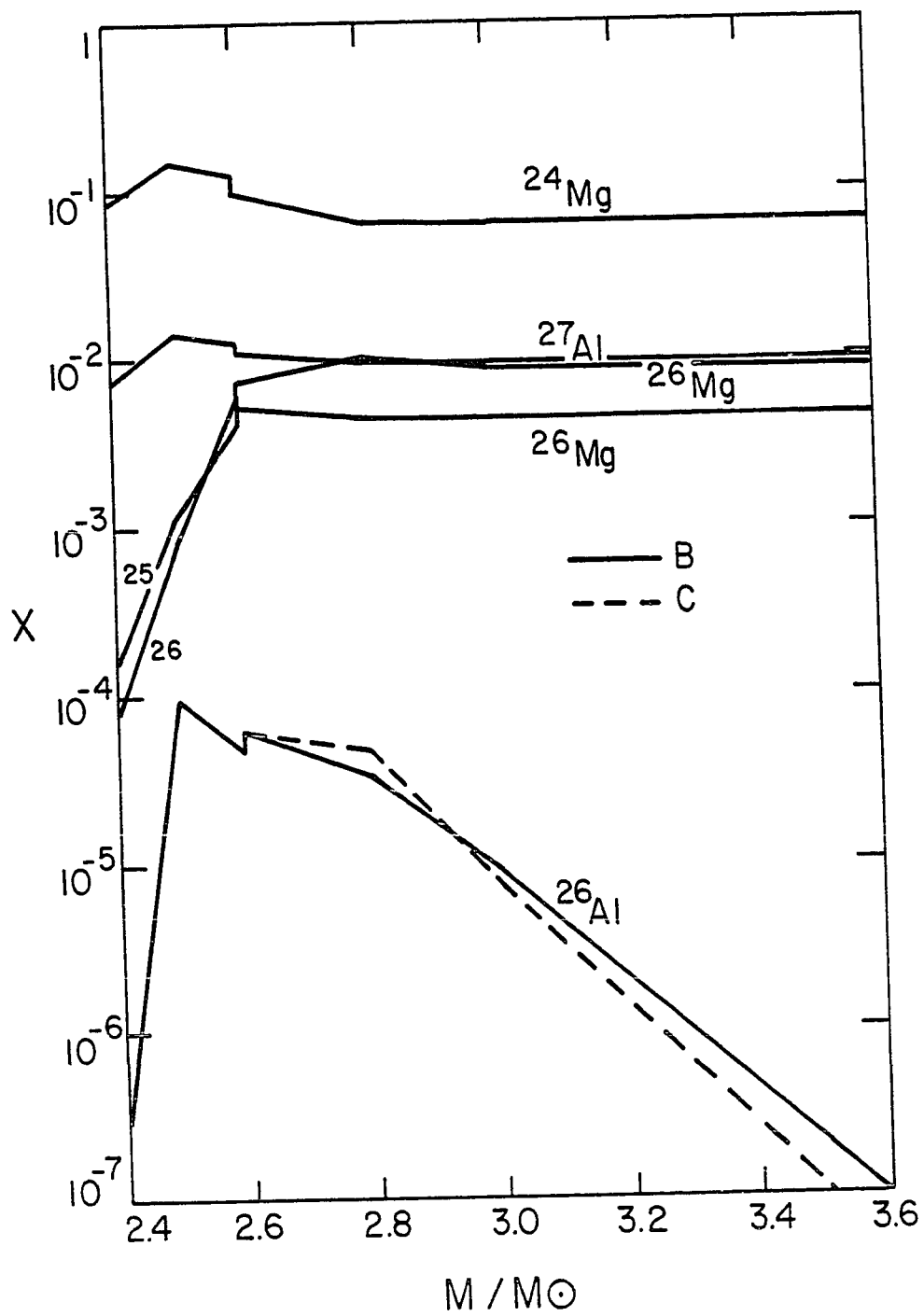
TABLE 7, continued:

Species	2.4 M_{\odot}	2.5 M_{\odot}	neon 2.6 M_{\odot}	carbon 2.6 M_{\odot}	2.8 M_{\odot}	3.0 M_{\odot}	3.5 M_{\odot}
peak ρ_5	10.98	7.86	6.43	6.43	4.76	3.16	1.81
peak τ_9	2.775	2.512	2.375	2.375	2.20	1.90	1.60
σ_1	5.54	5.69	5.81	5.81	6.06	6.02	6.22
$\Delta\sigma$	0.275	0.280	0.262	0.262	0.266	0.263	0.272

FIGURE 24 Distribution of nuclear burning products with mass in the supernova ejecta, at freezeout, for Model A with $\chi = 1$ and 2.

FIGURE 25 Same as for Figure 25, for Models B and C with $\chi = 1$.





leading to integrated abundances which show only small differences from the case with $\chi = 1$.

The same qualitative behavior appears in Figure (25) for profiles B and C; the final abundances for Mg and ^{27}Al change little, although ^{26}Al shows some differences. Compared to Model A, the systematic alteration of the pattern for Models B and C causes the small peak in ^{24}Mg and ^{27}Al to move in in mass, whereas setting $\chi = 2$ in Model A causes these features to move out in mass. As before, the qualitative features of the distribution and the integrated yields will not differ significantly, in light of uncertainties in reaction rates, from the results for Model A. However, for completeness, Table (8) presents the raw nucleosynthetic yields for profiles B and C, where the figures for $2.4 M_{\odot}$ from Model A have been used in Models B and C, as the slightly higher peak conditions in Model A should occur in Models B and C at a point slightly interior to $2.4 M_{\odot}$, according to Figure (24). Simple interpolation suggests this happens at $2.38 M_{\odot}$, close enough for astrophysics.

Before proceeding to the calculation of bulk yields, it is both interesting and suggestive to examine briefly the energetics of Model A. A tacit assumption of the approach taken to the hydrodynamics of mass ejection in these calculations is that the thermonuclear explosion which accompanies shock passage plays an ancillary role in the dynamics, as discussed by Arnett (1978), and in contrast to earlier notions of detonation of nuclear fuel in supernovae (Fowler and Hoyle, 1964; Arnett, 1969, 1969a). The energetics figures provided by BRUNO make possible a kind of consistency test of this assumption, when compared

TABLE 8

Raw Yields for Models B and C, with $X = 1$

Species	$2.5 M_{\odot}$ B,C	neon $2.6 M_{\odot}$ B,C	carbon $2.6 M_{\odot}$ B,C	$2.8 M_{\odot}$ B	$2.8 M_{\odot}$ C	$3.0 M_{\odot}$ B	$3.0 M_{\odot}$ C	$3.5 M_{\odot}$ C
^{12}C	1.281×10^{-3}	1.384×10^{-3}	2.499×10^{-2}	3.709×10^{-2}	3.824×10^{-2}	3.989×10^{-2}	4.002×10^{-2}	4.006×10^{-2}
^{16}O	6.753×10^{-1}	6.035×10^{-1}	5.899×10^{-1}	5.606×10^{-1}	5.596×10^{-1}	5.590×10^{-1}	5.590×10^{-1}	5.590×10^{-1}
^{20}Ne	6.948×10^{-2}	2.106×10^{-1}	2.351×10^{-1}	2.960×10^{-1}	2.978×10^{-1}	2.987×10^{-1}	2.967×10^{-1}	2.987×10^{-1}
^{22}Ne	9.715×10^{-7}	2.202×10^{-5}	4.570×10^{-5}	4.619×10^{-5}	5.458×10^{-5}	7.715×10^{-5}	7.829×10^{-5}	7.853×10^{-5}
^{23}Na	8.208×10^{-5}	2.597×10^{-4}	9.766×10^{-4}	5.125×10^{-3}	6.134×10^{-3}	7.211×10^{-3}	7.249×10^{-3}	7.256×10^{-3}
^{24}Mg	1.482×10^{-1}	1.244×10^{-1}	9.859×10^{-2}	6.531×10^{-2}	6.339×10^{-2}	6.141×10^{-2}	6.132×10^{-2}	6.129×10^{-2}
^{25}Mg	1.132×10^{-3}	4.174×10^{-3}	5.146×10^{-3}	4.454×10^{-3}	4.438×10^{-3}	4.429×10^{-3}	4.426×10^{-3}	4.428×10^{-3}
^{26}Mg	8.299×10^{-4}	6.284×10^{-3}	7.098×10^{-3}	9.675×10^{-3}	9.329×10^{-3}	8.891×10^{-3}	8.875×10^{-3}	8.872×10^{-3}
^{26}Al	9.415×10^{-5}	4.665×10^{-5}	5.955×10^{-5}	3.286×10^{-5}	4.769×10^{-5}	8.806×10^{-6}	7.455×10^{-6}	1.071×10^{-7}
^{27}Al	1.377×10^{-2}	1.281×10^{-2}	1.078×10^{-2}	9.665×10^{-3}	9.597×10^{-3}	9.554×10^{-3}	9.553×10^{-3}	9.553×10^{-3}
^{28}Si	6.351×10^{-2}	2.198×10^{-2}	1.511×10^{-2}	7.488×10^{-3}	7.245×10^{-3}	7.027×10^{-3}	7.018×10^{-3}	7.016×10^{-3}
^{29}Si	1.564×10^{-2}	8.121×10^{-3}	6.993×10^{-3}	1.969×10^{-3}	1.766×10^{-3}	1.600×10^{-3}	1.595×10^{-3}	1.593×10^{-3}
^{30}Si	7.699×10^{-3}	4.429×10^{-3}	3.270×10^{-3}	1.140×10^{-3}	1.062×10^{-3}	9.996×10^{-4}	9.978×10^{-4}	9.974×10^{-4}
^{31}P	2.093×10^{-3}	1.086×10^{-3}	6.683×10^{-4}	4.430×10^{-4}	4.450×10^{-4}	4.471×10^{-4}	4.472×10^{-4}	4.472×10^{-4}
peak ν_5	7.10	5.69	5.69	4.05	3.88	2.80	2.44	1.57
peak τ_9	2.4	2.25	2.25	2.05	2.00	1.80	1.70	1.50
α_1	5.69	5.81	5.81	6.06	6.06	6.02	6.02	6.22
λ_{d}	0.180	0.161	0.161	0.138	0.103	0.161	0.085	0.150

with $\frac{1}{2} v_{ps}^2$, the kinetic energy/mass imparted by the shock. The integrated nuclear energy release, tabulated for selected mass zones from Model A appears in Table (9) alongside $\frac{1}{2} v_{ps}^2$ and the ratio of representative values of the neutrino energy loss to the nuclear energy generation for each zone. These last are much less than unity, implying that neutrino losses play a negligible part in the dynamics of shock passage. The nuclear energy released in the inner zones of the model ($m \leq 3.0 M_{\odot}$) exceeds the kinetic energy density of the shocked matter, and may thus play a role in the dynamics of the postshock expansion. It is, however, released over a fairly long period of time, $t \gtrsim 0.1 \tau_{HD}$, and should not affect shock propagation in this model. The integrated nuclear energy released is about 2.1×10^{50} ergs, significantly smaller than $\frac{1}{2}(M_{\alpha} - m)v_{ps}^2 = 8.78 \times 10^{50}$ ergs for Model A at $4.0 M_{\odot}$.

2. Bulk Isotopic Yields

The mass fractions of the major burning products for Model A are obtained by integrating over the raw nucleosynthetic yields from Table (6), and multiplying by $1 M_{\odot} = 1.989 \times 10^{33}$ g to convert to grams. The results of a trapezoidal rule integration, extended over the unprocessed material with $m > 3.5 M_{\odot}$, where the post-helium burning abundances used to start static carbon burning are taken for $7.0 \leq m/M_{\odot} \leq 8.0$, appear in Table (10). The integrated isotopic ratios for Mg and Al, which are crucial to an assessment of the supernova trigger hypothesis, are

TABLE 9

Energetics Figures for Selected Zones

M/M_{\odot}	$\Delta E_{\text{nuc}} (\text{erg g}^{-1})$	$\frac{1}{2} v_{\text{ps}}^2 (\text{erg g}^{-1})$	$\bar{\epsilon}_v / \bar{\epsilon}_{\text{nuc}}$
2.4	2.35×10^{17}	1.45×10^{17}	1.4×10^{-6}
2.5	2.62×10^{17}	1.33×10^{17}	1.75×10^{-6}
2.6*	3.50×10^{17}	1.24×10^{17}	8.00×10^{-6}
2.8	7.90×10^{16}	1.19×10^{17}	4.00×10^{-5}
3.0	9.65×10^{16}	1.01×10^{17}	8.00×10^{-4}

* carbon burning only

TABLE 10

Model A Integrated Yields of Major Burning Products,
 $2.4 \leq M/M_{\odot} \leq 8.0$, in grams

Species	$X = 1$	$X = 2$	neon (average, 1.4-2.6)	carbon (2.6-3.5)	carbon (3.5-7.0)	post-helium (7.0-8.0)
^{12}C	9.46×10^{32}		3.74×10^{29}	6.29×10^{31}	2.79×10^{32}	6.05×10^{32}
^{16}O	6.53×10^{33}		2.80×10^{32}	1.03×10^{33}	3.89×10^{33}	1.33×10^{33}
^{20}Ne	2.58×10^{33}		1.07×10^{31}	4.82×10^{32}	2.08×10^{33}	5.89×10^{30}
^{23}Na	5.96×10^{31}		1.57×10^{28}	9.09×10^{30}	5.05×10^{31}	2.65×10^{28}
^{24}Mg	6.09×10^{32}	6.59×10^{32}	4.74×10^{31}	1.34×10^{32}	4.27×10^{32}	2.67×10^{29}
^{25}Mg	5.10×10^{31}	5.07×10^{31}	2.16×10^{28}	7.67×10^{30}	3.08×10^{31}	1.23×10^{31}
^{26}Mg	8.48×10^{31}	8.38×10^{31}	1.55×10^{29}	1.45×10^{31}	6.18×10^{31}	8.35×10^{30}
^{26}Al	6.19×10^{28}	6.20×10^{28}	1.70×10^{28}	4.50×10^{28}	$\lesssim 10^{26}$	
^{27}Al	9.02×10^{31}	9.03×10^{31}	4.54×10^{30}	1.80×10^{31}	6.65×10^{31}	1.22×10^{30}
^{28}Si	1.15×10^{32}		4.22×10^{31}	2.26×10^{31}	4.88×10^{31}	1.10×10^{30}
^{29}Si	2.56×10^{31}		7.26×10^{30}	6.88×10^{30}	1.11×10^{31}	3.92×10^{29}
^{30}Si	1.83×10^{31}		3.37×10^{30}	6.77×10^{30}	6.94×10^{30}	1.20×10^{30}
^{31}P	5.26×10^{30}		8.51×10^{29}	1.08×10^{30}	3.11×10^{30}	2.15×10^{30}

$$^{25/24}\text{Mg} = 8.05 \times 10^{-2} \quad 64\% \quad (5.1a)$$

$$^{26/24}\text{Mg} = 1.286 \times 10^{-2} \quad 92\% \quad (5.1b)$$

$$^{26/27}\text{Al} = 7.123 \times 10^{-4}$$

$$^{27}\text{Al}/^{24}\text{Mg} = 1.318 \times 10^{-1} \quad 115\% \quad (5.1c)$$

Percentages next to the stable isotope ratios are the fraction of the solar system values reported by Catanzano et al. (1966). The yield of ^{26}Al by mass is

$$^{26}\text{Al} = 6.19 \times 10^{28} \text{g} \quad (5.2a)$$

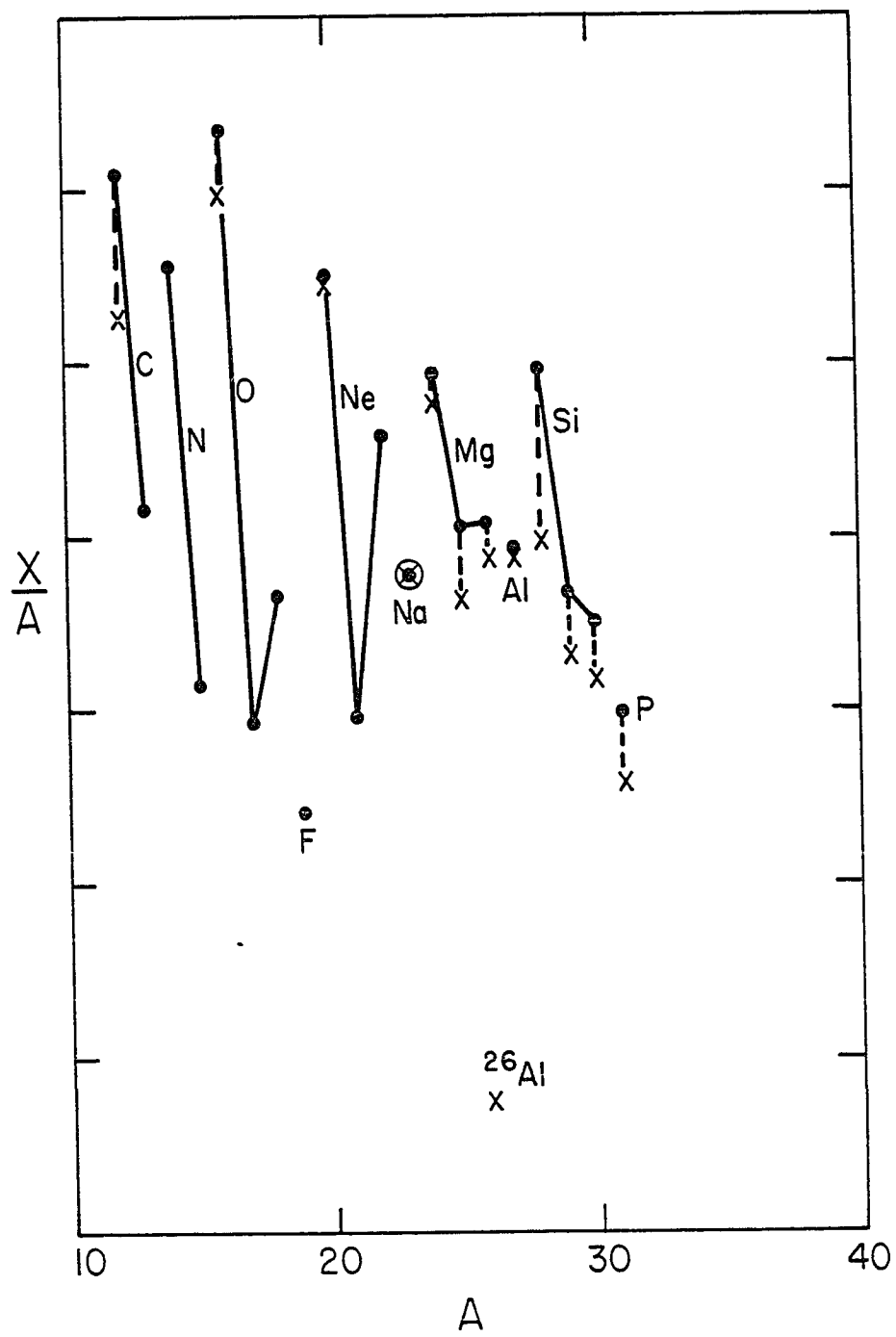
$$= 10.36 M_{\odot} \quad (5.2b)$$

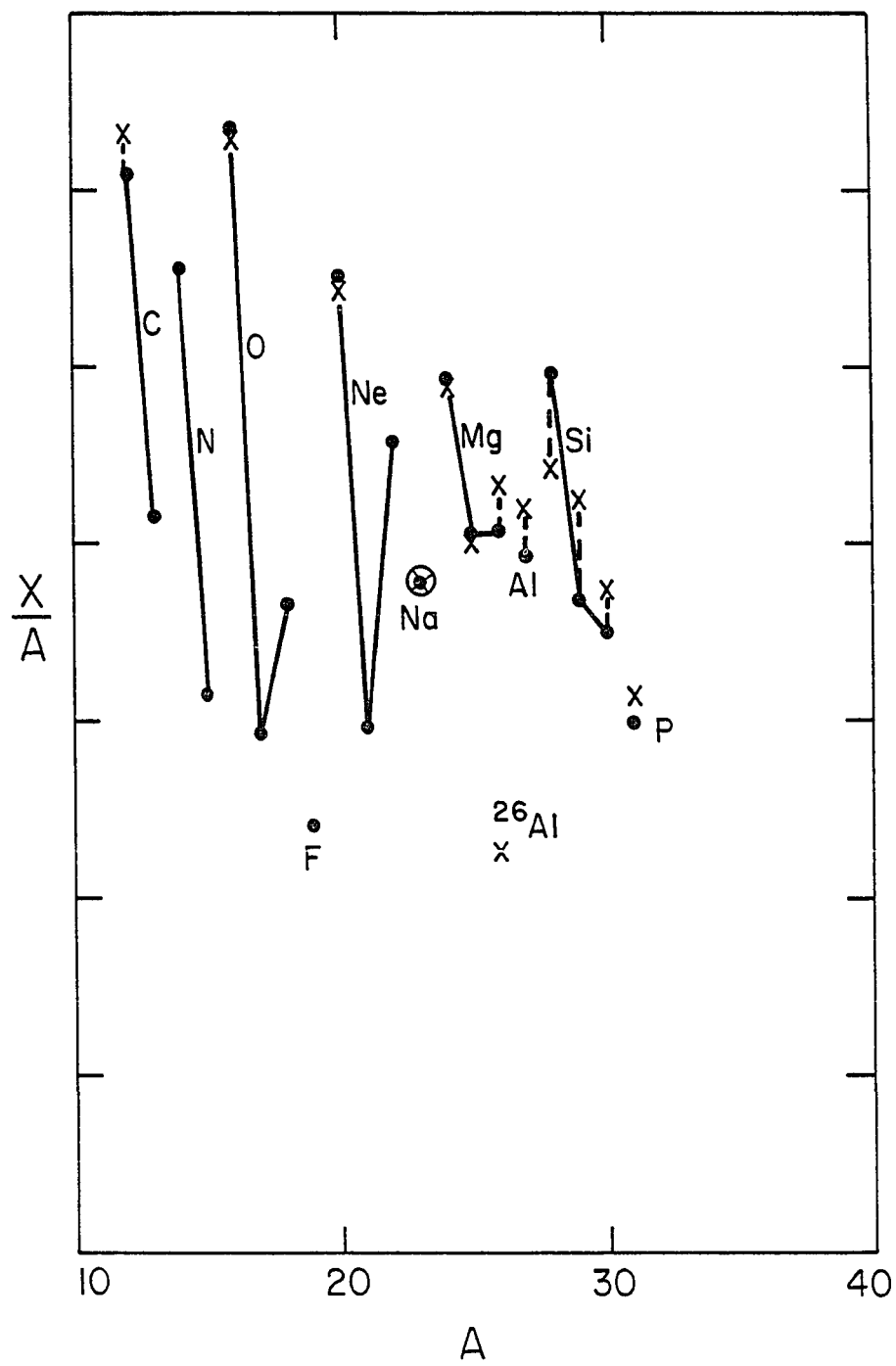
in terms of a more memorable unit. Table (9) also includes integrated yields for various subdivisions of the mass interval 2.4-8.0 M_{\odot} , including the post-helium burning abundances supplied by Arnett.

The bulk abundances represented by Table (6) appear plotted against the solar system pattern from Cameron (1973) in Figure (26). Overall, as comparison with Figure (27) shows, the yields resemble the results of standard ECB fairly closely (excluding ^{12}C and ^{16}O), even though the pattern is something like 90% due to static burning products ejected with no alteration. There is a systematic trend of slightly underproducing the nuclei heavier than ^{24}Mg relative to the standard case, which is worst for Si, and, of course, the general level of burning products relative to ^{12}C in this model is very much greater than in an explosion that starts out with $X(^{12}\text{C}) = 50\%$, but the qualitative agreement at the factor-of-two level with both standard ECB and

FIGURE 26 Integrated final abundances for neon, carbon, and post-helium burning zones in Model A.

FIGURE 27 Final abundances for standard explosive carbon burning.





with the solar system pattern for $20 \leq A \leq 27$ is encouraging.

The isotopic yields for the region between the neon zone and the helium zone may be incorporated into a crude model for the bulk yields of the elements between carbon and silicon by augmenting them with estimates of the yield of α -particle nuclei from the rest of the star, on the reasonable assumption that very little of the important non- α -particle nuclei come from outside these zones. A small network including only (α, γ) links on ^{12}C , ^{20}Ne , ^{24}Mg and ^{28}Si was used to estimate the yields from oxygen burning at 2.1 and 2.3 M_{\odot} with $\chi = 1$; these results showed little change when $\chi = 1$ and $\chi = 10$ were used. For regions exterior to the helium core, the required abundances were estimated from Figure 2a of Weaver et al. (1978). Finally, 0.2 M_{\odot} of matter with $\approx 60\%$ ^{28}Si was added arbitrarily in order to simulate the ejection of unburned silicon from beneath the oxygen zone. The resulting abundances, shown in Figure (28), are intended mainly for heuristic purposes, as an example of the way ejecta from a massive star might approximate the "cosmic" abundance pattern. Note that ^{12}C , ^{16}O , ^{20}Ne and ^{24}Mg change little from Figure (26). The relative underproduction of ^{12}C in this model reflects a curious property of Weaver et al.'s model, which may mean that most ^{12}C does not come from stars like the "typical nucleosynthetic event" of $m \gtrsim 20 M_{\odot}$, but rather from stars of lower mass. The Mg and Al figures become

$$^{25}/^{24}\text{Mg} = 7.592 \times 10^{-2} \quad 60\% \quad (5.3a)$$

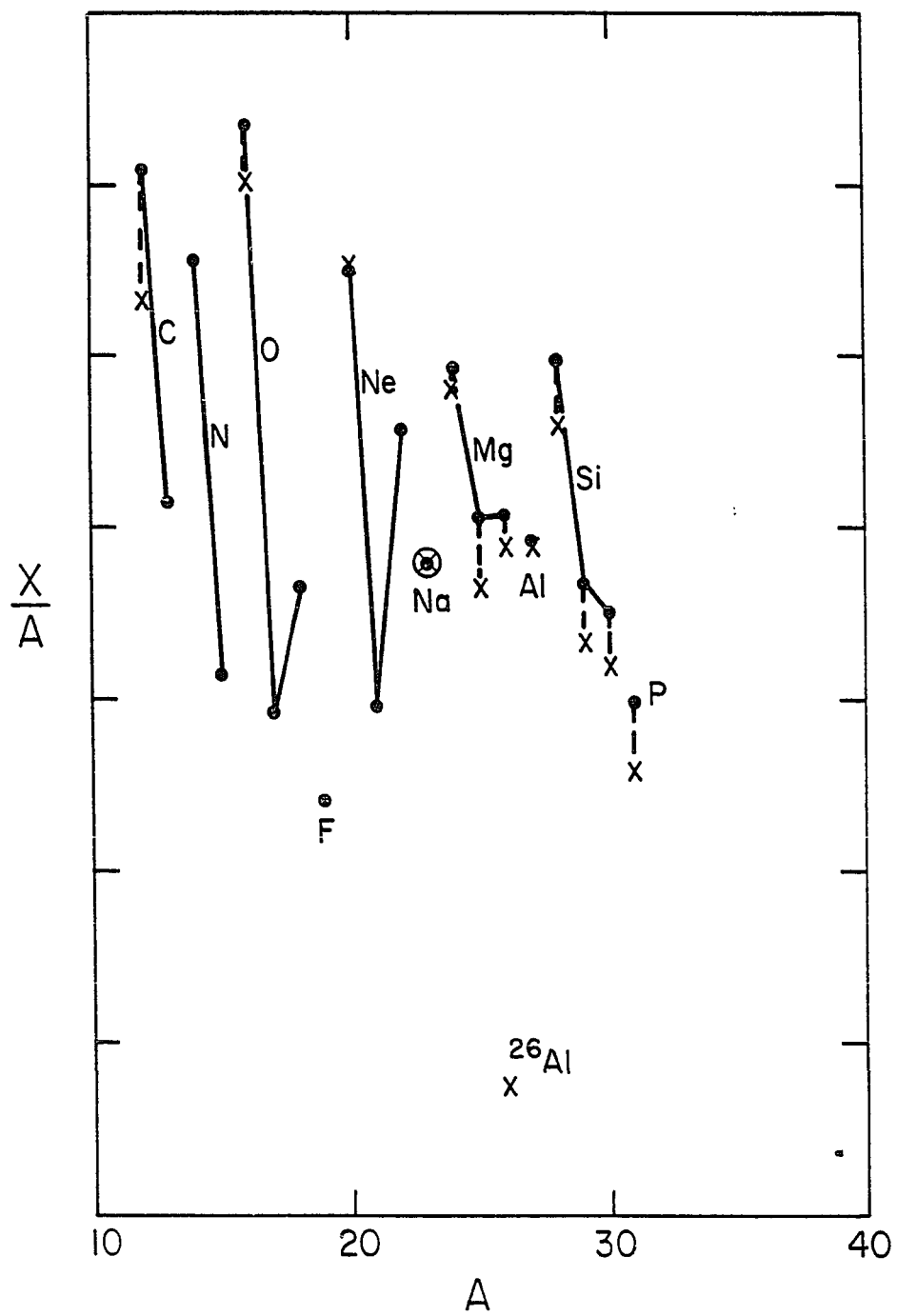
$$^{26}/^{24}\text{Mg} = 1.213 \times 10^{-1} \quad 84\% \quad (5.3b)$$

$$^{24}\text{Al}/^{24}\text{Mg} = 1.243 \times 10^{-1} \quad 109\% \quad (5.3c)$$

for the whole star.

FIGURE 28

Integrated final abundances for the
whole star, Model A.



3. Neutron Capture Synthesis of Heavy Nuclei

The free neutron histories in Figures (22) and (23) allow one to estimate the importance of neutron capture on heavy seed in explosive neon and carbon burning for the production of the long-lived radioactivities ^{129}I ($t_{1/2} = 15.9 \times 10^6 \text{ yr}$) and ^{40}K ($1.28 \times 10^9 \text{ yr}$), and of the short-lived ^{107}Pd ($6.5 \times 10^6 \text{ yr}$), all of which play a role in solar system chronology. In the model of Cameron and Truran (1977), the triggering supernova does not inject much r-process material, allowing the ^{244}Pu and ^{129}I chronologies conventionally interpreted in terms of galactic nucleosynthesis to be produced by the late trigger, so a "mini-r-process" accompanying explosive nucleosynthesis in various zones is invoked to produce certain key heavy nuclei. This process, very similar to one proposed by Howard *et al.* (1972) in order to account for rare light nuclei, assumes that the neutron burst from explosive carbon burning is sufficiently intense to cause rapid, multiple capture on a pre-existing set of seed nuclei.

As free neutron levels in explosive carbon and neon burning in this study are typically one to two orders of magnitude lower than those given by "standard" ECB, it is not clear that any such mechanism can operate. The number of neutron captures/heavy seed proposed by Cameron and Truran, of order 10/seed, contrasts sharply with the maximum of 2 captures/ ^{56}Fe estimated for neon burning at $2.4 M_{\odot}$ of Model A (see Table (11)). Although the oversimple prescription used to account for the role of heavy nuclei in the neutron economy may distort the free neutron history somewhat, the integrated neutron exposure is

TABLE 11

Estimated Neutron Exposures

M/M_{\odot}	captures/ ^{56}Fe	ϕ (sec)
2.4	1.9	6×10^{-13}
2.5	1.3	4×10^{-13}
2.6 (neon)	1.0	1.6×10^{-13}
2.6 (carbon)	1.7	1.2×10^{-12}
2.8	0.42	1.6×10^{-13}
3.0	0.0047	2.5×10^{-15}
3.5	$< 10^{-5}$	---

dictated largely by the amount of nuclear burning that takes place under the constraints of thermodynamics and timescales, and the results of the explosive survey may thus be used to place limits on the possible enhancement of heavy nuclei by neutron capture in the mantle of a massive supernova.

Consider a chain of nuclei connected by (n,γ) links; they may be successive members of the s-process path along the stability line, or isotopes of a single element, as in this discussion, so long as the chain of transmutations is unique. Then the evolution of abundances of members of the chain is given by

$$\frac{dY_1}{dt} = -\lambda_1 Y_n Y_1 \quad (5.4a)$$

$$\frac{dY_2}{dt} = -\lambda_2 Y_n Y_2 + \lambda_1 Y_n Y_1 \quad (5.4b)$$

$$\begin{array}{c} \dots \\ \frac{dY_k}{dt} = -\lambda_k Y_n Y_k + \lambda_{k-1} Y_n Y_{k-1} \end{array} \quad (5.4c)$$

where the λ_k are (n,γ) rates as defined in Chapter II. The system (5.4) has an elegant analytic solution, the Bateman solution (Clayton, 1968, pp.563-565). Here we simply quote the solution for the case $k = 3$, for a chain of three isotopes exposed for time Δt to a constant neutron level Y_n , experiencing an integrated exposure

$$\phi = Y_n \Delta t \quad (5.5)$$

The (n,γ) rates are also taken to be constant. The solution is

$$Y_1(\Delta t) = Y_1(0) \exp(-\lambda_1 \phi) \quad (5.6a)$$

$$Y_2(\Delta t) = Y_1(0) \left[\frac{\lambda_1}{\lambda_2 - \lambda_1} \right] \left[\exp(-\lambda_1 \phi) - \exp(-\lambda_2 \phi) \right] \quad (5.6b)$$

$$Y_3(\Delta t) = Y_1(0) \lambda_1 \lambda_2 \left[\frac{\exp(-\lambda_1 \phi)}{(\lambda_3 - \lambda_1)(\lambda_2 - \lambda_1)} + \frac{\exp(-\lambda_2 \phi)}{(\lambda_3 - \lambda_2)(\lambda_1 - \lambda_2)} + \frac{\exp(-\lambda_3 \phi)}{(\lambda_2 - \lambda_3)(\lambda_1 - \lambda_3)} \right] \quad (5.6c)$$

This simple solution may not hold under conditions of sufficiently high temperature or sufficiently low free neutron density, if photodisintegration significantly impedes the addition of neutrons; in analogy to the r-process, one expects that as successive neutron captures drive seed nuclei towards neutron-rich isotopes, neutron separation energies, and thus (γ,n) lifetimes, will decrease until a point is reached at which the photodisintegration lifetime is shorter than that for neutron capture on the nearest neighbor to the neutron-poor side. This terminus for the capture chain is called a "waiting point" in discussions of the r-process. The ratio of the photodisintegration lifetime at mass $A + 1$ to the neutron capture lifetime at mass A is (Clayton, 1968, p.584)

$$\log_{10} \left(\tau_{(\gamma,n)}^{A+1} / \tau_{(n,\gamma)}^A \right) = \log_{10} \left(\frac{G_{A+1}}{G_A} \right) + \log_{10} N_n - \frac{3}{2} \log \left(\frac{A}{A+1} \right) T_9 + \frac{5.031}{T_9} S_n^{A+1} - 34.075 \quad (5.7)$$

where G_A is the partition function for nucleus A , N_n is the neutron density in cm^{-3} , and S_n^{A+1} is the neutron separation for mass $A + 1$ in MeV. Table (12) shows $\log_{10} \left[\tau_{(\gamma,n)} / \tau_{(n,\gamma)} \right]$ for a number of potential parents of ^{129}I , ^{107}Pd and ^{40}K evaluated for peak neutron densities and temperatures in the base of the neon zone ($2.4 M_\odot$) and for two locations in the carbon zone (2.6 and $2.8 M_\odot$). Evidently, any nucleus with $S_n \lesssim 7.2\text{--}7.5$ MeV, depending on the location, has $\log_{10} \left[\tau_{(\gamma,n)} / \tau_{(n,\gamma)} \right] < 0$ and will thus photodisintegrate as fast as it is formed by neutron capture. In practice, this means that the heavy seed from which ^{107}Pd or ^{129}I are to be made can capture at most 2-3 neutrons before reaching a waiting point, even though approximately 10 neutrons may be available for capture, as estimated by Cameron and Truran. Furthermore, as has been emphasized in discussions of the production of CCF Xe by Heymann and Dzickaniec (1979), the rapid fall off of free neutrons during the late stages of explosive burning while temperatures are still high will mean that photodisintegration may well dominate the overall flows for many nuclei, perhaps leading to the formation of neutron-poor isotopes (Woosley and Howard, 1977). The neon zones, which experience a short but intense neutron burst, may be especially prone to this kind of late (γ,n) erosion.

These imponderables make any quantitative estimates of ^{129}I or ^{107}Pd production treacherous without careful analysis. It seems clear, however, that interesting amounts of synthesis can in principle occur. The most favorable parent for ^{129}I is ^{128}Te , and for ^{107}Pd , ^{106}Pd .

TABLE 12

Comparison of Neutron Capture and Photodisintegration
Lifetimes for Selected Nuclei (peak explosive conditions)

Species	Sn	$\log_{10} \left[\tau_{(\gamma,n)}^{A+1} / \tau_{(n,\gamma)}^A \right]$		
		2.4 M_{\odot}	2.6(carbon)	2.8 M_{\odot}
^{126}Te	9.11 MeV	-1.596	-1.181	-1.266
^{127}Te	6.296	0.479	1.658	2.112
^{128}Te	8.772	-1.983	-1.632	-1.789
^{129}Te	6.087	-0.153	0.915	1.338
^{130}Te	8.413	-2.504	-2.205	-2.349
^{105}Pd	---	2.128	3.551	4.120
^{106}Pd	9.561	-1.158	-0.667	-0.703
^{107}Pd	6.543	1.449	2.767	3.228
^{108}Pd	9.225	-1.837	-1.466	-1.590
^{104}Pu	---	-2.658	-2.363	-2.134
^{39}K	---	0.544	1.423	1.627
^{40}K	7.800	3.547	5.134	5.736
^{41}K	10.096	-0.431	0.367	0.537

Both nuclei are waiting points. The ratio of productive to destructive lifetimes from Table (7) shows that steady-state leakage results in transient concentrations in the range $1-2 \times 10^{-2}$ for $^{129/128}\text{Te}$ and $7 \times 10^{-2} - 2 \times 10^{-1}$ for $^{107/106}\text{Pd}$. One must bear in mind that these figures apply only to the peak conditions in each zone, during the early part of the explosion, as discussed in the preceding paragraph, and may not reflect the levels that survive the explosion. Finally, $S_n = 8.84$ MeV for ^{129}I and $= 6.457$ MeV for ^{130}I , so that any leakage to mass 129 in iodine will likely halt there.

The Bateman solution (5.6) may be applied to estimate the alteration that occurs in the isotopes of potassium, as photodisintegration is less important, especially in the carbon zone. Equations (5.6) were evaluated for the three locations used for the estimates of heavy-nucleus synthesis, with (n, γ) rates estimated from the tables of Woosley et al. (1975) and neutron exposures taken from Table (11): $^{40/39}\text{K} = 8.3 \times 10^{-1}$ ($2.4 M_\odot$), 9.7×10^{-1} ($2.6 M_\odot$, carbon), and 9.9×10^{-2} ($2.8 M_\odot$). Equations (5.6) actually overestimate the ^{40}K production, as the diminished efficacy of $^{39}\text{K}(n, \gamma)^{40}\text{K}$ because of photodisintegration is not taken into account. It does seem, however, as if the possibility exists of making $^{40/39}\text{K} \approx 1$ in at least part of the neon and carbon zones.

4. Possible Effects of Dust Formation

The distribution of burning products with mass in the ejecta is of great interest with respect to dust formation. A few comments on the possibilities can be made on the basis of Figures (24) and (25),

and Table (10). First, the Al/Mg ratio is essentially constant over the entire neon-carbon portion of the mantle, so that there is no way to implant a distinct chemistry which correlates very strongly with the gradient of the heavier isotopes that occurs near the base of the carbon zone and throughout the neon zone. Second, any surviving imprint of such a correlation will produce a negative ^{26}Mg anomaly of about the same level as the residual anomaly in ^{25}Mg , as the ^{26}Mg contributed by ^{26}Al decay will be at a much smaller level. Most Al resides in MgAl_2O_4 (Spinel; Clayton, 1977), so that the ^{26}Al contribution will be wiped out. On the other hand, most Mg resides in minerals devoid of Al, and the noise level in the isotopic content of individual dust grains will cause a much larger range of variations in the matter from which chondritic inclusions form, so it is hard to see how to account for positive ^{26}Mg excesses very easily. On the other hand, there is the possibility of explaining the odd spinel with a deficit of ^{26}Mg , as observed by Lee et al. (1977b).

CHAPTER VI

DISCUSSION

The preceding chapters have elaborated the nucleosynthetic history of the elements with $20 \leq A \leq 30$ contributed by the carbon- and neon-burning zones of a massive star which ends its life as a supernova. Apart from the interest of a nucleosynthetic model of the explosion products of an O star to nucleosynthesis generally, the model developed in these pages represents a significant improvement upon idealized "standard" explosive nucleosynthesis calculations for purposes of estimating the effect of a late supernova injection on the early solar system on two grounds: (1) The inclusion of static burning results in more realistic starting abundances for the explosion. (2) The model for shock passage provides meaningful constraints on peak burning conditions for differing locations in the presupernova mantle. Predictions of the model therefore allow a more quantitative evaluation of aspects of the supernova trigger hypothesis than Cameron and Truran were able to provide, but some caution should be exercised in this application. In particular, the choice of a $25 M_{\odot}$ star for the model, dictated by the assumption that a supernova whose progenitor mass lies close to the mass of the average contributor to galactic nucleosynthesis (Arnett and Schramm, 1973; Arnett, 1978) will inject

matter with nearly solar abundance patterns, which constraint can then be used as a requirement of the model, is a likely, but not necessarily the best possible, choice for the progenitor of a solar system trigger. In some ways, $15 M_{\odot}$, identified by Arnett and Schramm (1973) as the progenitor mass for the average supernova, is a more advantageous value. The presupernova abundances will differ in such a case from those reported here, as examination of Figure 4 of Reeves (1978) shows, and the systematics of explosive burning will also change somewhat. However, such effects should not make qualitative changes from the main results of this study.

The following conclusions may be drawn from the results presented in the preceding chapter.

1. Of the elements ejected primarily from the region between the neon shell source and the base of the hydrogen envelope of the presupernova star, roughly 90% of their production occurs during hydrostatic carbon burning prior to the final outburst. In the model, this effect comes about because of the impossibility of shocking most of the carbon zone to explosive conditions without at the same time exposing too much matter near the base of the zone to conditions outside the allowed range of carbon burning parameters or imparting kinetic energies $> 10^{51}$ ergs to the ejecta. This conclusion agrees with the argument of Arnett (1978) that extensive explosive modification of the products of static nuclear burning would seriously distort the yields of major burning products

2. ^{26}Al represents a departure from this pattern, being produced almost entirely during the explosion. A significant contribution ($\approx 30\%$) to the final production comes from explosive neon burning. The $^{26}/^{27}\text{Al}$ ratio in the ejecta, $\approx 7 \times 10^{-4}$, is near the lower limit suggested by Cameron and Truran for the trigger.

If we assume a free-decay interval for the ^{26}Al of $\approx 10^6$ yr, then the initial ratio $^{26,27}\text{Al}$ in the Allende inclusions (and possibly in Murchison and Leoville) allows a dilution by "normal" matter of at most 4.5; assuming no decay allows a maximum dilution of the injected Al of 12. Therefore, the ejecta must have been mixed with other protosolar matter in a highly inhomogeneous manner. The isotopic yields of this model are thus consistent with the possibility of a supernova trigger in terms of the crucial ^{26}Al abundance, if we assume the material that formed the chondrites somehow managed to receive a heavy dose of it. There is another simple calculation one can do with the $^{26}/^{27}\text{Al}$ ratio, suggested by Reeves, who argues that if the solar system formed in an OB association, there is no real need for a single supernova trigger, as $\gtrsim 20$ massive stars can be expected to supernova during the few million years the protosolar cloud might be expected to take in passing to a solar nebula with meteoritic parent bodies, so that it should be liberally sprayed with supernova fallout. Consider an interstellar cloud of $\approx 10^5 M_{\odot}$, contaminated with the debris from ≈ 20 supernovae. By Reeve's (1978) estimate, this cloud will contain $\approx 8.1 M_{\odot}$ of ^{27}Al ; it will also have $20 \times 6.2 \times 10^{28} \text{ g} = 6.2 \times 10^{-4} M_{\odot}$ of ^{26}Al for an average ambient ratio (assuming no decay) of $^{26}/^{27}\text{Al} = 8.0 \times 10^{-5}$.

in the cloud. An average free decay period of 2.9×10^5 yr will bring this down to 6×10^{-5} . A bonus for star formation comes from the observation by Lada et al. (1978) that luminous members of an OB association are capable of driving a shock into dense clouds; potentially, an O star might do as much damage with its ionization front as by exploding, for the energies in the two processes are similar. Thus a nearby supernova could conceivably contaminate a cloud which has already been forced to collapse by such a process. This scenario might help explain the small amount of dilution or free decay the ^{26}Al can have experienced.

3. While photodisintegration limits the number of neutron captures on heavy seed nuclei which can accompany the explosion, it appears that favorable conditions for the production of the long-lived radioactivities ^{129}I , ^{107}Pd , and ^{40}K at some non-trivial level exist in the explosive burning of the carbon and neon zones, which together correspond to the "carbon" zone in the study of Cameron and Truran, who invoke a rapid neutron capture sequence as a source of long-lived cosmochronometers.

In summary, we have shown that the ^{26}Al production from a massive supernova is consistent with values assumed in theories for the origin of ^{26}Mg excesses in chondritic meteorites which provide some role for a supernova explosion in the events surrounding the origin of the solar system and in star formation generally.

BIBLIOGRAPHY

- Allen, Macklin and Gibbons 1971, Nucleosynthesis and Neutron Capture Cross Sections, in Advances in Nuclear Physics, Vol. 4, eds. M. Baranger and E. Vogt (Plenum Press).
- Arnett, W. D. 1969, Astrophys. J., 157, 1369.
- Arnett, W. D. 1969a, Astrophysics and Space Science, 5, 180.
- Arnett, W. D. 1972, Astrophys. J., 176, 681.
- Arnett, W. D. 1972a, Astrophys. J., 176, 699.
- Arnett, W. D. 1973, Ann.Rev. Astron. Ap., 11, 73.
- Arnett, W. D. 1973a, Astrophys. J., 179, 249.
- Arnett, W. D. 1974, Astrophys. J., 194, 373.
- Arnett, W. D. 1974a, Astrophys. J., 193, 169.
- Arnett, W. D. 1977, Astrophys. J. Supp., 35, 145.
- Arnett, W. D. 1978, Astrophys. J., 219, 1008.
- Arnett, W. D., and Clayton, D. D. 1970, Nature, 227, 780.
- Arnett, W. D., and Schramm, D. N. 1973, Astrophys. J., 184, L47.
- Arnett, W. D., and Truran, J. W. 1969, Astrophys. J., 157, 339.
- Arnett, W. D., and Wefel, J. P. 1978, Astrophys. J., 224, L139.
- Assousa, G. E., Herbst, W., and Turner, K. C. 1977, Astrophys. J., 218, L13.
- Bethe, H. A., Brown, G. T., Applegate, J., and Lattimer, J. M. 1978, Nordita preprint.
- Beaudet, G., Petrosian, V., and Salpeter, E. E. 1964, Astrophys. J., 150, 979.
- Birkeland, K. 1912, Compt. rend. acad. sci., 155, 892.
- Bludman, S. A., and Van Riper, K. A. 1972, Astrophys. J., 212, 859.

- Bruenn, G. W. 1975, Ann. N.Y. Acad. Sci., 262, 80.
- Buffon, G.L.L. 1745, De la Formation des Planetes (Paris).
- Burbidge, E. M., Burbidge, G. R., Fowler, W. A., and Hoyle, F. 1957, Rev. Mod. Phys., 29, 457.
- Cameron, A.G.W. 1963, in Origin of the Solar Systems, ed. R. Jastrow and A.G.W. Cameron (Academic Press, New York).
- Cameron, A.G.W. 1973, in Explosive Nucleosynthesis, eds. D. N. Schramm and W. D. Arnett (University of Texas Press).
- Cameron, A.G.W., and Truran, J. W. 1977, The Supernova Trigger for Formation of the Solar System, ICARUS, 30, 447-461.
- Cameron, A.G.W., and Truran, J. W. 1977, Astrophys. J., 219, 226.
- Chamberlin, J. 1901, Astrophys. J., 14, 17.
- Chiu, H. Y. 1968, Stellar Physics (Blaisdell).
- Clark, D. H., and Stephenson, F. R. 1977, The Historical Supernovae (Pergamon Press).
- Clayton, D. D. 1968, Principles of Stellar Evolution and Nucleosynthesis (McGraw-Hill, New York).
- Clayton, D. D. 1978, An Interpretation of Special and General Isotopic Anomalies in r-Process Nuclei, to be published.
- Clayton, D. D. 1978a, Precondensed Matter: Key to the Early Solar System, presented at Symposium, "Protostars and Planets," Tucson, 3-7 January, 1978.
- Clayton, D. D., Dwek, E., and Woosley, S. E., Astrophys. J., 214, 300.
- Clayton, R. N., Grossman, L., and Mayeda, T. K. 1973, Science, 182, 485.
- Colgate, S. A., and White, R. H. 1966, Astrophys. J., 143, 626.
- Couch, R. G., Schmeidekamp, A. B., and Arnett, W. D., 1974, Astrophys. J., 190, 95.
- Cox, J. P., and Guili, R. T. 1968, Principles of Stellar Structure (Gordon and Breach).
- Descartes, R. 1644, Principia Philosophiae (Amsterdam).
- Despain, K. H. 1977, Astrophys. J., 212, 774.

- DeWitt, H. E., Gabroske, H. G., and Cooper, M. S. 1973, Astrophys. J., 181, 439.
- Divine, N. 1966, Astrophys. J., 142, 1652.
- Dwek, E. 1978, Astrophys. J., 221, 1026.
- Endal, A. S. 1975, Astrophys. J., 195, 187.
- Endal, A. S. 1975a, Astrophys. J., 197, 405.
- Forcefield, Mad Dr. 1977, Interstellar Weapon Physics (Rip-off Press, San Francisco).
- Fowler, W. A., Caughlin, G. R., and Zimmerman, B. A. 1967, Ann. Rev. Astron. Ap., 5, 525.
- Fowler, W. A., Caughlin, G. R., and Zimmerman, B. A. 1975, Ann. Rev. Astron. Ap., 13, 69.
- Fowler, W. A., Greenstein, J. L., and Hoyle, F. 1962, Geophysical J., 6, 148.
- Fowler, W. A., and Hoyle, F. 1964, Astrophys. J., 139, 909.
- Fowler, W. A., and Hoyle, F. 1964a, Nucleosynthesis in Massive Stars and Supernovae (U. Chicago Press, Chicago, 1964).
- Goldschmidt, V. M. 1937, Skrifter Norske Videnskap-Akad. Oslo I. mat. Natur, K1 #4.
- Gray, G. M., and Compston, W. 1974, Nature, 251, 495.
- Hansen, C. J. 1966, Ph.D. Dissertation, Yale University.
- Heymann, D., and Dzickaniec, M. 1976, Science, 191, 79.
- Heymann, D., Dzickaniec, M., Walker, H., Huss, G., and Morgan, J. A. 1978, Astrophys. J., 225, 1030.
- Herbst, W., and Assousa, G. E. 1977, Astrophys. J., 217, 443.
- Hillebrandt, W., Takahashi, K., and Kodama, T. 1976, Astron. and Astrophys., 52, 63.
- Howard, W. M., Arnett, W. D., Clayton, D. D., and Woosley, S. E. 1972, Astrophys. J., 175, 201.
- Hoyle, F. 1944, Proc. Cambridge Phil. Soc., 40, 256.
- Huang, K. 1968, Statistical Mechanics (John Wiley & Sons).

- Ikeuchi, S., Nakazawa, K. Murai, T., Hoshi, R., and Hyashi, C. 1971, Prog. Theor. Phys., 46, 1713.
- Ishennik, V. S., and Nadyozhin, D. K. 1974, in Late Stages of Stellar Evolution, IAU Symp. #66, ed. R. J. Tayler (D. Neidel, Dordrecht).
- Kant, I. 1755, Allgemeine Naturgeschichte und Theorie des Himmels.
- Kohman, T. P. 1961, J. Chem. Educ., 38, 73.
- Kuiper, G. P. 1949, Astrophys. J., 109, 308.
- Lada, C. J., Blitz, L., and Elmegreen, B. G. 1978, in Protostars and Planets, ed. T. Gehrels, p.341.
- Lamb, S. A., Howard, W. M., Truran, J. W., and Iben, I. 1977, Astrophys. J., 217, 213.
- Lamb, S. A., Iben, I., and Howard, W. M. 1976, Astrophys. J., 207, 209.
- Landau, L. D., and Lifshitz, E. M. 1959, Fluid Mechanics (Pergamon Press).
- Laplace, P. S. de 1796, Exposition du système du Monde (Paris).
- Lee, T. 1978, Astrophys. J., 224, 217.
- Lee, T., and Papanastassiou, D. A. 1974, Geophys. Res. Lett., 1, 225.
- Lee, T., Papanastassiou, D. A., and Wasserborg, G. J. 1977, Astrophys. J. Lett., 211, L107.
- Lee, T., Papanastassiou, D. A., and Wasserborg, G. J. 1977a, Geochim. et Cosmochim. Acta, 41, 1473.
- Lee, T., Papanastassiou, D. A., and Wasserborg, G. J. 1977b, Geophys. Res. Lett., 4, 299.
- Lee, T., Papanastassiou, D. A., and Wasserborg, G. J. 1978, Astrophys. J. Lett., 250, L21.
- Lorin, J., Shimizu, N., Michel-Levy, M. C., and Allegre, C. J. 1978, Meteoritics, 12, 299.
- Lucretius (55 B.C.E.), De Rerum Natura, tr. by R. E. Lattimer as On the Nature of the Universe (Penguin Books, Baltimore, Md., 1971), pp.183-184.
- Lyttleton, R. A. 1941, M.N.R.A.S., 101, 216.

- McCulloch, M. T., and Wasserburg, G. J. 1978, Astrophys. J. Lett., 220, L15.
- MacDougall, J. D., and Phinney, D. 1978, Fractionated Mg Isotopes in Murchison Refractory Inclusions, presented at Isotope Geology Conference, Aspen, 1978.
- MacDougall, J. D., and Stoner, E. C. 1938, Phil. Trans. Roy. Soc., 237, 67.
- Manuel, D. K., Hennecke, E. W., and Sabu, D. P. 1972, Nature, 240, 99.
- Mathews, J., and Walker, R. W. 1970, Mathematical Method of Physics (W. A. Benjamin).
- Michaud, G., and Fowler, W. A. 1970, Phys. Rev. C 2, 2041.
- Moulton, T. 1905, Astrophys. J., 22, 165.
- Nørgaard, H. 1978, Nordita preprint.
- Ono, Y., Sakashita, S., and Ohyama, N. 1961, Supp. Prog. Theor. Phys., 20, 85.
- Pardo, R. C., Couch, R. G., and Arnett, W. D. 1974, Astrophys. J., 191, 711.
- Patterson, J. R., Winkler, H., Zaidans, C. S. 1969, Astrophys. J., 157, 367.
- Phinney, D., Whitehead, B., and Anderson, D. 1978, Proceedings of the Ninth Lunar and Planetary Science Conference.
- Rakav, G., Shaviv, G., and Zinamon, Z. 1967, Astrophys. J., 150, 131.
- Reeves, H. 1978, in Protostars and Planets, ed. Gehrels, p.399.
- Rutherford, E. 1929, Nature, 123, 313.
- Sakurai, A. 1950, J. Fluid Mechanics, 1, 436.
- Sedov, L. I. 1959, Similarity and Dimensional Methods in Mechanics (Academic Press).
- Suess, H. C., and Urey, H. C. 1956, Rev. Mod. Phys., 28, 53.
- Taylor, G. I. 1950, Proc. Roy. Soc., A201, 155.
- ter Haar, D. 1948, Tgl. Danske Videnskab Selskab, mat-Fys. Medd., 25, 3.

- Urey, H. C. 1951, Geochim. et Cosmochim. Acta, 1, 209.
- van den Bergh 1976, Astrophys. J. Lett., 208, L17.
- Van Riper, K. A. 1978, Astrophys. J., 221, 304.
- Van Riper, K. A., and Arnett, W. D. 1978, Astrophys. J., 225, L129.
- von Neumann, John 1943, Theory of Shock Waves, U.S. Dept. Com. Off. Tech. Serv. #PB32719; reprinted in the collected works, Vol. VI (Pergamon Press, New York, 1963), p.178.
- von Neumann, John 1943a, in Blast Wave, AEC REport LA-2000.
- von Neumann, John, and Richtmeyer, R. D. 1950, A Method for the Numerical Calculation of Hydrodynamic Shocks, J. App. Phys., 21, 3, 232-237; reprinted in von Neumann's collected works, Vol. VI (Pergamon Press, New York, 1963), p.380.
- von Weizäcker, C. F. 1944, Z. Ap., 22, 319.
- Wagoner, R. V. 1969, Astrophys. J. Supp., 162, 247.
- Weaver, T. A., Zimmerman, G. B., and Woosley, S. A. 1978, Astrophys. J., 225, 1021.
- Wehr1, A. 1978, Rev. Mod. Phys., 50, 221.
- Wetherill, G. W. 1975, Radiometric Chronology of the Early Solar System, Ann. Rev. Nucl. Sci., 25, 283.
- Whipple, F. 1948, Harvard Observatory Monographs #7.
- Wilson, J. R. 1971, Astrophys. J., 163, 209.
- Wilson, J. R. 1974, Phys. Rev. Lett., 32, 849.
- Woosley, S. E., Arnett, W. David, and Clayton, Donald D. 1973, The Explosive Burning of Oxygen and Silicon, Astrophys. J. Supp., 26, 231, 231-312.
- Woosley, S. E., Fowler, W. A., Holmes, J. A., and Zimmerman, B. A. 1975, Table of Thermonuclear Reaction Rate Data for Intermediate Mass Nuclei, Orange Aid Preprint OAP-422.
- Woosley, S. E., and Howard, W. M. 1977, Astrophys. J. Suppl, 36, 285.
- Zeld'ovich, Ya. B., and Raizer, Yu. P. 1966, Physics of Shock Waves and High-Temperature Hydrodynamic Phenomena (Academic Press).

PLEASE NOTE:

In all cases this material has been filmed in the best possible way from the available copy.
Problems encountered with this document have been identified here with a check mark ✓.

1. Glossy photographs or pages _____
2. Colored illustrations, paper or print _____
3. Photographs with dark background ✓
4. Illustrations are poor copy _____
5. Pages with black marks, not original copy ✓
6. Print shows through as there is text on both sides of page _____
7. Indistinct, broken or small print on several pages ✓
8. Print exceeds margin requirements _____
9. Tightly bound copy with print lost in spine _____
10. Computer printout pages with indistinct print _____
11. Page(s) _____ lacking when material received, and not available from school or author.
12. Page(s) _____ seem to be missing in numbering only as text follows.
13. Two pages numbered _____. Text follows.
14. Curling and wrinkled pages ✓
15. Dissertation contains pages with print at a slant, filmed as received ✓
16. Other _____

University
Microfilms
International

—

RICE UNIVERSITY

HF SIDEBANDS IN THE IONOSPHERE

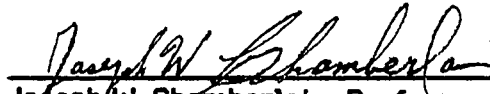
by

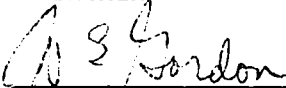
ZHONG- HAO HUANG


A THESIS SUBMITTED
IN PARTIAL FULFILLMENT OF THE
REQUIREMENTS FOR THE DEGREE

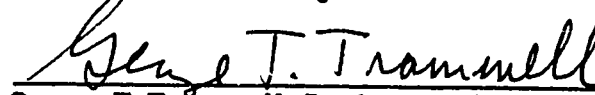
DOCTOR OF PHILOSOPHY

APPROVED, THESIS COMMITTEE:


Joseph W. Chamberlain, Professor of
Space Physics and Astronomy
Chairman


William E. Gordon, Distinguished
Professor Emeritus


Patricia H. Reiff, Associate Research
Scientist of Space Physics & Astr.


George T. Trammell, Professor of
Physics

HOUSTON, TEXAS
APRIL 1987

ABSTRACT

HF Sidebands in the Ionosphere

Sidebands on the high frequency (HF) waves received from two transmitted waves separated by small frequency intervals were first observed by Gordon and Ganguly in January, 1984 at Arecibo, Puerto Rico. Papadopoulos proposed that HF sidebands would arise from the nonlinear interaction of an ELF wave with the two high frequency waves. The nonlinear mechanism for ELF and HF sideband generation is parametric decay of a high frequency radio wave into a low frequency compressional Alfvén wave and a high frequency sideband [Papadopoulos et al., 1982].

In 1984 Fejer proposed another nonlinear mechanism (phase modulation theory) for HF sideband generation. Fejer points out that the effect of the ponderomotive force is a reduction in the electron density and an increase in the phase delay which is greater for more powerful waves. Numerical solutions show that the phase delay would relate to the power density of the HF wave. This modulation index theory using the W.K.B. approximation shows that the amplitude of sidebands is related to: [1] the effective HF power; [2] the HF frequency; [3] the temperature of the electrons; [4] the scale height of the ionosphere; and [5] the difference frequency of the two pump waves. Observations of HF sidebands were again made in January, 1986. The 430 MHz incoherent radar provided the ionospheric background measurements. The modulation index theory provides the most complete interpretation of the observations.

ACKNOWLEDGEMENTS

I would like to extend a special thanks to Dr. William E. Gordon, my thesis advisor, for providing me with a research opportunity in nonlinear ionospheric plasma physics. This research would not have been possible without the patient support, guidance and encouragement of Dr. Gordon. I also would like to thank Professor Joseph W. Chamberlain, my Professor of the Theory of Planetary Atmospheres, who has served my official advisor since Dr. Gordon retired as Rice's provost and vice president; Dr. Reiff and Dr. Trammell also both have served as my Ph. D. committee members.

I am indebted to Dr. Fejer whom I met and worked with at the Arecibo Observatory in 1984 and who has since advised on my theoretical work. This research represents a collaborative effort that included Dr. S. Noble of SRS International, Dr. James McCoy of the Johnson Space Center, NASA, Dr. Lewis M. Duncan of Los Alamos National Laboratory and Dr. F. T. Djuth of Aerospace Corporation. They participated in these experiments. I am indebted for their help, which ranged from technical support to theoretical discussions. I would also like to acknowledge the aid of the scientific staff at the Arecibo Observatory.

Finally I want to thank Professor Henry G. Booker who was mainly instrumental in getting me interested in the incoherent scattering radar. As a graduate student I had the good fortune to attend his lecture in 1981. Dr. Booker also has been kind enough to evaluate my thesis.

This research was supported by the Atmospheric Research Section of the National Science Foundation under Grant Nos. ATM-4813306.

TABLE OF CONTENTS

1. INTRODUCTION.....	1
2. THEORETICAL BACKGROUND.....	7
2.1 Waves and Instabilities in the Ionosphere.....	7
2.2 General Coupled Mode Formalism.....	12
2.3 Saturation Mechanisms of the Ionosphere.....	19
2.4 Incoherent Scatter.....	24
3. TWO HF HEATING THEORY.....	31
3.1 Papadopoulos Theory.....	31
3.2 Fejer-Huang Phase Modulation Theory.....	36
3.3 Gordon-Huang Modulation Index Theory.....	44
4. EXPERIMENT.....	56
4.1 High Frequency Heating Facility.....	56
4.2 Arecibo Observatory.....	64
4.3 Two Frequency Experiment.....	66
5. EXPERIMENTAL RESULTS.....	72
5.1 Brief Summaries.....	73
5.2 Extended Observations.....	73
(A) February 3, 1986.....	73
(B) February 4, 1986.....	83
(C) February 5, 1986.....	96
(D) February 7, 1986.....	106
(E) February 8, 1986.....	115
6. ANALYSIS AND CONCLUSIONS.....	129